ACCURATE MEASUREMENTS AND MODELING OF THE $P\rho T$ BEHAVIOR OF PURE SUBSTANCES AND NATURAL GAS-LIKE HYDROCARBON MIXTURES

A Dissertation

by

IVAN DARIO MANTILLA

Submitted to the Office of Graduate Studies of
Texas A&M University
in partial fulfillment of the requirements for the degree of

DOCTOR OF PHILOSOPHY

August 2012

Major Subject: Chemical Engineering

ACCURATE MEASUREMENTS AND MODELING OF THE $P\rho T$ BEHAVIOR OF PURE SUBSTANCES AND NATURAL GAS-LIKE HYDROCARBON MIXTURES

A Dissertation

by

IVAN DARIO MANTILLA

Submitted to the Office of Graduate Studies of
Texas A&M University
in partial fulfillment of the requirements for the degree of

DOCTOR OF PHILOSOPHY

Approved by:

Co-Chairs of Committee,	Kenneth Hall
	Tahir Cagin
Committee Members,	James Holste
	Sam Mannan
	Robert Wattenbarger
Head of Department,	Charles Glover

August 2012

Major Subject: Chemical Engineering

ABSTRACT

Accurate Measurements and Modeling of the $P\rho T$ Behavior of Pure Substances and Natural Gas-Like Hydrocarbon Mixtures. (August 2012)

Ivan Dario Mantilla, B.S., Universidad Industrial de Santander

Co-Chairs of Advisory Committee, Dr. Kenneth Hall
Dr. Tahir Cagin

The scale of the energy business today and a favorable and promising economic environment for the production of natural gas, requires study of the thermophysical behavior of fluids: sophisticated experimentation yielding accurate, new volumetric data, and development and improvement of thermodynamic models. This work contains theoretical and experimental contributions in the form of 1) the revision and update of a field model to calculate compressibility factors starting from the gross heating value and the mole fractions of diluents in natural gas mixtures; 2) new reference quality volumetric data, gathered with state of the art techniques such as magnetic suspension densimetry and isochoric phase boundary determinations; 3) a rigorous first-principles uncertainty assessment for density measurements; and 4) a departure technique for the extension of these experimental data for calculating energy functions. These steps provide a complete experimental thermodynamic characterization of fluid samples.

A modification of the SGERG model, a standard virial-type model for prediction of compressibility factors of natural gas mixtures, matches predictions from the master GERG-2008 equation of state, using least squares routines coded at NIST. The

modification contains new values for parametric constants, such as molecular weights and the universal gas constant, as well as a new set of coefficients.

A state-of-the-art high-pressure, single-sinker magnetic suspension densimeter is used to perform density measurements over a wide range of temperatures and pressures. This work contains data on nitrogen, carbon dioxide, and a typical residual gas mixture (95% methane, 4% ethane, and 1% propane). Experimental uncertainty results from a rigorous, first-principles estimation including composition uncertainty effects.

Both low- and high-pressure isochoric apparatus are used to perform phase boundary measurements. Isochoric *P-T* data can determine the phase boundaries. Combined with density measurements, isochoric data provides isochoric densities. Further mathematical treatment, including noxious volume and thermal expansion corrections, and isothermal integration, leads to energy functions and thus to a full thermodynamic characterization.

To

All my Teachers in Life

and

All my Families around the World

ACKNOWLEDGEMENTS

Let me hereby take a few lines to extend a grateful acknowledgement to everyone who participated in the development and completion of any activity related to this dissertation work, and most especially to my advisors Dr. Kenneth Hall, Dr. James Holste, Dr. Tahir Cagin, Dr. Sam Mannan and Dr. Robert Wattenbarger for their advice, patience, support and friendship, and to all members of the thermodynamics research group.

I would like to acknowledge the important contributions of Dr. Mark McLinden and Dr. Eric Lemmon at NIST, and visiting professor Dr. Gustavo Iglesias, their support, advice and friendship.

Especial thanks to Randy in the CHEN shop and Jason in the electronics physics shop for their support and technical wisdom.

Thanks to my family for the initial boost, for the constant thoughts and questions, and for the final prayers. And thanks very much indeed to all my friends who made many moments unforgettable. Thanks for all the time, and for all.

NOMENCLATURE

α	Balance atmosphere factor
A	Helmholtz free energy (kJ/kmol)
β	Thermal expansion coefficient
b	Exclusion volume, constant in Redlich-Kwong EoS, intermediate coefficient for calculation of second virial coefficient of mixture
B	Second virial coefficient
c	Intermediate coefficient for calculation of third virial coefficient of mixture
C	Third virial coefficient
C_P	Constant pressure heat capacity
C_v	Constant volume heat capacity
Δ, δ	Experimental value minus equation of state prediction
D	Fourth virial coefficient
Φ	Coupling factor
g	Empirical coefficient in heating value correlation with molecular weight
G	Gibbs free energy (kJ/kmol)
H	Enthalpy (kJ/kmol)
H_{CH}	Equivalent hydrocarbon heating value
m	Mass (g, kg)
M	Molar mass, molecular weight
n	Number of moles
N	Number of data points, or number of components in a mixture

P	Pressure (MPa)
ρ	Density (kg/m^3, kmol/m^3)
R	Universal gas constant (8.314472 kJ/kmol-K)
Ψ	Any independent experimental variable contributing to the uncertainty
σ	Standard deviation
S	Entropy (kJ/kmol-K)
T	Temperature (K)
u	Uncertainty
U	Internal energy (kJ/kmol)
V	Molar volume (m^3/kmol), or physical volume (m^3, cc)
w	Weight, mass reading from balance
χ	Joule-Thomson coefficient
x	Molar fraction
X	Energy function
Z	Compressibility factor

TABLE OF CONTENTS

LIST OF FIGURES

FIGURE Page

LIST OF TABLES

TABLE Page

1. INTRODUCTION

The study of the $P\rho T$ behavior of fluids has been an endeavor occupying many scientists and engineers over the past three centuries. The possibility of generating usable energy by burning, expanding, compressing, cooling, or heating different fluids in the most inventive ways has motivated work by many brilliant minds and led to astonishing observations that gave birth to what we know as classical thermodynamics. The scale of the energy business today and the relative simplicity of industrial operations demand still more accurate data and simpler more powerful predictive models.

1.1. Energy Landscape

Recently, energy has become a pressing topic. All media, including scientific and non-scientific literature reflect diverse and keen ideas, opinions, analyses, and developments towards securing a safe, clean, sustainable and affordable energy future. The toughest challenges should happen in the near future as the most widely used and developed energy sources become scarcer and the energy demand continues rising in an accelerating fashion, mainly driven by big developing economies like China, India and Brazil.

This dissertation follows the style of *Journal of Chemical & Engineering Data.*

In the world energy landscape described by the most important contributors from academia, industry and governments[1-6], natural gas appears as the world's fastest-growing fossil fuel, being relatively clean, cheap and abundant. A favorable economic framework has allowed important technological developments at the operational level. In the US, the abundance of natural gas makes it a candidate to achieve and secure a dependable energy future. This idea underlies the strong effort that academic, industrial and governmental institutions have undertaken to develop the most advanced technologies in exploration, exploitation, production, processing and distribution of natural gas from conventional and non-conventional sources.

Thermodynamics, the science containing thermophysical behavior of substances and equilibrium, appears at the scientific core of the subject matter imposing limits to operating conditions. Natural gas (primarily a mixture of hydrocarbons) has driven most of the equations of state development for mixtures.

1.2. Natural Gas Custody Transfer Operations and Business: Importance of Measurements

The industrial importance of thermodynamic measurements is most evident when dealing with custody transfer operations summarized in the following equation:

$$\frac{\$}{day} = \left(\frac{\$}{J}\right)\left(\frac{J}{kg}\right)\left(\frac{kg}{m^3}\right)\left(\frac{m^3}{day}\right) \tag{1.1}$$

Equation 1.1 estimates the amount of money per unit time traded in the natural gas business by taking the price per unit energy ($/J) and multiplying it by the heating value (J/kg), times the density of the fluid (kg/m^3) at the transfer conditions, times the volume transferred per unit time (m^3/day, volumetric flow).

Typical uncertainty levels of density values of well and sale gases predicted with the most widely used and accurate equations of state are around 0.1 to 1.0 %.

US total net imports of natural gas were roughly 70 billion m^3 in 2011,[1] or about 200 million m^3/day. At current prices of ~2 USD/mcf ($0.07/$m^3$), natural gas imports cost roughly $14 million per day ($5 billion/year). An uncertainty of 1.0 % in the density value amounts to $50 million/year assuming all other variables are 100 % accurate.

Now, considering US measures 20 to 70 trillion cf each year, and assuming an average price of $2/mcf, a reduction of 0.01 % in measurement uncertainty (either density or flow) would save the industry $4 to 14 million per year.

The current natural gas economy is a shifting entity. The market has experienced rapid diversification and globalization driven by liquefied natural gas (LNG) and gas to liquids (GTL) technologies. The supply has increased because of improved production technologies (hydraulic fracture) that have made it economical to produce shale gas and tight gas resources. Global gas demand should grow about twice as fast as the demand for oil over the next 20 years according to the International Energy Agency (IEA).[2]

Higher accuracy in densities, flow measurements, and heating value estimations for natural gas can improve transactions and trust. Natural gas can also provide a clean, sustainable and dependable energy supply for the near future.

From the scientific viewpoint, mixtures of hydrocarbons are the simplest industrial substances with the widest applicability. This fact provides motivation to work on thermodynamic characterization until reaching a model simple, general and powerful enough to predict thermodynamic properties to the lowest achievable experimental uncertainties.

1.3. Equations of State

An equation of state (EoS) is a model that correlates the properties of substances, such as the volumetric ($P\rho T$) behavior. Such a model must smoothly extrapolate to the ideal gas state as P and $\rho \rightarrow 0$, as well as account for the deviation of real behavior from ideal. Equation 1.2 is the ideal gas EoS.

$$PV = RT \tag{1.2}$$

A simple, general way to model the $P\rho T$ behavior of "real" gases is the compressibility factor, Z

$$Z = \frac{PV}{RT} = \frac{P}{\rho RT} \tag{1.3}$$

in which P is the pressure, T is the absolute temperature, R is the universal gas constant, and V is the molar volume, reciprocal of the molar density ρ.

The task becomes, to find a way to predict Z, knowing it should equal unity when at the ideal gas state. The more general, in the sense of the more fluids it describes, the wider the range of conditions (pressure, temperature, and density), and the lower the

uncertainty and the deviations of its predictions from experimental data, the better and more powerful the EoS model is.

1.3.1. The Virial Equation of State

The virial formulation expresses the compressibility factor Z as an infinite power series in ρ, a *virial expansion*.

$$Z = 1 + B(T)\rho + C(T)\rho^2 + D(T)\rho^3 + \ldots \tag{1.4}$$

Where B, C, D, … are the *virial coefficients*, functions of temperature and composition. Clearly, the ideal gas state is when $Z \rightarrow 1$ as $\rho \rightarrow 0$. Ideal gas particles do not interact with each other.

Thus, the virial EoS has a strong theoretical connection with the interaction potential such that the *second* virial coefficient B accounts for binary interactions between particles, the *third* virial coefficient C accounts for ternary interactions, and so on. Mathematically, B and C are the intercept and the slope of the function $(Z-1)/\rho$ at zero pressure, respectively.

$$B(T) = \left(\frac{\partial (Z-1)}{\partial \rho} \right)_T = \lim_{\rho \to 0} \frac{(Z-1)}{\rho} \tag{1.5}$$

$$C(T) = \left(\frac{\partial^2 (Z-1)}{\partial \rho^2} \right)_T = \lim_{\rho \to 0} \frac{\left(\frac{Z-1}{\rho} - B \right)}{\rho} \tag{1.6}$$

Viral coefficient estimates come from fitting volumetric data gathered isothermally to a truncated version of the virial expansion. Truncation selection depends

upon the accuracy of the experimental techniques and the conditions under which experiments are performed. Usually, for a particular substance, isothermal data sets are fit at once and values of virial coefficients at different temperatures are extracted from those isothermal correlations.

The *least squares* method has been used to fit thermodynamic data for most virial coefficient determinations, varying only in the experimental techniques and setups used, and, with them, the accuracy and precision of data. Among those techniques are compressibility measurements via Burnett apparatus, direct density measurements (weighing methods), and energy determinations (heats of formation and vaporization, heat capacity determinations, and Joule-Thomson coefficients). For the former (volumetric techniques), the numerical procedures involve a direct polynomial fit. For the latter (energy measurements) less accurate values result because the procedure involves a simplified inverse problem and different indirect models. Here are some examples:

$$H - H^0 = RT\left(\frac{B - B_1}{V} + \frac{2C - C_1}{2V^2} + \cdots\right) \tag{1.7}$$

$$C_p - {C_p}^0 = -R\left\{\frac{B_2}{V} - \frac{(B - B_1)^2 - (C - C_1) - \frac{C_2}{2}}{V^2} + \cdots\right\} \tag{1.8}$$

$$S - S^0 = -R\left\{lnP + \frac{B_1}{V} + \frac{(B^2 - C + C_1)}{2V^2} + \cdots\right\} \tag{1.9}$$

$$\chi = \frac{1}{C_p}\left(T\left(\frac{\partial V}{\partial T}\right)_p - V\right) \tag{1.10}$$

$$\chi = \frac{1}{{C_p}^0}\left\{(B_1 - B) + \frac{2B^2 - 2B_1B - 2C + C_1}{V} + \frac{R}{{C_p}^0}\left(\frac{B_2(B_1 - B)}{V}\right) + \cdots\right\} \qquad (1.11)$$

Subcripts 1 and 2 indicate first and second derivative with respect to *T* respectively.

$$B_1 = \frac{dB}{dT}; \qquad B_2 = \frac{d^2B}{dT^2}; \qquad (1.12)$$

$$C_1 = \frac{dC}{dT}; \qquad C_2 = \frac{d^2C}{dT^2}; \qquad (1.13)$$

The uncertainty of the resulting virial parameters depends upon the truncation of the virial expansion, the number of data points used, and the uncertainty of the measured properties. The truncation selection depends, in turn, upon the conditions and the substance, making it a matter of engineering judgment.

The best results so far (lowest uncertainties/standard errors) are the direct polynomial correlations of data gathered with Burnett apparatus and sophisticated weighing methods like Magnetic Suspension Densimetry (MSD). The numerical algorithms are usually simple and deterministic (least squares, Levenberg–Marquardt).

1.3.2. Cubic Equations of State

Cubic equations of state, such as Redlich-Kwong[7] or Peng-Robinson[8] are the predictive models most widely used by industry because they are simple, fast, and still acceptably accurate for most design and operational needs. In these equations the pressure, *P,* is an explicit cubic function of *V*. These equations preserve a theoretical

foundation from the first developments by Van der Waals, and implement empirical parameters to fit different fluids and phase equilibrium behavior, but lack the structure to predict the behavior over all the thermodynamic space.

In general, they remain viable as the simplest and most reliable attempts to produce a fundamental and general model, and their use is subject to manipulation and adjustment of their parameters for specific systems and applications, as experimental data become available and new applications develop.

1.3.3. Standard/Reference Equations of State

Data-based Reference equations of state (EoS) have evolved greatly during the last 20 years becoming the most accurate representation of the thermodynamic behavior of pure fluids. A nitrogen equation by Span et al.[9] and a carbon dioxide equation by Span et al.[10] are examples of these reference equations. These multi-parametric equations define the Helmholtz energy of the substance by a mathematical function and derive from it all other properties necessary to fit its parameters to diverse experimental data. They contain many terms, which makes them computationally demanding when implementing them in calculation algorithms.

Reference equations of state like AGA-8[11] and GERG-08[12] use departure functions, which contain interaction parameters for mixtures, to produce the standard models for mixtures. Although widely accepted by academia and the community of

standards, the level of complexity of these models requires many parameters, raising the computational cost of using them to unpractical levels for industrial applications.

1.3.4. SGERG Model

The SGERG model[13, 14] is a virial-type, multi-parametric model. It follows the concept of the virial EoS explained above (equation 1.4), and uses its empirical flexibility to fit mixture virial coefficients in a multi-parametric manner similar to the one used by standard/reference EoS. In other words, it represents an interesting combination of the multi-parametric standard EoS and the virial equation: it carries the conceptual, mathematical simplicity of the virial EoS, and the high accuracy of the standard models, to an extent practical enough for single phase predictions over a limited range of conditions. Section 2 is a detailed revision and update of this model.

1.4. Density Measurements

Experimentally, researchers have developed many techniques over the last century.[15] Indirect methods, such as speed of sound [16-19] or thermal properties [20-23] mentioned above, vibrating wires [24-26] and tubes [27-31], whose vibration frequencies are sensitive to the density of a surrounding or contained fluid, expansion methods like the Burnett apparatus [32-35], and direct continuous weighing methods like pycnometers [36-38]. The most sophisticated and versatile of all is the magnetic suspension densimeter

(MSD)[39-44], which uses one of the oldest and most elegant of all experimental techniques: Archimedes principle. For it to be used over a wide range of temperatures and pressures, the MSD uses a closed container in which a magnetic coupling accesses the element (sinker) submerged in the fluid to measure its apparent mass. The buoyancy force experienced by the sinker is proportional to the density of the fluid. In the work described by this dissertation, we measure densities using a high-pressure, single-sinker MSD. An explanation of the technique, apparatus, procedures, and uncertainties appears in section 3.

1.5. Uncertainties

Uncertainty is an important quantity associated to any measurement. It is a way to quantify the level of accuracy, precision and reliability of data collected with a particular technique or apparatus. Extensive documents exist in the literature[45-48] dedicated to a standard way to express the uncertainties of measurements.

Different techniques and apparatus have different sources of uncertainty. The thorough knowledge and understanding of the physical devices and methods used in the experiment leads to the most reliable estimation of specific uncertainties. Sample composition effects upon the uncertainty of density measurements either has been ignored or taken for granted. In this work, we calculate uncertainties in density measurements using a rigorous approach that involves first-principles mathematical

treatment of all experimental variables involved in MSD measurements, including composition.

1.6. Phase Boundaries

The design of compression systems and pipelines for hydrocarbon processes and operations requires knowledge of the phase equilibrium of substances to impose limits on operating conditions. Phase boundaries, dew and bubble points in the case of vapor-liquid equilibrium (VLE), are pairs of coordinates, generally *(T, P)* or *(T, ρ)*, at which the aggregation state of a substance stops being a single phase, like gas or liquid, and two phases begin to coexist. At a dew point, liquid begins to form from a vapor. Conversely, at a bubble point, vapor begins to form as bubbles from a liquid.

Many techniques are available to measure vapor-liquid equilibrium.[49-51] At low pressures, methods like a recirculating still[52, 53] or open container static methods[54, 55] have been used. At high pressures, several researchers have developed various versions of the VLE apparatus during the last decades of the 20th century.[15, 56, 57]

The isochoric VLE method appeared in the literature in 1986 as a versatile, static, closed-cell method for measurements over wide ranges of temperature and pressure. It relies upon the change in slope of isochoric lines as they cross vapor-liquid phase boundaries[15].

1.7. Full Thermodynamic Characterization

Isothermal and isochoric $P\rho T$ data can be enough to calculate all thermodynamic properties including energy functions (internal energy U, entropy S, enthalpy H, and Gibbs G and Helmholtz A free energies) and provide a full thermodynamic characterization of a sample. Mathematical treatment, correction and manipulation of experimental quantities are not trivial tasks. Section 5 contains a technique for the calculation of energy functions from experimental $P\rho T$ data.

1.8. Objectives of This Work

Thermodynamicists seek to increase and improve thermodynamic knowledge in the forms of data tabulations, correlations of data, predictive equations of state, etc., which are critical to developments driven by the energy economy framework. The two main objectives of this work are: 1) contributing a wider and deeper understanding of the thermodynamic behavior of pure fluids and natural gas-type (NG-type) mixtures, and 2) validating and improving of the predictive power of existing thermodynamic models.

The contributions of this dissertation are fourfold: 1) suggesting a revision and updating of ISO Standard: 12213-3 "Natural gas – Calculation of compression factor – Part 3: Calculation using physical properties"; 2) new density and phase boundary data for pure substances and NG-type mixtures acquired using high-accuracy/high-precision techniques such as magnetic suspension densimetry (MSD) and isochoric "slope-break"

phase boundary determinations featuring high pressure capabilities, up to 200 MPa; 3) a rigorous approach to experimental uncertainty assessment; and 4) a calculation routine for energy functions from experimental $P\rho T$ data that involves crossing of isothermal and isochoric curves in the thermodynamic space. Experimental and theoretical methodologies implemented to accomplish these objectives appear in each section.

2. STANDARD GERG VIRIAL EQUATION FOR FIELD USE – REVISION 2010

In 1991 the Groupe Europeen de Recherches Gazieres (GERG) developed a standard virial-type equation for calculating the compressibility factor (Z) of natural gas and similar mixtures (SGERG model). When a complete molar composition is not available, this model uses a simplified set of input requirements, namely, the *gross* heating value, the relative density, and the concentration of diluents in the fluid (nitrogen, carbon dioxide, carbon monoxide, and hydrogen). AGA report No. 8 developed by Starling et al.[11] describes this model as the *gross method*. In 1997, this model became an international standard under the reference number ISO 12213-3.

The current model is a thorough revision of the original model and the calculation methodologies. Optimization techniques coded at NIST for fitting/tuning the model include new data that has become available to match the predictions of the master GERG-2008 standard equation of state for compressibility factors of natural gas mixtures at the working conditions of the simplified model within 0.1 % deviations.

2.1. Methodology

The applicability ranges of the original model reported in the ISO 12213-3:2006(E) document appear in table 2.1.

Table 2.1. Applicability ranges of the SGERG model.

Quantity	**Range**
Pressure	0 - 12 MPa
Temperature	270 - 330 K
Heating value	30 - 45 MJ/m3
Relative density	0.55 - 0.90
Mole fraction composition	
N_2	0 - 0.2
CO_2	0 - 0.2
CO	0 - 0.03
H_2	0 - 0.10
C_1	0.7 - 1.0

The general method works for natural gas mixtures basically composed of aliphatic hydrocarbons (C_1 – C_{10}) and some major diluents or impurities (N_2, CO_2, H_2, CO). The model estimates the second and third virial coefficients of the mixture using empirical correlations with the heating value and the compositions (mole fractions) of the diluting substances. The hydrocarbon compositions should follow a common, empirical rule: the mole fraction of C_2 should be around 1/3 that of C_1, C_3 1/3 of C_2, and so on. This rule guaranties average hydrocarbon chain lengths between 1.0 and 1.2 can apply in table 2.1 and equation (2.1) is valid.

In order to match the master GERG-2008 EoS, the fitting methodology used here uses *Z*-predictions from GERG-2008 as input data. First, the mixture composition is fed into a calculation routine, based upon the GERG-2008 EoS, that retrieves density (ρ) and *Z* data at *T, P* conditions within the working ranges of the model, (270 – 330) K in temperature, up to 12 MPa in pressure, 0.6 – 0.9 relative densities, and 1.0 – 1.2 average chain lengths. Within those limits the original experimental data used to develop the GERG-2008 model claims total uncertainties lower than 0.05 %. With these *raw data* for

each mixture, the program calculates the equivalent hydrocarbon composition and its corresponding heating value (H_{CH}) converting the complex multicomponent natural gas mixture into a simpler 5-component mixture (equivalent hydrocarbon (1), nitrogen (2), carbon dioxide (3), hydrogen (4) and carbon monoxide (5)). When applying the SGERG model in real operations, the heating value of the equivalent hydrocarbon (H_{CH}) is used internally to calculate the molar mass of the equivalent hydrocarbon mixture M_{CH} using the empirical correlation:

$$M_{CH} = g_1 + g_2 H_{CH} \tag{2.1}$$

where g_1 and g_2 are -2.709328 and 0.021062199 respectively.

During the model fitting procedure, equation (2.1) provides the heating value from the molar mass of the equivalent hydrocarbon, which can be calculated from the compositions and the individual molar masses, M_i, of the diluents in the mixture and the relative density.

$$x_{CH} M_{CH} = (M_S - x_2 M_2 - x_3 M_3 - x_4 M_4 - x_5 M_5) \tag{2.2}$$

$$x_{CH} = x_1 = 1 - x_2 - x_3 - x_4 - x_5 \tag{2.3}$$

These molar masses of the main diluents as well as the value of the gas constant R are updated in this revision. Table 2.2 contains the old and new values of these quantities.

M_S in equation (2.2) is the molar mass of the sample. It is calculated using the mass density of air at normal conditions and the relative density, γ, of the sample in the definition of the compressibility factor.

$$M_S = \frac{\gamma Z_0 RT}{P \rho_{0,air}} \tag{2.4}$$

Table 2.2. New values of constants used in the gross method.

Constant	Old value		Updated value	
$M_2 = M_{N2}$	28.0135	kg/kmol	28.0134	kg/kmol
$M_3 = M_{CO2}$	44.010	kg/kmol	44.0095	kg/kmol
$M_4 = M_{H2}$	2.0159	kg/kmol	2.01588	kg/kmol
$M_5 = M_{CO}$	28.010	kg/kmol	28.0101	kg/kmol
R	8.31451	bar·m3/kmol·K	8.314472	bar·m3/kmol·K

Then, the SGERG model estimates the second and third virial coefficients of the 5-component mixture:

$$B_{mix}(T) = x_1^2 B_{11} + 2x_1 x_2 B_{12} + 2x_1 x_3 B_{13} + 2x_1 x_4 B_{14} + 2x_1 x_5 B_{15} + x_2^2 B_{22} + 2x_2 x_3 B_{23} + 2x_2 x_4 B_{24} + x_3^2 B_{33} + x_4^2 B_{44} + x_5^2 B_{55} \quad (2.5)$$

$$C_{mix}(T) = x_1^3 C_{111} + 3x_1^2 x_2 C_{112} + 3x_1^2 x_3 C_{113} + 3x_1^2 x_4 C_{114} + 3x_1^2 x_5 C_{115} + 3x_1 x_2^2 C_{122} + 6x_1 x_2 x_3 C_{123} + 3x_1 x_3^2 C_{133} + x_2^3 C_{222} + 3x_2^2 x_3 C_{223} + 3x_2 x_3^2 C_{233} + x_3^3 C_{333} + x_4^3 C_{444} \quad (2.6)$$

Pure-component and simpler-mixture second and third virial coefficients appear in equations (2.1) and (2.2). In general, those intermediate values are expressed as second degree polynomials in temperature, with the exception of those involving the equivalent hydrocarbon.

$$B_{ij} = \sum_{n=0}^{2} b_{ij}(n) T^n \quad (2.7)$$

B_{11}, the virial coefficient of the equivalent hydrocarbon, is also correlated to the heating value using a quadratic polynomial.

$$B_{11} = b_H(0) + b_H(1) H_{CH} + b_H(2) H_{CH}^2 \quad (2.8)$$

And the coefficients $b_H(m)$ are each, in turn, quadratic polynomials in temperature.

$$b_H(m) = \sum_{n=0}^{2} b_H(m,n)T^n \tag{2.9}$$

B_{12} is the arithmetic mean of B_{11} and B_{22} multiplied by an empirical second polynomial in temperature. The coefficients of this polynomial are released and fit in the new version of the model.

$$B_{12} = (b_{12}(0) + b_{12}(1)T + b_{12}(2)T^2) \cdot \left[\frac{B_{11} + B_{22}}{2}\right] \tag{2.10}$$

B_{13} is the geometric mean of B_{11} and B_{33}. Only one additional binary interaction parameter is fit in that calculation.

$$B_{13} = b_{13}\sqrt{B_{11}B_{33}} \tag{2.11}$$

B_{24} is held constant.

Likewise, the third virial coefficient of the equivalent hydrocarbon C_{111} is correlated as a quadratic polynomial to the heating value, and the intermediate third virial coefficients are expressed as quadratic polynomials in temperature:

$$C_{111} = c_H(0) + c_H(1)H_{CH} + c_H(2)H_{CH}^2 \tag{2.12}$$

$$c_H(m) = \sum_{n=0}^{2} c_H(m,n)T^n \tag{2.13}$$

$$C_{ijk} = \sum_{n=0}^{2} c_{ijk}(n)T^n \tag{2.14}$$

Equation (2.14) applies for the pure ones (i=j=k), and for C_{115}, C_{223} and C_{233}. The rest of them, which involve the equivalent hydrocarbon (C_{112}, C_{122}, C_{113}, C_{133}, C_{114},

and C_{123}) are calculated as the geometric mean of the pure ones multiplied by a ternary interaction parameter linearly dependent of temperature.

$$C_{ijk} = \left(c_{ijk}(0) + c_{ijk}(1)T\right)\sqrt[3]{C_{iii}C_{jjj}C_{kkk}} \tag{2.15}$$

With B_{mix} and C_{mix} the SGERG model calculates the compressibility factor Z of each sample at each pair of conditions *(T, P)*. Those Z values are compared to values calculated from the master GERG-2008 equation of state. The model builder uses non-linear algorithms coded at NIST to sequentially and randomly vary all coefficients involved in the model to minimize the sum of squares of the differences between both calculated values (SGERG – GERG-08).

2.2. Results

The fitting program outputs a new set of coefficients that appear compared with the original set in tables 2.3 and 2.4. Table 2.3 contains the coefficients involved in the calculation of B_{mix} and table 2.4 the ones involved in the calculation of C_{mix}.

Table 2.3. Coefficients for the calculation of B_{mix} in the SGERG model.

Coefficient	**SGERG-88**	**SGERG-10**
$b_H(0,0)$	-0.425468	-0.302240
$b_H(0,1)$	0.877118×10^{-3}	0.767948×10^{-3}
$b_H(0,2)$	-0.824747×10^{-6}	-0.823864×10^{-6}
$b_H(1,0)$	0.286500×10^{-2}	0.252605×10^{-2}
$b_H(1,1)$	-0.556281×10^{-5}	-0.530365×10^{-5}
$b_H(1,2)$	0.431436×10^{-8}	0.425120×10^{-8}
$b_H(2,0)$	-0.462073×10^{-5}	-0.519082×10^{-5}
$b_H(2,1)$	0.881510×10^{-8}	0.104068×10^{-7}
$b_H(2,2)$	$-0.608319 \times 10^{-11}$	$-0.683855 \times 10^{-11}$
$b_{22}(0)$	-0.144600	-0.642573×10^{-1}
$b_{22}(1)$	0.740910×10^{-3}	-0.641890×10^{-4}
$b_{22}(2)$	-0.911950×10^{-6}	0.763542×10^{-6}
$b_{33}(0)$	-0.868340	-1.910016
$b_{33}(1)$	0.403760×10^{-2}	0.109716×10^{-1}
$b_{33}(2)$	-0.516570×10^{-5}	-0.168165×10^{-4}
$b_{44}(0)$	-0.110596×10^{-2}	-0.110596×10^{-2}
$b_{44}(1)$	0.813385×10^{-4}	0.813385×10^{-4}
$b_{44}(2)$	-0.987220×10^{-7}	-0.987220×10^{-7}
$b_{55}(0)$	-0.130820	-0.130820
$b_{55}(1)$	0.602540×10^{-3}	0.602540×10^{-3}
$b_{55}(2)$	-0.644300×10^{-6}	-0.644300×10^{-6}
$b_{12}(0)$	2.640000	6.827586
$b_{12}(1)$	-0.120000×10^{-1}	-0.419421×10^{-1}
$b_{12}(2)$	0.187500×10^{-4}	0.705347×10^{-4}
b_{13}	-0.865000	-0.815773
$b_{14}(0)$	-0.521280×10^{-1}	-0.521280×10^{-1}
$b_{14}(1)$	0.271570×10^{-3}	0.271570×10^{-3}
$b_{14}(2)$	-0.250000×10^{-6}	-0.250000×10^{-6}
$b_{15}(0)$	-0.687290×10^{-1}	-0.687290×10^{-1}
$b_{15}(1)$	-0.239381×10^{-5}	-0.239381×10^{-5}
$b_{15}(2)$	0.518195×10^{-6}	0.518195×10^{-6}
$b_{23}(0)$	-0.339693	2.373498
$b_{23}(1)$	0.161176×10^{-2}	-0.169762×10^{-1}
$b_{23}(2)$	-0.204429×10^{-5}	0.297491×10^{-4}
b_{24}	0.120000×10^{-1}	0.120000×10^{-1}

Table 2.4. Coefficients for the calculation of C_{mix} in the SGERG model.

Coefficient	**SGERG-88**	**SGERG-10**
$c_H(0,0)$	-0.302488	-0.282888
$c_H(0,1)$	0.646422×10^{-3}	0.605700×10^{-3}
$c_H(0,2)$	-0.332805×10^{-6}	-0.316963×10^{-6}
$c_H(1,0)$	0.195861×10^{-2}	0.190798×10^{-2}
$c_H(1,1)$	-0.422876×10^{-5}	-0.414262×10^{-5}
$c_H(1,2)$	0.223160×10^{-8}	0.223263×10^{-8}
$c_H(2,0)$	-0.316302×10^{-5}	-0.314791×10^{-5}
$c_H(2,1)$	0.688157×10^{-8}	0.688768×10^{-8}
$c_H(2,2)$	$-0.367713 \times 10^{-11}$	$-0.375913 \times 10^{-11}$
$c_{222}(0)$	0.784980×10^{-2}	0.515240
$c_{222}(1)$	-0.398950×10^{-4}	-0.326914×10^{-2}
$c_{222}(2)$	0.611870×10^{-7}	0.574871×10^{-5}
$c_{333}(0)$	0.205130×10^{-2}	0.108865
$c_{333}(1)$	0.348880×10^{-4}	-0.682136×10^{-3}
$c_{333}(2)$	-0.837030×10^{-7}	0.109431×10^{-5}
$c_{223}(0)$	0.552066×10^{-2}	0.657071
$c_{223}(1)$	-0.168609×10^{-4}	-0.421258×10^{-2}
$c_{223}(2)$	0.157169×10^{-7}	0.818212×10^{-5}
$c_{233}(0)$	0.358783×10^{-2}	-5.860405
$c_{233}(1)$	0.806674×10^{-5}	0.382236×10^{-1}
$c_{233}(2)$	-0.325798×10^{-7}	-0.661664×10^{-4}
$c_{444}(0)$	0.104711×10^{-2}	0.104711×10^{-2}
$c_{444}(1)$	-0.364887×10^{-5}	-0.364887×10^{-5}
$c_{444}(2)$	0.467095×10^{-8}	0.467095×10^{-8}
$c_{115}(0)$	0.736748×10^{-2}	0.736748×10^{-2}
$c_{115}(1)$	-0.276578×10^{-4}	-0.276578×10^{-4}
$c_{115}(2)$	0.343051×10^{-7}	0.343051×10^{-7}
$c_{112}(0)$	0.920000	0.299859
$c_{112}(1)$	0.130000×10^{-2}	-0.186313×10^{-3}
$c_{122}(0)$	0.920000	-0.139366
$c_{122}(1)$	0.130000×10^{-2}	-0.137934×10^{-2}
$c_{113}(0)$	0.920000	0.893855
$c_{113}(1)$	0.000000	0.693277×10^{-3}
$c_{133}(0)$	0.920000	3.747595
$c_{133}(1)$	0.000000	0.429716×10^{-1}
$c_{114}(0)$	1.200000	1.200000
$c_{123}(0)$	1.100000	1.372576
$c_{123}(1)$	0.000000	0.256380×10^{-2}

Figures 2.1 and 2.2 are side-by-side plots that compare the performance of the new SGERG-10 model against the old SGERG-88 and the current standard GERG-2008.

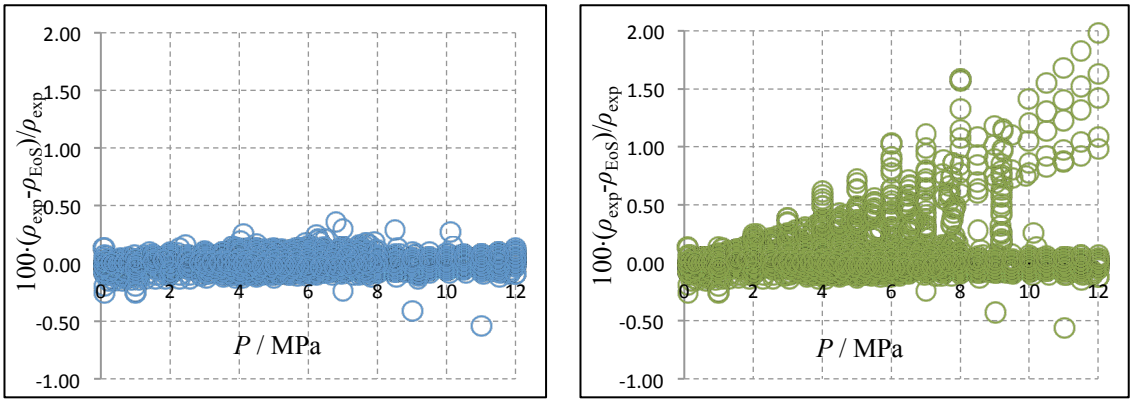

Figure 2.1. Percent deviations of GERG data base of experimental data up to 12 MPa from models SGERG-10 (left, blue) and SGERG-88 (right, green).

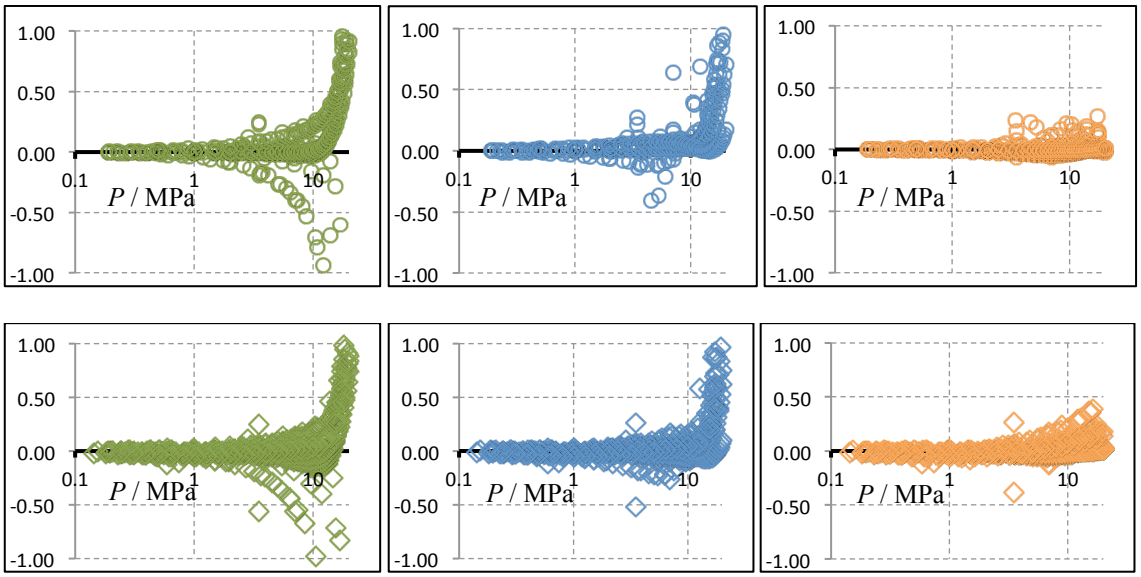

Figure 2.2. Percent deviations of Round Robin samples data from models SGERG-88 (green symbols), SGERG-10 (blue), and GERG-2008 (orange). ○ NIST1, ◇ NIST2, □ GU1, △ GU2, and × RG2. The abscisa is logarithmic pressure.

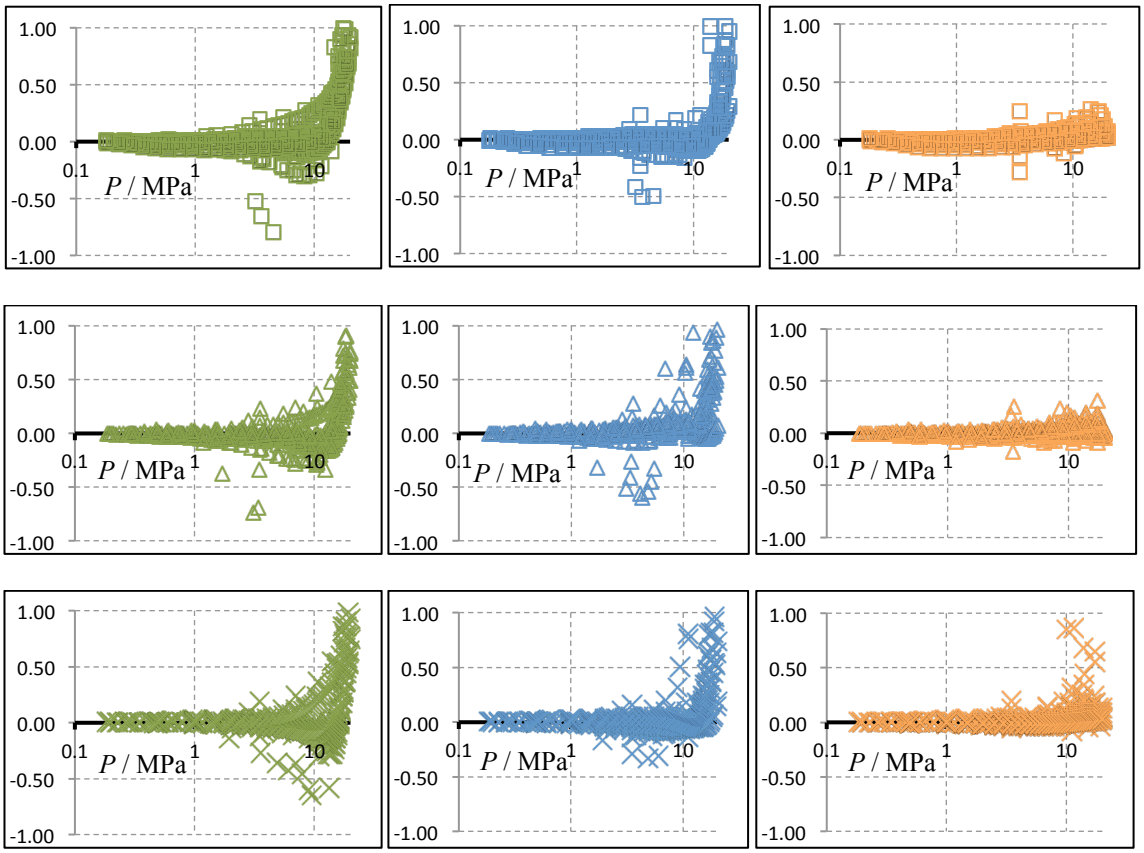

Figure 2.2. Continued.

3. DENSITY MEASUREMENTS

3.1. The Magnetic Suspension Densimeter

The Thermodynamics Research Group in the Chemical Engineering Department at Texas A&M University has a high-pressure, single-sinker magnetic suspension densimeter (MSD). This device uses Achimedes principle to determine the density of sample fluids over a wide range of temperatures and pressures, by measuring the buoyancy force experienced by a piece of metal (sinker) of well-known mass and volume submerged into a sample fluid. In order to perform measurements on gaseous fluids at high-pressures (up to 200 MPa), the MSD uses a magnetic suspension system to couple the sinker inside the cell to an analytical balance outside. The system comprises a high-pressure Be-Cu cell with a suspension coupling connected to an analytical balance, an independent compression system, and ancillary equipment for pressure and temperature control and monitoring.

A PRT (model S1059PA5X6 platinum resistance thermometer from Minco Products), installed at the bottom of the cell, with fixed temperature points defined by ITS-90 and calibrated by a PRT traceable to the National Institute of Standards and Technology (NIST) measures the temperature of the cell with an uncertainty of 2.5 mK and a stability of 5 mK. A thermopile measures and controls the difference between top and bottom of the cell. The pressure measurement instruments are two Digiquartz transducers ((40 and 200) MPa, (6000 and 30000) psia) from Paroscientific, Inc. with

uncertainties of 0.01 % of full scale ((0.6 and 3.0) psia respectively). Table 3.1 summarizes the ranges and accuracies of these devices.

Table 3.1. Measuring range and accuracy of MSD system devices.

Device	**Range**	**Accuracy**
Balance	0 - 200 g	± 0.003 % (r)
6k *P* Transducer	0 - 6000 psia	± 0.01 % (fs)
30k *P* Transducer	0 - 30000 psia	± 0.01 % (fs)
PRT	-80 - 250 °C	± 3 mK (r)

Two radiation shields enclose the cell. Those have heat exchange tubing coils and resistors for temperature control. The bath contains one vacuum isolation shield.

The core of the MSD technique lies in the suspension coupling. Inside the cell resides a hollowed cylinder (sinker) made of titanium, calibrated for mass (ms = 30.39159 g) and volume (6.741043 cm^3) by state-of-the-art techniques traceable to NIST.[58]

Also inside the cell, a lifting shaft with a permanent magnet head rises by virtue of its interaction with an electromagnet outside the cell that hangs from the balance. The electromagnet is energized externally using a control box to two different positions: zero point (ZP, w_1) and measurement point (MP, w_2). At ZP, the electromagnet raises the lifting shaft while the sinker rests over the walls of the cell. At MP, the electromagnet raises both the lifting shaft and the sinker. The difference between those two readings $(w_2 - w_1)$ indicates the apparent mass of the sinker. The difference between the apparent mass of the sinker in vacuum and when submerged in a fluid indicates the buoyancy force experienced by the sinker, which is proportional to the density of the fluid by

Archimedes principle. Figure 3.1 shows a schematic diagram of the magnetic suspension coupling.

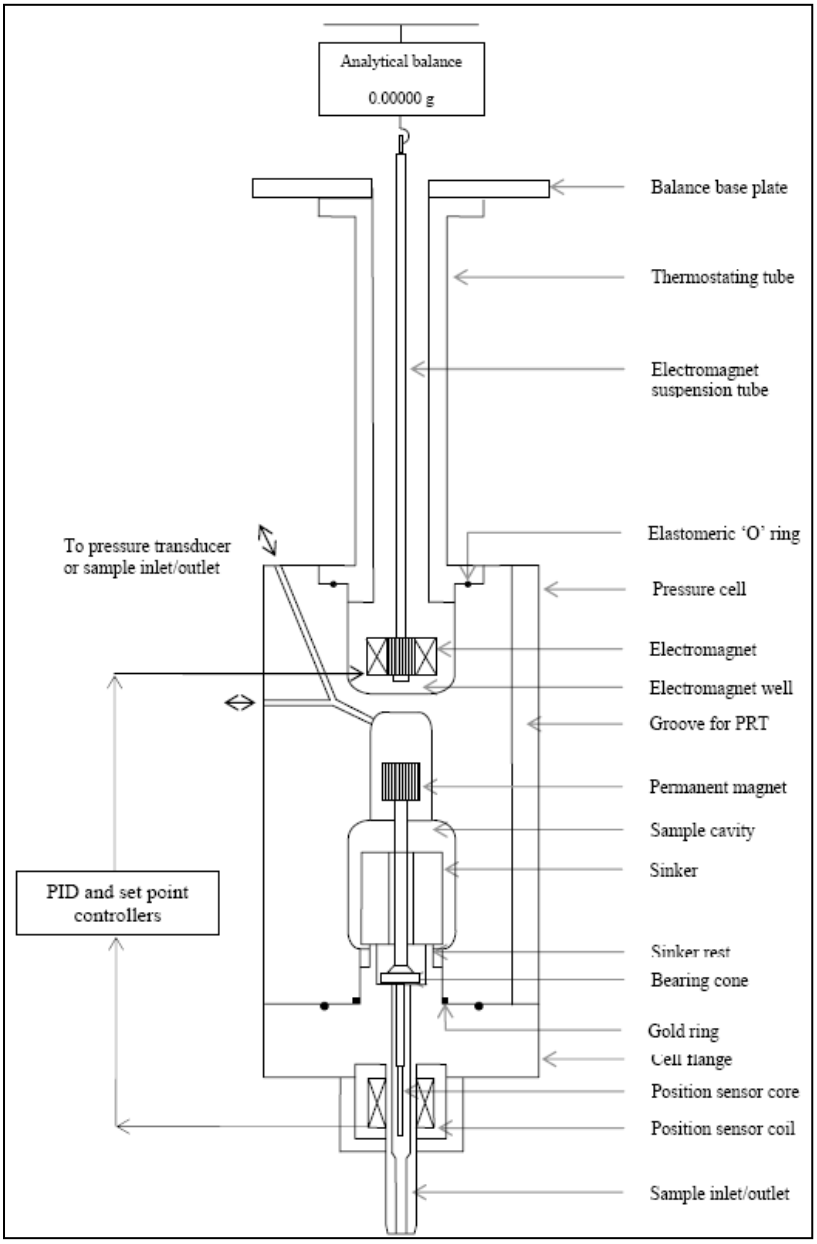

Figure 3.1. Schematics of the magnetic suspension coupling.

3.2. Force Transmission Error

The MSD technique works by turning a magnetic force (between the permanent magnet and the electromagnet) into a gravitational force measured by the balance (from the hanging electromagnet). This force transmission is not completely accurate because the cell wall and the fluid effect the magnetic interaction. This error is inherent to the technique and must be quantified.

Equations (3.1) and (3.2) are the force balances that define the two balance readings (ZP and MP1) involved in a typical measurement process.

$$w_1 = \alpha\left\{\phi\left[m_{\mathrm{pm}} - \rho_{\mathrm{f}} V_{\mathrm{pm}}\right] + m_{\mathrm{em}} + m_{\mathrm{c1}} - \rho_{\mathrm{a}}\left(V_{\mathrm{em}} + V_{\mathrm{c1}}\right) + w_{\mathrm{zero}}\right\} \tag{3.1}$$

$$w_2 = \alpha\left\{\phi\left[m_{\mathrm{s}} + m_{\mathrm{pm}} - \rho_{\mathrm{f}}\left(V_{\mathrm{s}} + V_{\mathrm{pm}}\right)\right] + m_{\mathrm{em}} + m_{\mathrm{c2}} - \rho_{\mathrm{a}}\left(V_{\mathrm{em}} + V_{\mathrm{c2}}\right) + w_{\mathrm{zero}}\right\} \tag{3.2}$$

in which α is the balance atmosphere factor, Φ is the coupling factor that represents the force transmission error (FTE), ρ_{f} is the fluid density, ρ_{a} is the density of the purge gas in the balance chamber (commonly air or dry nitrogen), V is the physical volume of the corresponding metal piece, m is mass, w is the balance reading, and w_{zero} is the balance reading with nothing on the balance pan or weighing hook (tare value), the subscripts denote: 1 the first balance position (ZP), pm the permanent magnet including the lifting shaft, em the electromagnet including the linking hook to the balance, s the sinker, c1 compensation weight 1 (tare mass), and c2 compensation weight 2 (calibration mass).

$$\alpha = \frac{(w_2 - w_1)}{(m_{c2} - m_{c1}) - \rho_a(V_{c2} - V_{c1})} \approx \frac{1}{1 - \frac{\rho_a}{\rho_{c2}}} \tag{3.3}$$

Subtracting w_1 from w_2 provides the corrected weight reading reported in the output files.

$$w_2 - w_1 = \alpha\left\{\phi\left[m_s - \rho_f V_s\right] + m_{c2} - m_{c1} - \rho_a\left(V_{c1} - V_{c2}\right)\right\} \tag{3.4}$$

Because $V_{c1} \approx V_{c2}$, the buoyancy terms from the external masses cancel.

$$w_2 - w_1 = \alpha\left\{\phi\left[m_s - \rho_f V_s\right] + \left(m_{c2} - m_{c1}\right)\right\} \tag{3.5}$$

The coupling factor, Φ, represents the correction to the force balance in the MSD caused by the Force Transmission Error. If we make a measurement of vacuum in the cell, $\rho_f = 0$ and the balance reading becomes

$$\left(w_2 - w_1\right)_0 = \alpha\left\{\phi_0 m_s + \left(m_{c2} - m_{c1}\right)\right\} \tag{3.6}$$

Here, Φ_0 accounts for the apparatus effect of the force transmission error, and can be determined by performing vacuum measurements (and solving for Φ_0 in equation 3.6). Combining equations (3.5) and (3.6),

$$\rho_f = \rho_s\left(1 - \frac{\phi_0}{\phi}\right) + \frac{\left(w_2 - w_1\right)_0 - \left(w_2 - w_1\right)_f}{\phi\alpha V_s} \tag{3.7}$$

Using the equivalence in (3.6) and rearranging,

$$\rho_f = \rho_s + \frac{\left(m_{c2} - m_{c1}\right) - \left(w_2 - w_1\right)_f / \alpha}{\phi V_s} \tag{3.8}$$

Equation (3.8) is the measuring equation for calculating and reporting fluid densities from the MSD. Equations (3.7) and (3.8) are equivalent.

McLinden et al.[59] suggest a technique to determine the coupling factor, Φ, and Cristancho et al.[60] have adapted the technique to our specific instrument. The result of the FTE analysis for a single-sinker MSD is:

$$\phi = \frac{\left(m_{c2} - m_{c1}\right)\left(\frac{1}{V_{s2}} - \frac{1}{V_{s1}}\right) - \frac{1}{\alpha}\left[\frac{\left(w_2 - w_1\right)_f^{s2}}{V_{s2}} - \frac{\left(w_2 - w_1\right)_f^{s1}}{V_{s1}}\right]}{\left[\rho_{\phi=\phi_0}^{s2} - \rho_{\phi=\phi_0}^{s1}\right] - \left[\rho_{s2} - \rho_{s1}\right]} \tag{3.9}$$

in which s1 and s2 denote two separate sinkers that have different densities.

3.2.1. Experimental Procedure

To perform the FTE analysis, and thus quantify the coupling factor Φ, requires a particular set of measurements to obtain density data and to perform a sufficient statistical analysis. Two different sinkers appear in equation (3.9). The second sinker should have essentially the same mass as s1 in order for the suspension coupling control to work properly with the same settings. Titanium is the material of the first sinker, and the second sinker is copper.

In order to perform a thorough analysis, we measured densities of four pure fluids (nitrogen, carbon dioxide, methane and ethane) over a wide range of temperatures. Essentially, we repeated the same measurements, at the same conditions, with both sinkers. The results showed that the apparatus component of the force transmission error ($\Phi = \Phi_0$; $(\Phi - 1)$ = 189 ppm ± 16 ppm) masks the fluid component in our apparatus.

3.3. Pure Substance Measurements

3.3.1. New $P\rho T$ Data for Nitrogen

This section contains new, accurate $P\rho T$ data for pure nitrogen collected isothermally at (265, 293, 298.15, 350 and 400) K, with the MSD system described in the previous sections. The nitrogen came from Scott Specialty Gases with a purity of 99.9995% mol.

Table 3.2. New $P\rho T$ data for pure nitrogen.

P / MPa	ρ (Exp) kg/m^3	ρ (EoS) kg/m^3	$100\cdot(\rho_{exp} - \rho_{EoS})/\rho_{exp}$
	T = 265.00 K		
0.967	12.355	12.357	-0.010
1.937	24.865	24.865	-0.002
3.929	50.840	50.841	-0.002
5.996	77.972	77.976	-0.004
7.985	104.063	104.061	0.002
9.835	128.039	128.053	-0.011
15.014	192.346	192.331	0.008
20.022	248.359	248.340	0.008
25.019	297.183	297.138	0.015
30.006	339.165	339.133	0.009
35.119	376.198	376.188	0.003
50.041	459.104	459.125	-0.005
74.887	549.760	549.772	-0.002
100.559	613.291	613.244	0.008
	T = 293.00 K		
0.965	11.119	11.115	0.037
1.933	22.306	22.310	-0.018
3.923	45.361	45.371	-0.024
5.988	69.244	69.255	-0.017
7.971	91.982	92.001	-0.020

Table 3.2. Continued

P / MPa	ρ (Exp) kg/m^3	ρ (EoS) kg/m^3	$100\cdot(\rho_{exp} - \rho_{EoS})/\rho_{exp}$
9.822	112.910	112.918	-0.007
14.872	167.663	167.699	-0.022
19.976	218.428	218.453	-0.012
24.948	262.722	262.742	-0.008
29.965	302.337	302.352	-0.005
34.993	337.389	337.399	-0.003
39.916	367.801	367.814	-0.004
50.130	421.000	421.008	-0.002
74.957	513.932	513.952	-0.004
99.903	578.472	578.495	-0.004
125.585	628.863	628.813	0.008
150.976	668.880	668.795	0.013
	T = 298.15 K		
10.005	112.564	112.602	-0.034
30.026	296.940	296.997	-0.019
49.844	413.221	413.252	-0.007
74.988	507.852	507.886	-0.007
100.175	573.318	573.325	-0.001
124.825	622.069	622.052	0.003
151.239	664.101	664.037	0.010
	T = 350.00 K		
2.974	28.486	28.490	-0.014
4.917	46.878	46.888	-0.020
5.971	56.772	56.770	0.003
7.481	70.762	70.787	-0.035
9.976	93.531	93.525	0.007
13.786	127.029	127.042	-0.010
17.230	155.891	155.899	-0.006
20.677	183.287	183.290	-0.002
24.132	209.197	209.197	0.000
27.582	233.510	233.524	-0.006
29.848	248.687	248.686	0.000
34.691	279.018	279.022	-0.002
49.978	358.872	358.864	0.002
74.999	452.980	452.998	-0.004
99.994	520.331	520.368	-0.007
124.395	571.157	571.212	-0.010

Table 3.2. Continued

P / MPa	ρ (Exp) kg/m^3	ρ (EoS) kg/m^3	$100\cdot(\rho_{exp} - \rho_{EoS})/\rho_{exp}$
150.364	614.997	615.056	-0.010
	T = 400.00 K		
1.004	8.432	8.433	-0.005
1.999	16.747	16.739	0.048
2.999	25.040	25.031	0.036
4.000	33.281	33.272	0.028
5.001	41.463	41.448	0.037
7.000	57.573	57.567	0.010
8.004	65.564	65.551	0.019
10.000	81.202	81.186	0.021
14.997	118.841	118.820	0.018
19.991	154.143	154.112	0.020
24.998	187.116	187.081	0.018
29.991	217.621	217.580	0.019
35.015	246.029	245.981	0.019
40.004	272.126	272.072	0.020
49.964	318.659	318.571	0.028
59.948	358.969	358.864	0.029
69.931	394.143	394.046	0.025
79.958	425.322	425.232	0.021
89.963	453.061	452.976	0.019
99.951	477.982	477.911	0.015
110.031	500.804	500.751	0.011
120.573	522.585	522.543	0.008

The coupling factor (Φ was 193, 197, 207, 201 and 202 ppm for (265, 293, 298.15, 350 and 400) K, respectively. The reproducibility of these values was always better than ±2 ppm.

The estimated experimental uncertainty is less than 3×10^{-4} kg/m^3 in density for pressures greater than 7 MPa and up to 5×10^{-4} kg/m^3 for pressures between 5 MPa and 7MPa. The data validate the performance of the equation of state developed by Span et

al. (2000) up to 150 MPa with better predictive capabilities than claimed for the EoS. Figure 3.2 depicts the deviations from table 3.2 along with other sets of data used in the development of the reference equation of state.

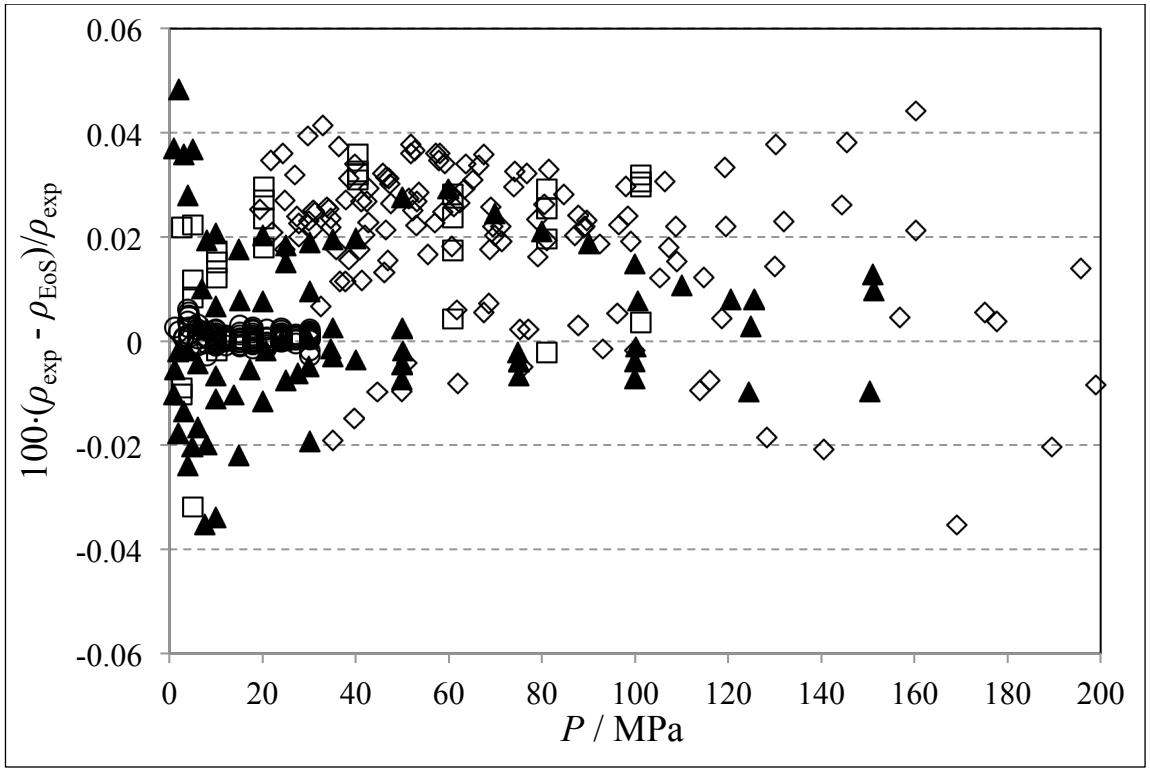

Figure 3.2. Percent deviation of experimental data using Span et al. as the reference. ▲This work[61]; ○ Klimeck [62] ◇ Michels [63] □ Wiebe [64].

Extrapolation of the linear behavior of the $(Z\text{-}1)/\rho$ to zero pressure determines the second and third virial coefficients with uncertainties of 0.28 cm^3/mol and 200 $(cm^3/mol)^2$ respectively. These values appear in table 3.3.

Table 3.3. Second and third virial coefficients for nitrogen.

T / K	B / cm^3/mol	C / (cm^3/mol)^2
265.00	-12.24	1538
293.00	-5.76	1435
350.00	3.48	1364
400.00	8.71	1442

Figures 3.3 and 3.4 present the absolute deviation of second and third virial coefficients presented in table 3.3 along with other sets of data from the literature.

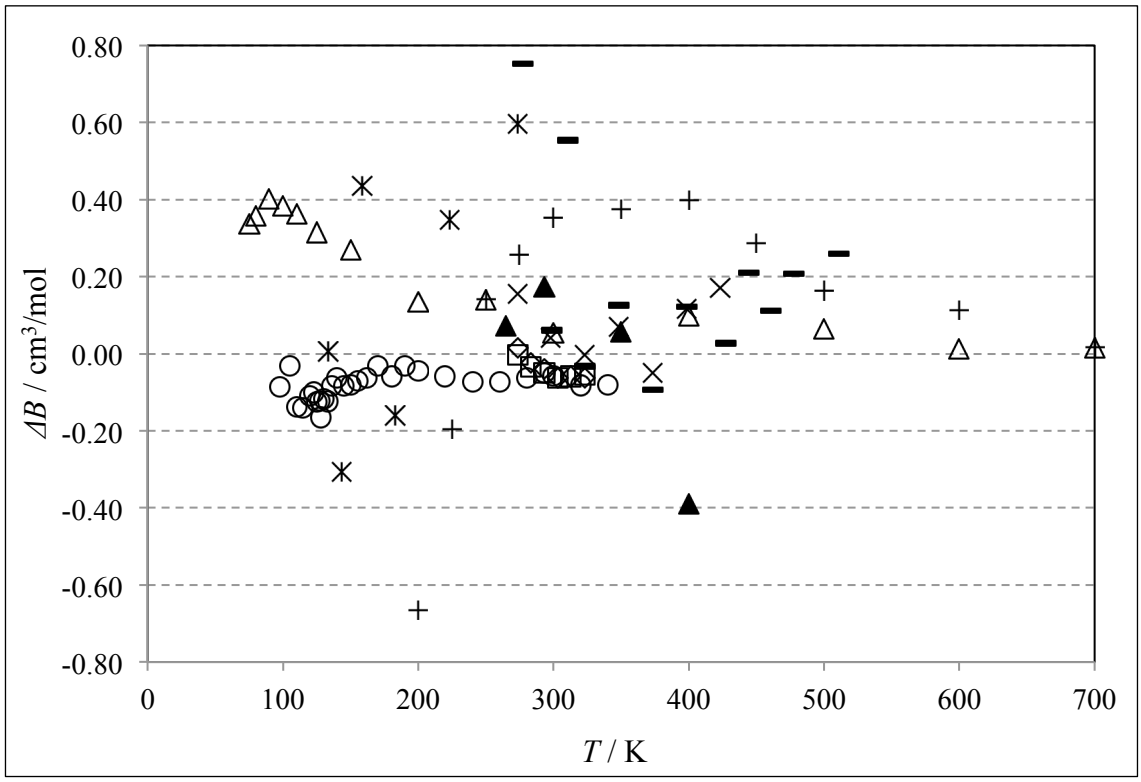

Figure 3.3. Absolute deviations of second virial coefficients using Span et al.[1] as the reference. $\Delta B=(B_{exp}-B_{calc})$. ▲ This work[61]; ○ Nowak [65]; ◇ Duschek [66]; □ Pieperbeck [67]; △ Ewing[68]; - Huff [69]; × Otto [70]; ∗ Canfield [71]; + Pocock [72].

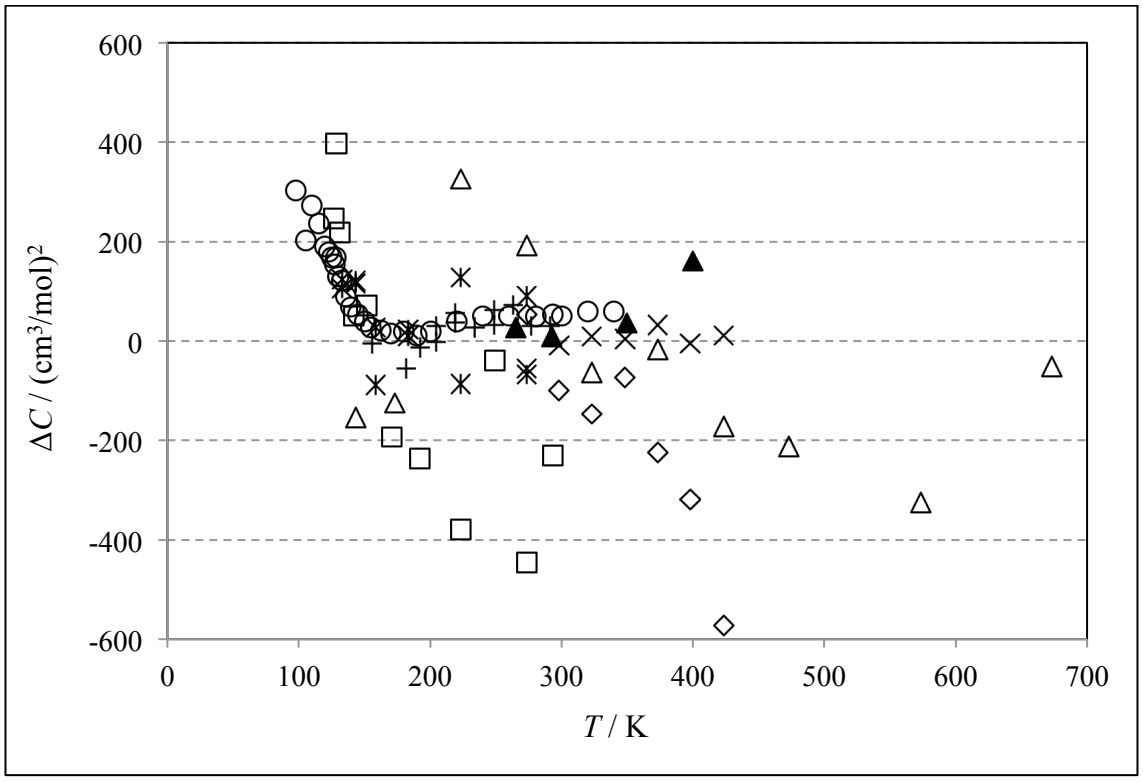

Figure 3.4. Absolute deviations of third virial coefficients using Span et al. as the reference. $\Delta C=(C_{exp}-C_{calc})$. ▲ This work [61]; ○ Nowak [65]; △ Holborn [73]; □ Kamerlingh [74]; ◇ Michels [63]; × Otto [70]; ∗ Canfield [71]; + Roe [75].

3.3.2. New *PρT* Data for Carbon Dioxide

The new *PρT* data for pure carbon dioxide uses sample provided by Matheson Tri-Gas with a purity of 99.999 mol%. The same high-pressure MSD system described in section 3.1 measured the mass densities isothermally at (310, 350, 400, 450) K up to 160 MPa. The coupling factor *(Φ -1)* for the FTE correction of these particular data sets was (195, 189, 204, and 194) ppm at (310, 350, 400, 450) K, respectively. The reproducibility of these values was better than ±2 ppm.

Table 3.4. New $P\rho T$ data for carbon dioxide.

P / MPa	ρ (Exp) kg/m^3	ρ (EoS) kg/m^3	$100\cdot(\rho_{exp} - \rho_{EoS})/\rho_{exp}$
	T = 310.000 K		
1.998	37.614	37.603	0.029
5.002	116.171	116.197	-0.022
10.014	686.160	686.431	-0.039
19.987	856.152	856.161	-0.001
29.966	921.817	921.860	-0.005
49.929	999.875	1000.131	-0.026
75.042	1062.566	1063.061	-0.047
100.055	1108.290	1108.777	-0.044
125.012	1144.813	1145.222	-0.036
139.289	1162.991	1163.314	-0.028
149.970	1175.569	1175.839	-0.023
159.844	1186.558	1186.760	-0.017
	T = 350.000 K		
2.011	32.349	32.353	-0.014
5.001	89.638	89.641	-0.003
9.986	228.244	228.298	-0.024
19.981	613.586	613.738	-0.025
30.013	758.897	759.108	-0.028
50.017	884.809	884.832	-0.003
74.904	969.636	969.722	-0.009
99.977	1027.564	1027.687	-0.012
124.895	1071.804	1071.896	-0.009
	T = 400.000 K		
0.999	13.455	13.464	-0.062
1.998	27.430	27.436	-0.022
4.998	72.779	72.772	0.010
10.021	161.960	161.938	0.014
14.986	267.104	267.101	0.001
20.028	381.082	381.115	-0.009
25.054	482.518	482.526	-0.002
29.994	561.435	561.412	0.004
35.005	623.368	623.290	0.012
39.985	672.037	671.953	0.012
49.967	745.445	745.244	0.027
59.920	799.163	798.946	0.027
69.997	842.031	841.747	0.034

Table 3.4. Continued

P / MPa	ρ (Exp) kg/m^3	ρ (EoS) kg/m^3	$100\cdot(\rho_{exp} - \rho_{EoS})/\rho_{exp}$
79.880	876.766	876.413	0.040
89.950	906.957	906.558	0.044
99.838	932.857	932.415	0.047
109.931	956.349	955.880	0.049
120.079	977.599	977.117	0.049
126.010	989.102	988.620	0.049
139.527	1013.251	1012.762	0.048
	T = 450.000 K		
4.998	62.269	62.269	0.000
9.998	131.635	131.605	0.023
19.983	284.802	284.880	-0.027
29.992	430.142	430.143	0.000
49.933	626.132	625.718	0.066
75.024	762.158	761.715	0.058
99.833	847.163	846.528	0.075
122.193	903.768	902.952	0.090

Table 3.4 contains the four isothermal data sets, each of which comprises several density measurement cycles (raw data) at each pair of conditions (*T, P*). The raw data were adjusted to nominal temperatures and pressures, and the mean density point was taken as the most likely value to report. The data compare well to values predicted by the Span and Wagner reference equation of state[10] as implemented in RefProp 9.0[76]. The last column in the table shows the percent difference between data and the equation.

Figure 3.5 is a log-linear plot[77] (linear scale delimited by the ±0.1 band and logarithmic scale beyond that) that shows the new data in comparison to other data sets used in the development of the reference equation of state. The data of Gokmenoglu[78] were not used in the fit process.

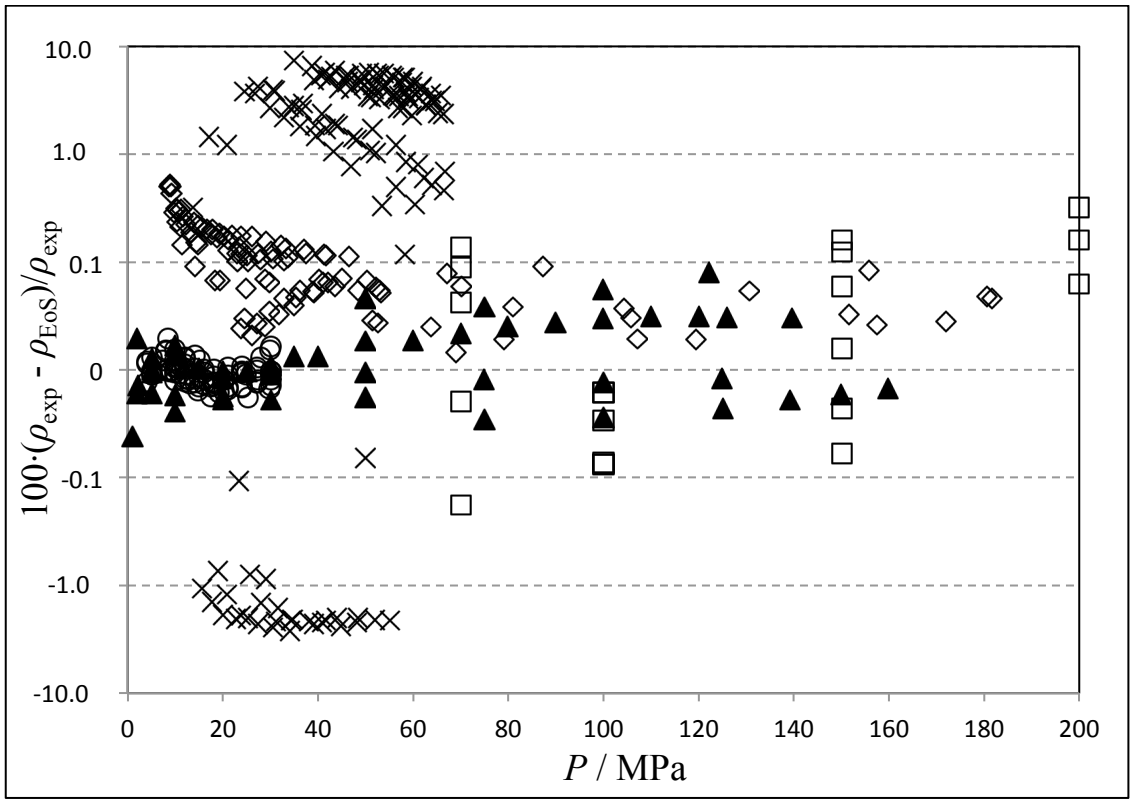

Figure 3.5. Percent deviation of experimental data compared to Span and Wagner equation of state. ▲ This work[79]; ○ Klimeck[80]; ◇ Michels [81]; □ Juza[82]; × Gokmenoglu [78].

Table 3.5 shows second (B) and third (C) virial coefficients obtained by extrapolating the linear behavior of the compressibility factor Z-1 at low pressures. Uncertainties of these values are estimated to be 2.5 cm^3/mol and 250 $(cm^3/mol)^2$ respectively. Figures 3.6 – 3.9 are comparative plots to other data and predictions from the EoS by Span and Wagner [10].

Table 3.5. Second and third virial coefficients for CO_2.

T / K	B / cm^3/mol	C / $(cm^3/mol)^2$
310.000	-111.85	4133
350.000	-83.70	3464
400.000	-59.70	2838
450.000	-43.10	2515

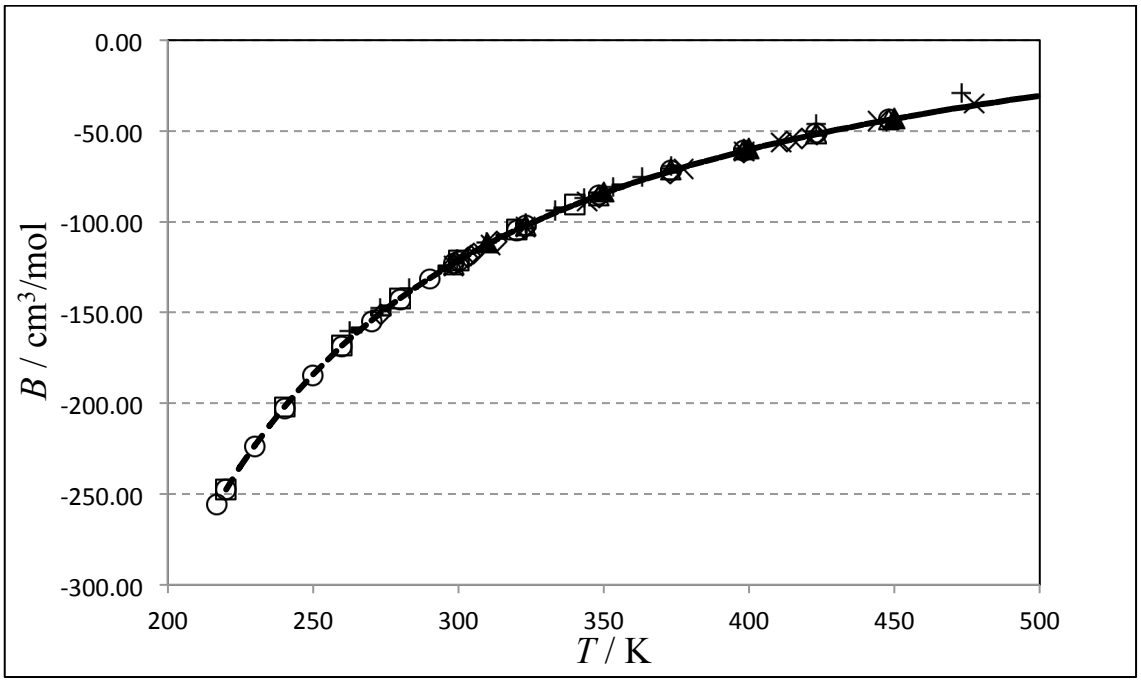

Figure 3.6. Second virial coefficients for CO_2. ▲ This work[79]; ○ Holste [83]; □ Duschek [84]; △ Patel [85]; + Butcher [86]; - Dadson [87]; × Huff [69]; ◇ Michels [88]; ⁎ Waxman [89]; --- EoS prediction.

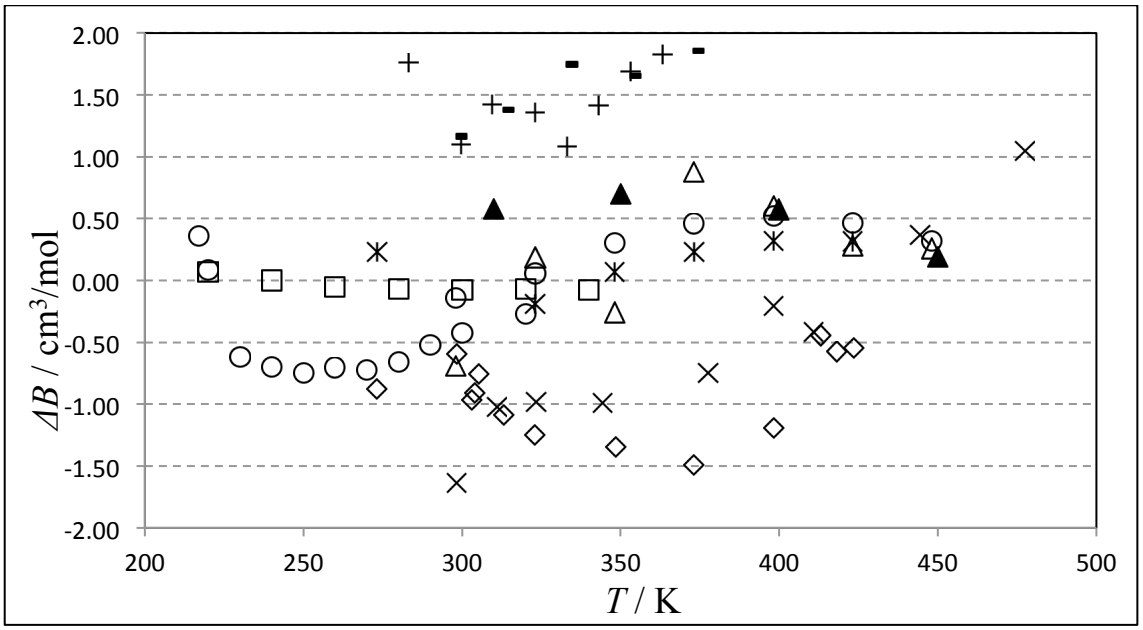

Figure 3.7. Absolute deviations of second virial coefficients from values predicted by the Span et al. equation of state $\Delta B=(B_{exp}-B_{calc})$. ▲ This work[79]; ○ Holste [83]; □ Duschek [84]; △ Patel [85]; + Butcher [86]; - Dadson [87]; × Huff [69]; ◇ Michels [88]; ⁎ Waxman [89].

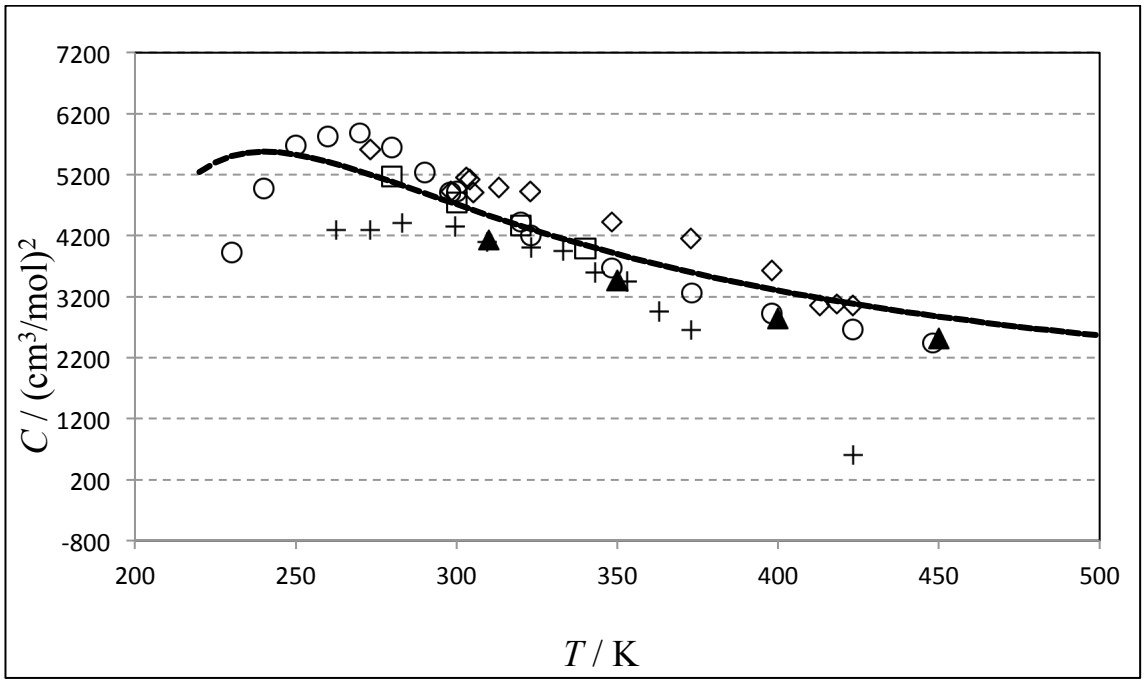

Figure 3.8. Third virial coefficients for CO_2. ▲ This work[79]; ○ Holste[83]; □ Duschek[84]; ◇ Michels[88]; + Butcher[86]; --- EoS prediction.

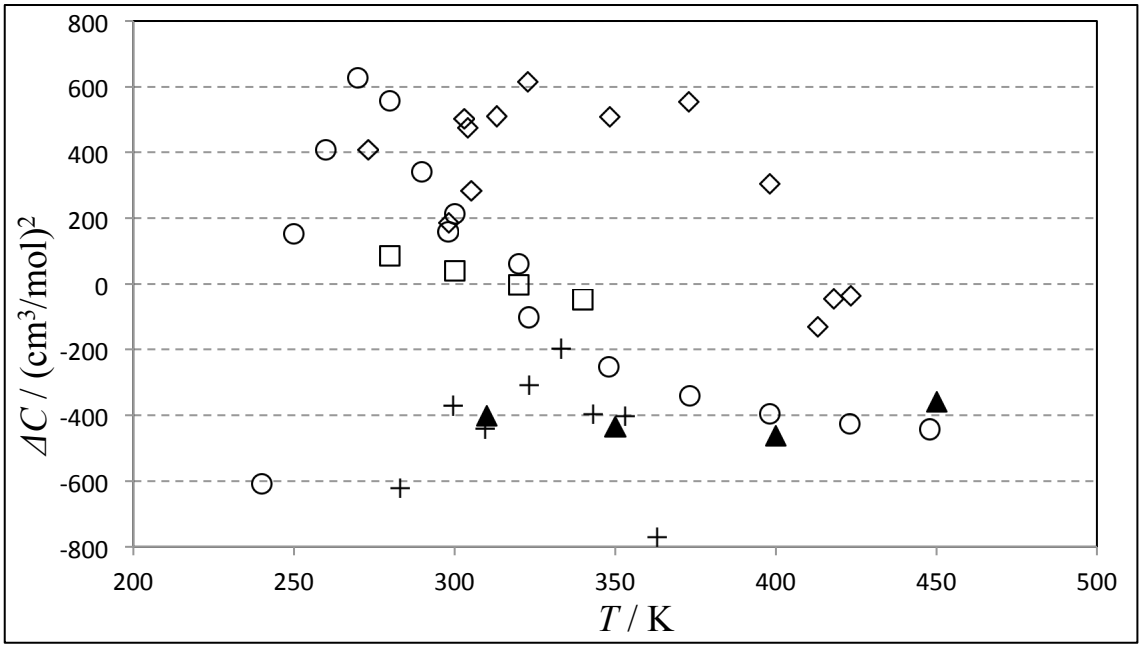

Figure 3.9. Absolute deviations of third virial coefficients from values predicted by the Span et al. equation of state $\Delta C=(C_{exp}-C_{calc})$. ▲ This work[79]; ○ Holste[83]; □ Duschek[84]; ◇ Michels[88]; + Butcher[86].

Experimental uncertainty of the density data is estimated to be better than 3×10^{-4} kg/m^3 for pressures greater than 7 MPa and up to 5×10^{-4} kg/m^3 for pressures between 5 MPa and 7MPa.

The Span and Wagner [10] EoS agrees well with the data up to 160 MPa. The uncertainties claimed for this reference EoS are ±0.03% to ±0.05% below 30 MPa and ±0.1% beyond that. However, in the high-pressure region the current uncertainties are lower than those of the data used to develop the EoS.

The new data reported here can improve the predictive capabilities of the reference EoS at high pressures.

3.4. Natural Gas Measurements: A Residual Gas Sample

Table 3.6 presents new density data for a synthetic residual gas sample with composition 95.014 % methane, 3.969 % ethane and 1.017 % propane, which resembles a typical pipeline gas, gathered with the MSD system described in 3.1. The data are organized by isotherms at (300, 325, 350, 375 and 400) K.

Table 3.6. New $P\rho T$ data for a synthetic residual gas sample.

***P* / MPa**	**ρ (Exp) kg/m3**	**ρ (GERG-08) kg/m^3**	**Deviation %**	**ρ (AGA-8) kg/m^3**	**Deviation %**
		T = 300.000 K			
4.999	37.306	37.286	0.054	37.289	0.046
7.503	58.646	58.618	0.048	58.622	0.041
10.002	81.394	81.354	0.049	81.357	0.045
12.505	104.869	104.811	0.055	104.815	0.051
14.999	127.822	127.773	0.038	127.775	0.037

Table 3.6. Continued

P / MPa	ρ (Exp) kg/m3	ρ (GERG-08) kg/m^3	Deviation %	ρ (AGA-8) kg/m^3	Deviation %
17.508	149.468	149.402	0.044	149.389	0.053
19.995	168.813	168.743	0.042	168.714	0.059
29.984	225.810	225.684	0.056	225.650	0.071
39.987	261.352	261.257	0.036	261.163	0.072
49.935	286.230	286.094	0.047	285.952	0.097
59.928	305.314	305.199	0.038	305.025	0.095
79.952	333.809	333.725	0.025	333.512	0.089
99.947	354.975	354.892	0.023	354.666	0.087
119.913	371.914	371.817	0.026	371.594	0.086
139.983	386.188	386.067	0.031	385.855	0.086
149.800	392.430	392.290	0.035	392.085	0.088
159.850	398.411	398.250	0.040	398.051	0.090
179.730	409.211	409.017	0.047	408.827	0.094
199.494	418.862	418.625	0.056	418.439	0.101
		T = 325.000 K			
5.000	33.485	33.473	0.036	33.475	0.028
10.000	70.876	70.839	0.051	70.850	0.037
12.500	90.289	90.251	0.042	90.265	0.026
15.006	109.585	109.523	0.057	109.538	0.043
17.507	128.112	128.034	0.061	128.041	0.056
19.996	145.414	145.322	0.063	145.312	0.071
30.059	201.282	201.159	0.061	201.120	0.080
40.015	238.616	238.498	0.050	238.456	0.067
49.963	265.488	265.332	0.059	265.249	0.090
59.992	286.267	286.133	0.047	286.012	0.089
79.963	317.017	316.922	0.030	316.756	0.082
99.953	339.762	339.680	0.024	339.506	0.075
119.937	357.863	357.777	0.024	357.622	0.067
139.769	372.872	372.750	0.033	372.629	0.065
149.914	379.699	379.562	0.036	379.462	0.062
159.898	385.959	385.815	0.037	385.735	0.058
179.838	397.373	397.189	0.046	397.152	0.056
		T = 350.000 K			
2.023	11.983	11.985	-0.022	11.986	-0.027
4.998	30.470	30.464	0.019	30.467	0.011
7.495	46.652	46.637	0.033	46.643	0.020
10.021	63.431	63.412	0.030	63.424	0.011

Table 3.6. Continued

P / MPa	ρ (Exp) kg/m3	ρ (GERG-08) kg/m^3	Deviation %	ρ (AGA-8) kg/m^3	Deviation %
12.526	80.209	80.198	0.014	80.217	-0.010
15.025	96.805	96.789	0.017	96.813	-0.009
17.544	113.084	113.050	0.030	113.074	0.009
20.021	128.379	128.334	0.035	128.349	0.024
30.062	180.758	180.727	0.017	180.684	0.041
40.025	218.503	218.483	0.009	218.455	0.022
49.958	246.513	246.455	0.023	246.424	0.036
59.953	268.419	268.384	0.013	268.326	0.035
80.013	301.223	301.235	-0.004	301.123	0.033
99.973	325.311	325.336	-0.008	325.201	0.034
119.974	344.476	344.484	-0.002	344.358	0.034
140.057	360.457	360.440	0.005	360.347	0.031
149.839	367.377	367.339	0.010	367.267	0.030
159.954	374.043	373.987	0.015	373.940	0.028
179.786	385.932	385.833	0.026	385.840	0.024
199.260	396.370	396.225	0.037	396.286	0.021
		T = 375.000 K			
5.017	28.131	28.140	-0.029	28.142	-0.039
10.019	57.578	57.571	0.012	57.583	-0.009
12.508	72.366	72.354	0.017	72.375	-0.012
14.970	86.847	86.828	0.023	86.856	-0.010
17.509	101.434	101.409	0.024	101.443	-0.009
20.011	115.297	115.272	0.022	115.304	-0.006
30.035	163.982	163.925	0.035	163.900	0.050
40.061	201.330	201.268	0.031	201.235	0.047
59.976	252.342	252.308	0.013	252.295	0.019
80.023	286.582	286.583	0.000	286.526	0.019
99.910	311.732	311.758	-0.008	311.666	0.021
119.931	331.832	331.847	-0.005	331.745	0.026
140.002	348.536	348.528	0.002	348.443	0.027
		T = 400.000 K			
2.054	10.539	10.543	-0.039	10.544	-0.049
5.009	26.058	26.058	0.002	26.061	-0.010
10.024	52.951	52.929	0.042	52.941	0.019
12.499	66.231	66.203	0.042	66.223	0.012
15.018	79.591	79.551	0.050	79.581	0.013
17.495	92.444	92.397	0.050	92.435	0.010

Table 3.6. Continued

***P* / MPa**	**ρ (Exp) kg/m3**	**ρ (GERG-08) kg/m^3**	**Deviation %**	**ρ (AGA-8) kg/m^3**	**Deviation %**
20.025	105.175	105.124	0.049	105.165	0.010
30.033	150.277	150.221	0.038	150.222	0.037
40.031	186.306	186.269	0.019	186.236	0.037
49.997	214.747	214.719	0.013	214.705	0.020
59.979	237.723	237.712	0.005	237.718	0.002
80.040	272.978	273.016	-0.014	273.006	-0.010
100.082	299.242	299.292	-0.017	299.244	-0.001
120.026	320.036	320.046	-0.003	319.973	0.020
139.961	337.257	337.242	0.004	337.168	0.026
150.019	344.956	344.923	0.010	344.857	0.029

The FTE corrections measured and applied to these data sets are $(\Phi - 1)$ = (201, 204, 196, 192 and 192) ppm at (300, 325, 350, 375 and 400) K, respectively.

Figure 3.10 is a plot of the data in table 3.6. Percent deviations with both GERG-08 and AGA-8 standard equations of state show agreement with the experimental data within 0.1 %, which coincides with the lowest uncertainty levels claimed for these models. The new data validates the performance of both equations at high pressures.

The experimental uncertainty must include the sample composition uncertainty. A novel thorough, robust, first principles analysis for the estimation of the total experimental uncertainty appears in the following section.

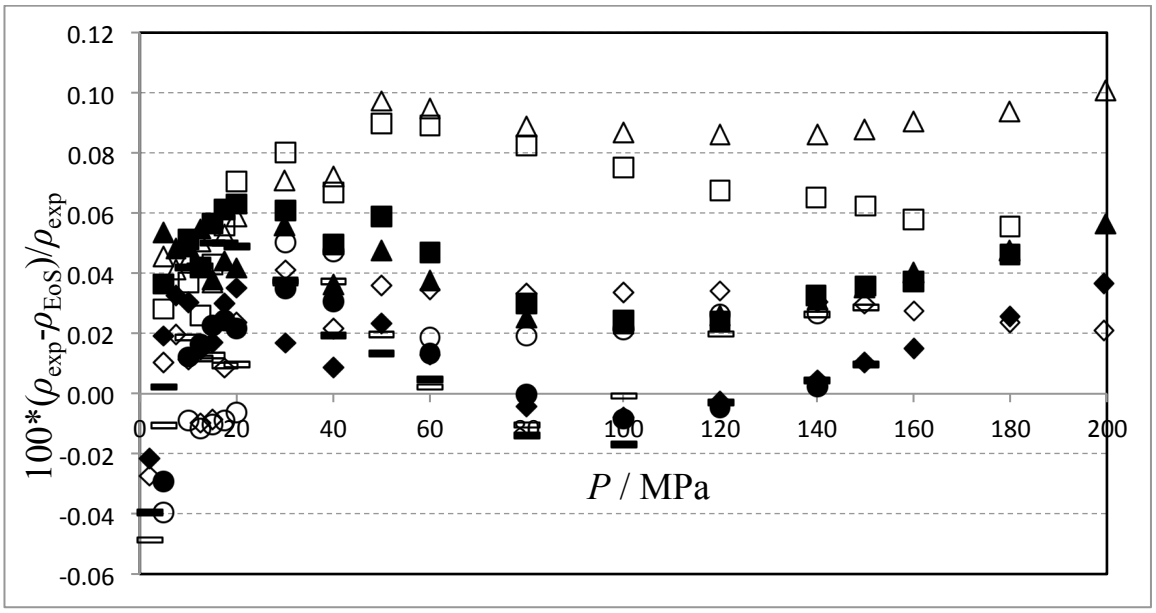

Figure 3.10. Percent deviation of experimental data compared to GERG-08 (full black symbols) and AGA-8 (open symbols) equations of state. Different shape markers represent different temperatures. ▲ 300 K; □ 325 K; ◇ 350 K; ○ 375 K; ━ 400 K.

3.5. Uncertainties

The uncertainty of an experimental quantity (the density in this case) can be expressed as a combination of independent contributions from all different variables involved in its determination:

$$[u^{app}(\rho)]^2 = \sum_i \left[\left(\frac{\partial \rho}{\partial \Psi_i}\right)_{\Psi_{j\neq i}}\right]^2 [u(\Psi_i)]^2 \tag{3.10}$$

or, in relative terms

$$\left[\frac{u^{app}(\rho)}{\rho}\right]^2 = \sum_i \left[\frac{\Psi_i}{\rho}\left(\frac{\partial \rho}{\partial \Psi_i}\right)_{\Psi_{j\neq i}}\right]^2 \left[\frac{u(\Psi_i)}{\Psi_i}\right]^2 \tag{3.11}$$

The superscript *app* refers to apparatus.

Equation (3.8) defines the experimental density of the fluid, and it is the starting point for a first principles uncertainty analysis of these density measurements. Experimental determination of the sinker density involves separate independent procedures for mass and volume.

$$\rho_f = \frac{m_s}{V_s} + \frac{(m_{c2} - m_{c1}) - (w_2 - w_1)_f/\alpha}{\phi V_s} \tag{3.12}$$

The uncertainty of ρ_f is a combination of the uncertainties of all experimental variables involved in the measurement, given by equation (3.12): mass and volume of the sinker, compensation masses, balance readings, and correcting factors α and Φ.

$$u^2(\rho) = \left(\frac{\partial \rho}{\partial m_s}\right)^2_{\Psi_i \neq m_s} u^2(m_s) + \left(\frac{\partial \rho}{\partial m_{c2}}\right)^2_{\Psi_i \neq m_{c2}} u^2(m_{c2}) + \left(\frac{\partial \rho}{\partial m_{c1}}\right)^2_{\Psi_i \neq m_{c1}} u^2(m_{c1})$$
$$+ \left(\frac{\partial \rho}{\partial (w_2 - w_1)}\right)^2_{\Psi_i \neq (w_2 - w_1)} u^2(w_2 - w_1) + \left(\frac{\partial \rho}{\partial V_s}\right)^2_{\Psi_i \neq V_s} u^2(V_s)$$
$$+ \left(\frac{\partial \rho}{\partial \alpha}\right)^2_{\Psi_i \neq \alpha} u^2(\alpha) + \left(\frac{\partial \rho}{\partial \phi}\right)^2_{\Psi_i \neq \phi} u^2(\phi) \tag{3.13}$$

Equation (3.13) is rewritten in relative terms in equation (3.14).

All masses were determined by performing sequential measurements that follow a symmetric design (ADABA) described by NIST[58], atmospheric buoyancy corrections and a statistical treatment.

A hydrostatic comparator determines the sinker volume at reference conditions *(T_0, P_0)* by comparing the sinker to silicon density standards. The experimental procedure also follows a symmetric design (ABACADADBDCDCBC) described by McLinden et al.[58] and provides the calibration volume V_{s0} and its uncertainty.

$$\left[\frac{u(\rho)}{\rho}\right]^2 = \left[\frac{m_s}{\rho}\left(\frac{\partial\rho}{\partial m_s}\right)_{\Psi_i\neq m_s}\right]^2\left[\frac{u(m_s)}{m_s}\right]^2 + \left[\frac{m_{c2}}{\rho}\left(\frac{\partial\rho}{\partial m_{c2}}\right)_{\Psi_i\neq m_{c2}}\right]^2\left[\frac{u(m_{c2})}{m_{c2}}\right]^2$$
$$+\left[\frac{m_{c1}}{\rho}\left(\frac{\partial\rho}{\partial m_{c1}}\right)_{\Psi_i\neq m_{c1}}\right]^2\left[\frac{u(m_{c1})}{m_{c1}}\right]^2$$
$$+\left[\frac{(w_2-w_1)}{\rho}\left(\frac{\partial\rho}{\partial(w_2-w_1)}\right)_{\Psi_i\neq(w_2-w_1)}\right]^2\left[\frac{u(w_2-w_1)}{(w_2-w_1)}\right]^2$$
$$+\left[\frac{V_s}{\rho}\left(\frac{\partial\rho}{\partial V_s}\right)_{\Psi_i\neq V_s}\right]^2\left[\frac{u(V_s)}{V_s}\right]^2 + \left[\frac{\alpha}{\rho}\left(\frac{\partial\rho}{\partial\alpha}\right)_{\Psi_i\neq\alpha}\right]^2\left[\frac{u(\alpha)}{\alpha}\right]^2$$
$$+\left[\frac{\phi}{\rho}\left(\frac{\partial\rho}{\partial\phi}\right)_{\Psi_i\neq\phi}\right]^2\left[\frac{u(\phi)}{\phi}\right]^2 \qquad (3.14)$$

Sinker volume changes with measurement conditions *(T, P)* according to the following equation:

$$V_s = V_{s0}\left[1+\beta(T-T_0)-3\frac{(1-2\vartheta)}{\gamma}(P-P_0)\right] \qquad (3.15)$$

in which β is the volumetric expansion coefficient, ϑ is the Poisson ratio, and γ is the Young's modulus. Each of these variables has an associated uncertainty based upon data available in the literature, the numerical interpolations used for specific conditions and engineering judgment. Thus, the sinker volume uncertainty resolves into independent pieces combined in the same way as equation (3.11).

The uncertainty of the balance readings $(w_2 - w_1)$ comes from a repeatability analysis.

$$u(w_2-w_1) = \frac{S_{(w_2-w_1)}}{\sqrt{N}} \qquad (3.16)$$

In formula (3.16), S is the standard deviation of the balance readings per measurement cycle, and N is the number of readings. In the MSD, measurement cycles are set to last 10 minutes total and record readings every 6 seconds. Typical values of S are around 3×10^{-5} g, but always below 5×10^{-5} g. $N = 120$.

Every isothermal set of measurements provides values of α and ϕ, so they can be treated in the same statistical way to estimate their uncertainty. The atmospheric correction factor α is given by equation (3.3). The force transmission analysis provides $\phi = \phi_0$ given by vacuum measurements according to equation (3.6).

$$\phi = \phi_0 = \frac{(w_2 - w_1)_0/\alpha - (m_{c2} - m_{c1})}{m_s} \tag{3.17}$$

Table 3.7 contains the values of the individual uncertainties that contribute to the apparatus uncertainty and their dimensionless sensitivity coefficients.

Other variables contribute to the uncertainty of the experimental density value. Uncertainties in the measuring conditions, temperature and pressure, as well as the composition of the sample motivate the following discussion.

Table 3.7. Typical values of uncertainty contributions to $u^{app}(\rho)$.

Quantity	Ψi	$u(\Psi i)$	$u(\Psi i)/\Psi i$	$\frac{\Psi_i}{\rho}\left(\frac{\partial \rho}{\partial \Psi_i}\right)_{\Psi_{j\neq i}}$
ms	30.39159 g	7.50×10^{-5} g	2.47×10^{-6}	6.8992
mc1	41.61804 g	7.50×10^{-5} g	1.80×10^{-6}	-9.4459
mc2	11.23311 g	7.50×10^{-5} g	6.67×10^{-6}	2.5495
(w2-w1)	-4.39569 g	4.56×10^{-6} g	-1.04×10^{-6}	0.9975
Vs	6.74078* cm^3	1.27×10^{-4} cm^3	1.88×10^{-5}	-1.0000
α	1.000150	5.25×10^{-5}	5.25×10^{-5}	-0.9972
ϕ	1.000189	1.60×10^{-5}	1.60×10^{-5}	5.8992

* Sinker volume changes with conditions. Value shown is the calibration volume V_{s0}.

In general, the total experimental uncertainty of densities measured with the MSD is a function of pressure, temperature and sample composition.

$$\rho_m = \rho_m\left(P,T,R,z_i\right) \tag{3.18}$$

The universal gas constant R is also an experimental quantity with an associated uncertainty.

$$\begin{aligned}\left[\frac{u\left(\rho_m\right)}{\rho_m}\right]^2 = &\left[\frac{u^{app}\left(\rho_m\right)}{\rho_m}\right]^2 + \left[\frac{P}{\rho_m}\left(\frac{\partial\rho_m}{\partial P}\right)_{T,R,z_i,M_i}\right]^2\left[\frac{u\left(P\right)}{P}\right]^2 + \left[\frac{T}{\rho_m}\left(\frac{\partial\rho_m}{\partial T}\right)_{P,R,z_i,M_i}\right]^2\left[\frac{u\left(T\right)}{T}\right]^2 \\ &+\left[\frac{R}{\rho_m}\left(\frac{\partial\rho_m}{\partial R}\right)_{P,T,z_i,M_i}\right]^2\left[\frac{u\left(R\right)}{R}\right]^2 + \sum_{i=1}^{N}\left[\frac{z_i}{\rho_m}\left(\frac{\partial\rho_m}{\partial z_i}\right)_{P,T,R,z_{j\neq i},M_i}\right]^2\left[\frac{u\left(z_i\right)}{z_i}\right]^2\end{aligned} \tag{3.19}$$

The sample composition can be measured by gas chromatography (GC) with an associated uncertainty of ~0.1%. This uncertainty is usually high compared to the apparatus uncertainty, so we could measure very accurately the mass density of a sample, but we would not know accurately the composition the sample. Assuming the sample is prepared gravimetrically, the composition term becomes a function of the individual masses of the pure substances that compose the sample, along with their molar masses.

$$z_i = \frac{n_i}{n} = \frac{\left(m_i / M_i\right)}{\sum_{k=1}^{N}\left(m_k / M_k\right)} \tag{3.20}$$

The mass density as a function of observables is then,

$$\rho_m = \rho_m\left(P,T,R,z_i\left\{m_i,M_i\right\}\right) \tag{3.21}$$

from which the total uncertainty in density would be

$$\left[\frac{u(\rho)}{\rho}\right]^2 = \left[\frac{u(\rho)^{app}}{\rho}\right]^2 + \left[\frac{p}{\rho}\left(\frac{\partial\rho}{\partial p}\right)_{T,R,m_i,M_i}\right]^2\left[\frac{u(p)}{p}\right]^2 + \left[\frac{T}{\rho}\left(\frac{\partial\rho}{\partial T}\right)_{p,R,m_i,M_i}\right]^2\left[\frac{u(T)}{T}\right]^2$$
$$+\left[\frac{R}{\rho}\left(\frac{\partial\rho}{\partial R}\right)_{p,T,m_i,M_i}\right]^2\left[\frac{u(R)}{R}\right]^2 + \sum_{i=1}^{N}\left[\frac{m_i}{\rho}\left(\frac{\partial\rho}{\partial m_i}\right)_{p,T,R,m_{j\neq i},M_i}\right]^2\left[\frac{u(m_i)}{m_i}\right]^2$$
$$+\sum_{i=1}^{N}\left[\frac{M_i}{\rho}\left(\frac{\partial\rho}{\partial M_i}\right)_{p,T,R,m_i,M_{j\neq i}}\right]^2\left[\frac{u(M_i)}{M_i}\right]^2 \qquad (3.22)$$

Table 3.8 contains the experimental uncertainties in *T*, *P* and *R*.

Table 3.8. Representative measurement uncertainties.

Quantity	**Uncertainty**
Temperature	$u(T)$ = 0.010 K
Pressure	
0-40 MPa Transducer	$u(p)$ = 0.0016 MPa
0-200 MPa Transducer	$u(p)$ = 0.0081 MPa
Gas constant	$u(R)/R = 1.8\times10^{-6}$

Table 3.9 contains the magnitudes of the gravimetric masses weighted in the preparation process of the residual gas sample. The uncertainty of these values is $u(m_i)$ = 0.1 g.

Table 3.9. Gravimetric masses.

Component	z_i	m_i/**kg**
Methane	0.95014	1.93891
Ethane	0.03969	0.1518
Propane	0.01017	0.05704

And table 3.10 has the uncertainties in molar masses calculated from variations in isotopic compositions for the constituents of each species.[90]

Table 3.10. Molar masses for natural gas constituents and their associated uncertainties.

Substance	M_i	$10^4 \cdot u(M_i)$	$10^4 \cdot u(M_i)/M_i$
CH_4	16.0425	8.5	0.53
C_2H_6	30.0690	16.5	0.55
C_3H_8	44.0956	24.6	0.56
C_4H_{10}	58.1220	32.8	0.56
C_5H_{12}	72.1488	40.9	0.57
C_6H_{14}	86.1754	49.0	0.57
C_7H_{16}	100.2019	57.1	0.57
C_8H_{18}	114.2285	65.2	0.57
C_9H_{20}	128.2551	73.3	0.57
$C_{10}H_{22}$	142.2817	81.5	0.57
N_2	28.0134	4.0	0.14
CO_2	44.0950	10.0	0.23
H_2O	18.0153	3.3	0.18
H_2S	34.0809	50.0	1.47

Results for the total experimental uncertainties, constructed from the contributions described above, appear in figure 3.11 plots. Clearly, the contribution from the gas constant *R* is negligible, and the predominant term is the apparatus contribution.

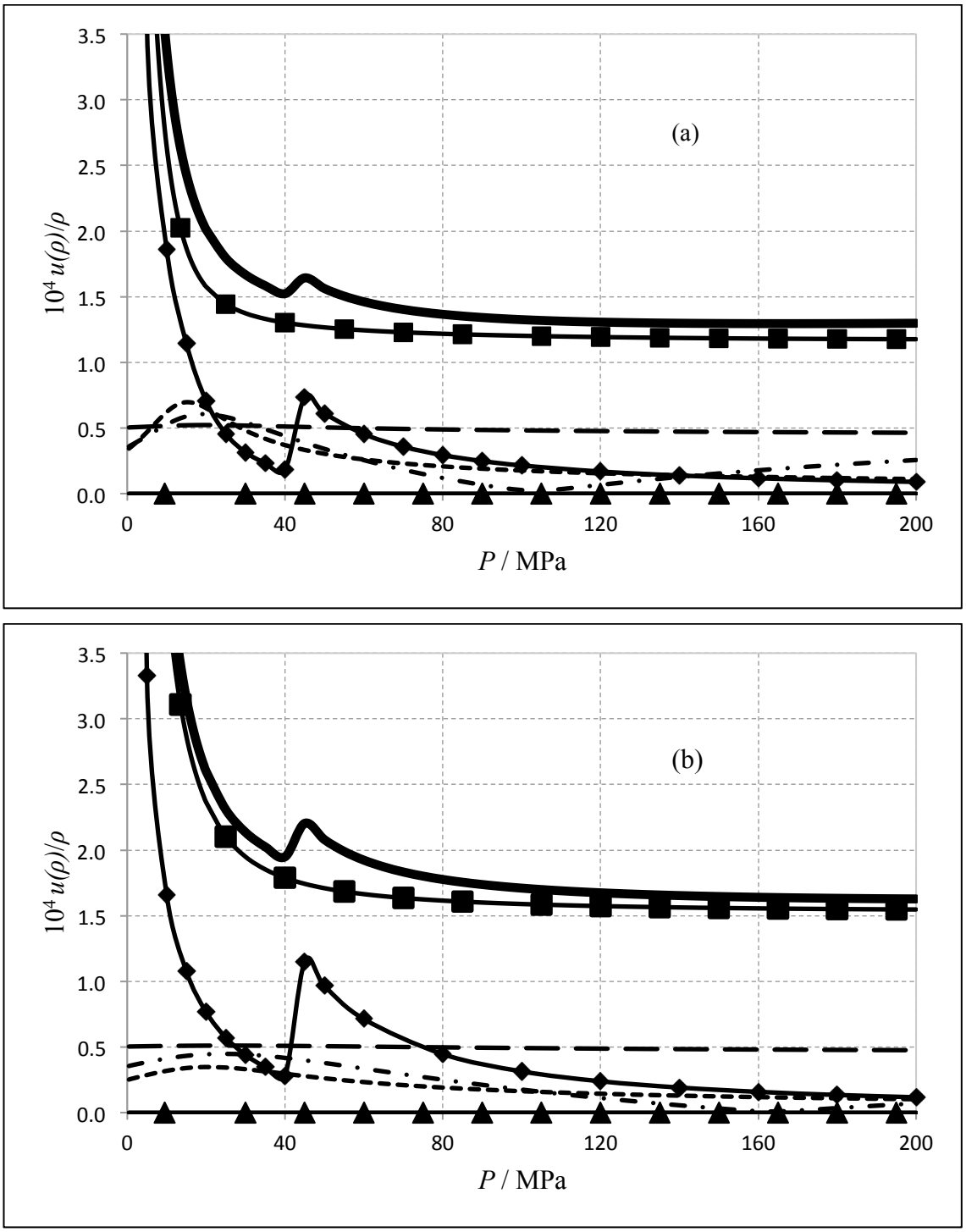

Figure 3.11. Uncertainty analysis for a residual gas mixture. (a) T = 300 K, and (b) T = 400 K. Gravimetric mass uncertainty $u(m_i)$ 0.1 g. ─ Total, -■- apparatus, -♦- pressure, ─ ─ molar mass, ─ · ─ gravimetric mass, ─▲─ gas constant, -- temperature.

4. ISOCHORIC MEASUREMENTS FOR PHASE BOUNDARY DETERMINATIONS

Accurate vapor-liquid equilibrium determination is a challenging area of experimental thermodynamics. Scientists have developed several different apparatus and techniques among which the isochoric change in slope technique is relatively simple experimentally and mathematically elegant.

4.1. The Isochoric Technique

The foundation of the isochoric technique lies in the principle that the slope of an isochoric (constant density) line changes abruptly at the phase boundary, i.e. when crossing from the single-phase region into the two-phase region.

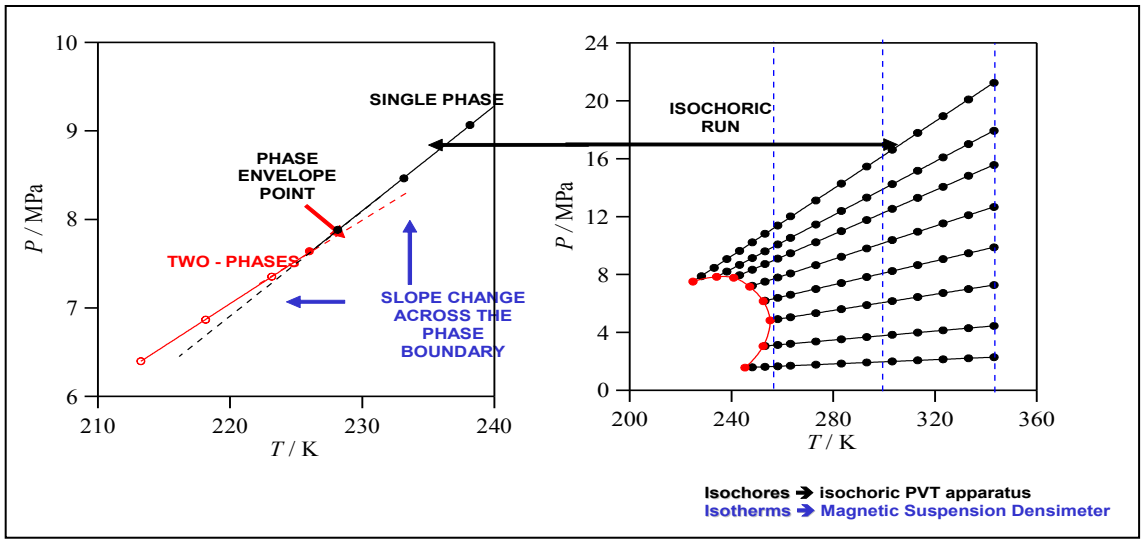

Figure 4.1. Isochoric technique for phase boundary determinations.

Griffiths[91] proved the co-linearity constraints to use isochoric data for phase equilibrium determinations.[92, 93] Several experimental approaches take advantage of that development, like the low- and high-pressure isochoric apparatus built at Texas A&M University recently. Figure 4.1 sketches the isochoric technique.

4.2. The Low-Pressure Isochoric Apparatus

The low-pressure isochoric apparatus is a closed isochoric cell made of stainless steel, equipped with surrounding heat exchange, temperature control, and automatic temperature and pressure monitoring systems. Temperature capabilities range from (100 to 500) K with a stability of ± 5 mK with pressures up to 20 MPa with 0.01 % full scale accuracy. Figure 4.2 is a schematic of the low pressure isochoric apparatus.

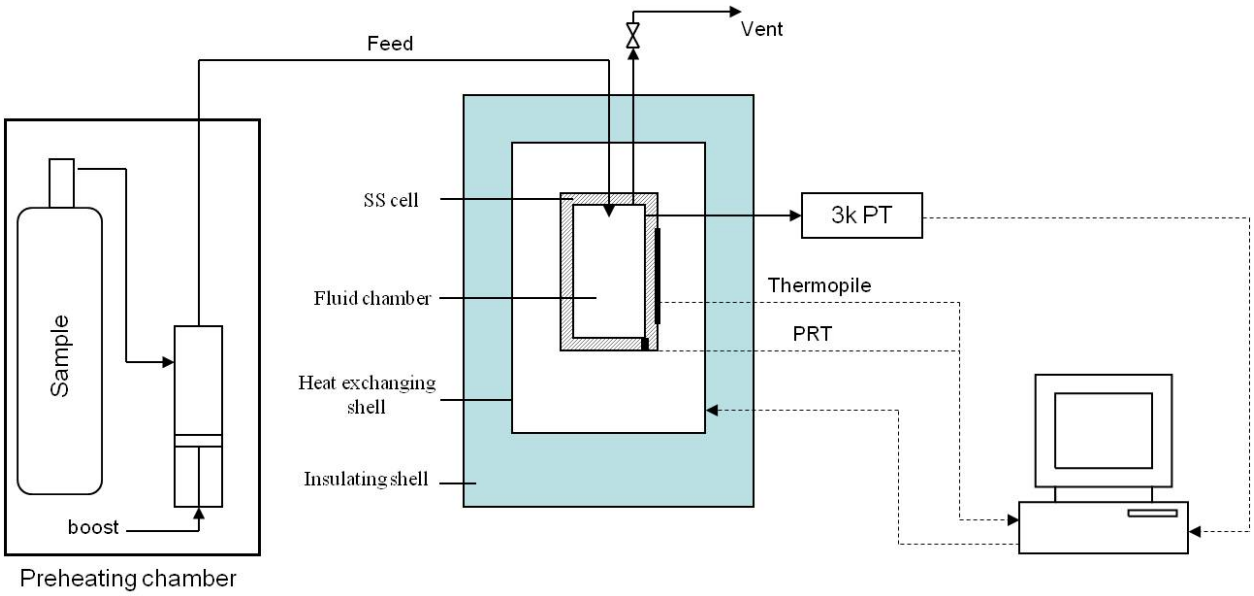

Figure 4.2. Low-pressure isochoric apparatus.

The experimental procedure followed to gather isochoric data involves loading the sample into the isochoric cell at initial conditions (say T = 300 K, P = 20 MPa), using the heat exchangers in the temperature control system to lower (or raise the temperature according to the experiment design) and waiting for the temperature and pressure to stabilize.

After stabilization, raw *(T, P)* data are collected and analyzed in 20-minute periods for each point, selecting the most stable region (random distribution of data points around set points and lowest standard deviation). A statistical analysis performed on the data near the phase boundaries reveals the change in slope mentioned above and allows determination of phase boundary coordinates (T_s, P_s) as well as dew points in the case of the low-density region.

4.3. The High-Pressure Isochoric Apparatus

The high-pressure isochoric apparatus follows the same conceptual design and construction. The high-pressure cell is smaller in volume (10.5 cm^3), has thicker walls and is copper-beryllium alloy (Cu-Be 175). The pressure limit is 200 MPa, one order of magnitude higher than the low-pressure system. This apparatus also has automated systems to monitor and control the temperature, and to record pressure.

A four wire PRT (Platinum Resistance Thermometer) from Minco® measures the temperature at the bottom of the isochoric cell, and a thermopile measures the

temperature gradient across the cell, top to bottom. The control system constrains temperature fluctuations to lower than 3 mK with virtually no gradients in the cell.

A 200 MPa quartz pressure transducer from Paroscientific measures the pressure within 0.01 % of full scale accuracy. Cristancho[94] presents additional details concerning this apparatus.

The procedure followed to collect data is essentially the same as that for the low-pressure apparatus. Initial conditions for sample loading are T = 300 K and P = 200 MPa, and the same time periods are analyzed to obtain each pair of (T, P) coordinates. Results from the statistical treatment near the phase boundaries determine bubble points in this case.

4.4. Phase Boundary Determination from Isochoric Data

Each experimental isochore comprises both single-phase and two-phase data gathered with the isochoric apparatus. The phase boundary in each case occurs when the slope of the isochore changes discontinuously.

To find the discontinuity in slope, and thus determine the phase boundary point for each data set, we fit the single-phase data in the vicinity of the boundary (P as a linear or quadratic function of T) and watch for large deviations of the two-phase data with respect to the extrapolation of the fit function evidenced by abrupt changes in the fit parameters. The actual statistical procedure illustrated in figure 4.3, involves selecting

the data set, sequentially adding points to the series to fit it to the corresponding function, and observe the change in the fit parameters.

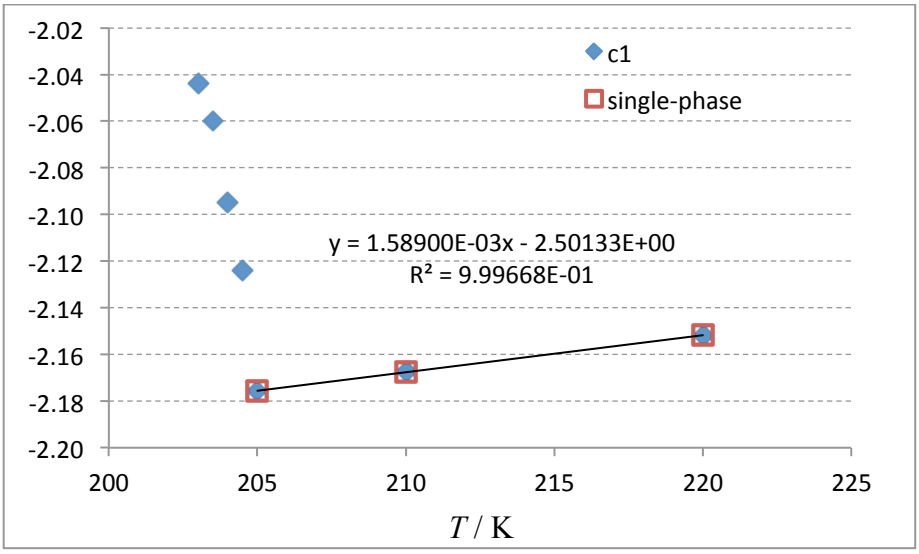

Figure 4.3. Statistical treatment of isochoric data for phase boundary determinations..c1 here is the linear coefficient in the fit.

In general, high-density isochoric data identifying bubble points have a much clearer change in slope, whereas low-density data identifying dew points show a much smoother curvature at the boundary making it more challenging to identify.

4.5. Isochoric Data for a Residual Gas Sample

Table 4.1 contains isochoric data collected with the isochoric apparatus on the residual gas sample with composition mentioned in section 3.4 (95.014 % methane, 3.969 % ethane and 1.017 % propane).

Table 4.1. Isochoric data for a typical residual gas sample.

T / K	P / MPa	T / K	P / MPa	T / K	P / MPa
Isochore 1					
300.000	199.8357	263.061	166.3106	200.000	103.1503
295.000	195.5887	259.991	163.1169	190.000	92.1353
290.000	191.1118	249.998	153.5939	179.999	81.0710
285.000	186.5976	239.999	143.8741	169.999	69.7925
280.000	182.0546	229.997	133.9730	159.999	58.3007
275.000	177.3862	220.000	123.8466	150.001	46.6373
270.000	172.7979	210.000	113.4992	140.984	36.1367
Isochore 2					
390.000	200.5475	275.000	120.0055	150.000	15.6461
380.000	194.0900	270.000	116.3288	140.000	6.9589
375.000	190.8577	260.000	108.6079	135.000	2.4331
370.000	187.5557	249.999	100.7470	131.999	0.5208
360.000	180.8950	239.999	92.7507	131.647	0.4258
350.000	174.1424	230.000	84.6076	131.552	0.3984
340.000	167.2950	219.991	76.3323	131.400	0.3766
330.000	160.3432	210.000	67.9246	130.647	0.3503
325.000	156.7287	199.994	59.3658	130.149	0.3391
320.000	153.2899	189.999	50.6782	129.651	0.3286
310.000	146.1376	180.000	41.8804	129.149	0.3183
300.000	138.9426	170.000	33.0344	128.649	0.3082
290.000	131.4393	160.000	24.2660	128.149	0.2978
280.000	123.9472				
Isochore 3					
449.998	193.8001	260.000	81.0900	149.001	2.0284
440.000	188.5609	250.000	74.6221	148.003	1.3871
430.000	183.2007	239.997	67.7519	147.901	1.2472
420.000	177.8295	229.999	60.8123	147.750	1.1683
410.000	172.3511	220.000	53.7677	147.650	1.1377
400.000	166.9505	209.993	46.6034	147.600	1.1278
390.000	161.3494	199.999	39.3682	147.500	1.1119
380.000	155.6739	190.000	32.0643	147.249	1.0387
370.000	149.9239	190.000	32.1835	147.001	0.9503
360.001	144.0859	180.001	24.8775	146.850	0.8693
350.001	138.1950	170.000	17.6030	146.750	0.8416
340.004	132.2390	159.999	10.3592	146.499	0.8131

Table 4.1. Continued

T / K	P / MPa	T / K	P / MPa	T / K	P / MPa
330.000	126.2030	159.000	9.6129	146.250	0.8039
325.002	123.1401	157.999	8.8618	146.001	0.7929
320.000	120.0714	156.999	8.1070	145.500	0.7753
310.002	113.8592	156.000	7.3478	145.000	0.7555
300.000	107.9277	155.000	6.5803	144.002	0.7213
290.000	101.5192	154.001	5.8079	143.008	0.6857
280.000	95.0098	153.000	5.0327	140.000	0.5873
275.000	91.3860	150.000	2.7312	134.999	0.4477
270.000	88.4209				
Isochore 4					
450.000	146.8766	340.001	96.1758	165.500	1.8114
440.000	142.5187	330.000	91.2519	165.250	1.7942
430.000	138.1020	320.000	86.2662	165.000	1.8326
419.999	133.6299	310.003	81.2292	164.750	1.7601
410.000	129.1274	300.000	76.1276	164.500	1.7431
400.000	124.5640	170.000	4.4876	164.250	1.7258
389.999	119.9614	169.000	3.8979	164.000	1.7098
380.000	115.3127	168.000	3.3371	163.500	1.6792
370.001	110.6114	167.000	2.7775	162.004	1.5868
360.000	105.8506	166.000	2.2596	161.000	1.5246
350.001	101.0393	165.750	1.8282	160.000	1.4645
Isochore 5					
299.999	35.7938	250.000	21.5229	209.986	9.5552
290.000	32.9943	240.000	18.5838	199.987	6.5142
279.998	30.1623	230.000	15.6107	189.999	4.0584
270.000	27.3064	220.000	12.5986	180.000	2.9906
260.000	24.4319				
Isochore 6					
299.995	20.5670	219.999	8.1088	202.501	5.4666
289.997	19.0228	209.998	6.5336	202.001	5.3979
279.999	17.4713	204.998	5.8064	201.001	5.2666
270.000	15.9142	204.501	5.7384	200.000	5.1590
260.000	14.3612	203.998	5.6806	199.000	5.0338
250.000	12.7953	203.497	5.6096	198.500	4.9733
239.999	11.2292	203.000	5.5330	198.000	4.9069
229.999	9.6663				

Table 4.1. Continued

T / K	P / MPa	T / K	P / MPa	T / K	P / MPa
Isochore 7					
420.000	20.1203	310.000	12.6772	209.250	5.3813
400.004	18.7896	300.001	11.9619	209.150	5.3731
390.000	18.1280	290.000	11.2683	209.000	5.4014
379.999	17.4609	280.001	10.5595	208.750	5.3457
370.000	16.7911	270.000	9.8629	208.500	5.2579
360.000	16.1160	260.000	9.1356	208.250	5.2804
350.000	15.4459	250.000	8.4135	208.000	5.2890
340.002	14.7662	240.000	7.6915	207.000	5.2121
330.000	14.0743	230.000	6.9525	206.000	5.1340
320.000	13.3757	220.000	6.1934		
Isochore 8					
450.000	10.6829	270.000	5.5494	211.100	3.7500
440.000	10.4061	260.000	5.2435	211.000	3.7467
430.000	10.1284	250.000	4.9443	210.900	3.7437
420.000	9.8503	240.000	4.6441	210.800	3.7405
409.999	9.5266	230.000	4.3360	210.700	3.7379
400.000	9.2908	220.000	4.0290	210.600	3.7351
390.000	9.0100	215.000	3.8742	210.500	3.7322
380.000	8.7273	213.000	3.8114	210.000	3.7368
369.998	8.4442	212.000	3.7801	209.900	3.7338
360.000	8.1259	211.750	3.7722	209.800	3.7308
350.000	7.8710	211.900	3.7774	209.700	3.7277
340.000	7.5845	211.800	3.7740	209.599	3.7247
330.000	7.2965	211.700	3.7703	209.500	3.7218
320.001	7.0076	211.600	3.7670	209.400	3.7187
309.998	6.7175	211.500	3.7627	209.300	3.7156
300.000	6.4207	211.400	3.7594	209.200	3.7127
290.001	6.1302	211.300	3.7565	208.999	3.7066
280.000	5.8407	211.200	3.7532	208.000	3.6766
Isochore 9					
500.000	9.6248	379.999	7.0443	260.000	4.3528
490.000	9.4141	369.999	6.8248	250.000	4.1218
480.000	9.2024	359.999	6.6045	240.000	3.8911
470.000	8.9899	350.001	6.3833	230.000	3.6634
460.000	8.7767	339.999	6.1611	220.000	3.4545

Table 4.1. Continued

T / K	*P* / MPa	*T* / K	*P* / MPa	*T* / K	*P* / MPa
450.000	8.5625	330.002	5.9385	215.000	3.3405
440.000	8.3478	320.000	5.7147	210.000	3.1933
430.000	8.1326	310.000	5.4899	205.000	3.0883
420.000	7.9157	300.000	5.2624	200.000	2.9580
410.000	7.6989	290.000	5.0378	195.000	2.8253
399.999	7.4814	280.000	4.8123	190.000	2.6785
390.000	7.2632	270.000	4.5851		
Isochore 10					
369.998	4.8223	310.001	3.9389	270.000	3.3358
360.000	4.6818	305.154	3.8681	260.000	3.1824
349.997	4.5335	299.996	3.7885	240.000	2.8739
340.000	4.3838	290.001	3.6393	220.000	2.5606
330.005	4.2136	279.998	3.4892	210.007	2.4023
319.999	4.0836				

Density values shown in table 4.1 are references to identify isochores. Accurate isochoric densities appear in section 5. Table 4.2 contains the phase envelope points resulting from the statistical treatment described in the previous section, performed using the isochoric data reported in table 4.1. Figure 4.4 illustrates the phase loop results.

Table 4.2. Phase boundaries determined by isochoric experiments.

Isochore	*T* / K	*P* / MPa
2	131.43	0.3815
3	146.54	0.8181
4	164.75	1.7601
5	194.76	5.2288
6	205.00	5.8062
7	209.25	5.3813
8	209.50	3.7218
9	206.64	3.1227

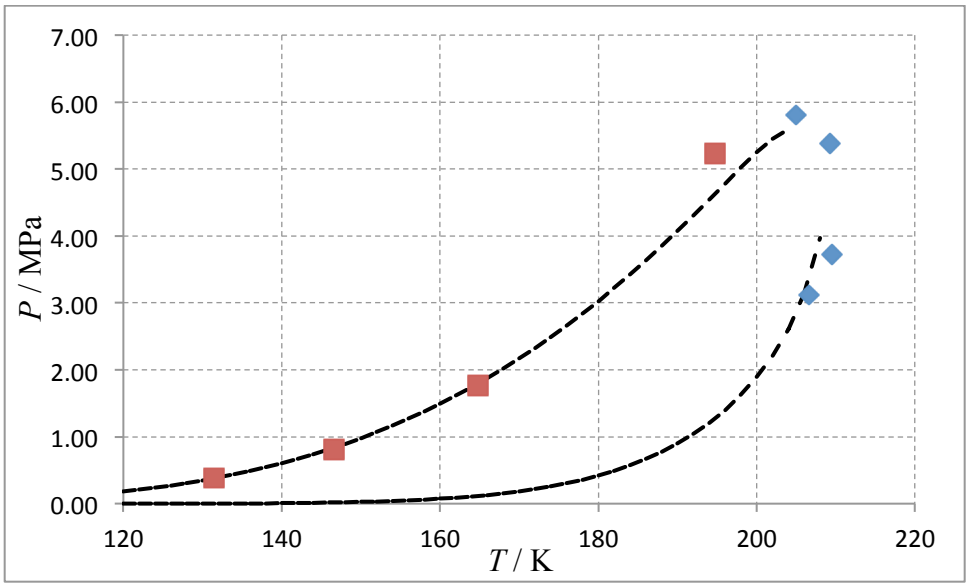

Figure 4.4. Phase loop for the residual gas sample. Red squares come from analysis of isochoric data collected with the high-pressure apparatus; blue diamonds from low- pressure isochoric experiments. The dashed line is the prediction of GERG-08 EoS.

4.6. Noxious Volume

The density of the isochoric lines is not strictly constant. This is caused by two independent effects: the volume of the cell changes with temperature and pressure and must be corrected at each point using the mechanical properties of the material, and the *noxious volume* effect.

In order to measure the pressure, the isochoric cell is connected to a pressure transducer, which means that a small portion of the sample leaves the cell and goes into the transducer. The pressure transducer is at a constant temperature (77 °C for the low-pressure system, and 36 °C for the high-pressure system). Along an isochore, as the temperature changes in the cell, the temperature gradient between the cell and the transducer also changes, and so does the distribution of sample between the two

subsystems. The total mass of sample in the system (cell + noxious volume) is constant throughout the isochoric experiment.

The noxious volume V_x is 0.34 % of the volume of the cell in the low-pressure apparatus and 1.5 % in the high-pressure system ($100 \times V_x/V_{cell}$). The amount of sample (number of moles) in the noxious volume must be accounted for in further calculations.

5. FULL THERMODYNAMIC CHARACTERIZATION

Figure 5.1 summarizes isothermal and isochoric data reported in sections 3 and 4 for the residual gas sample.

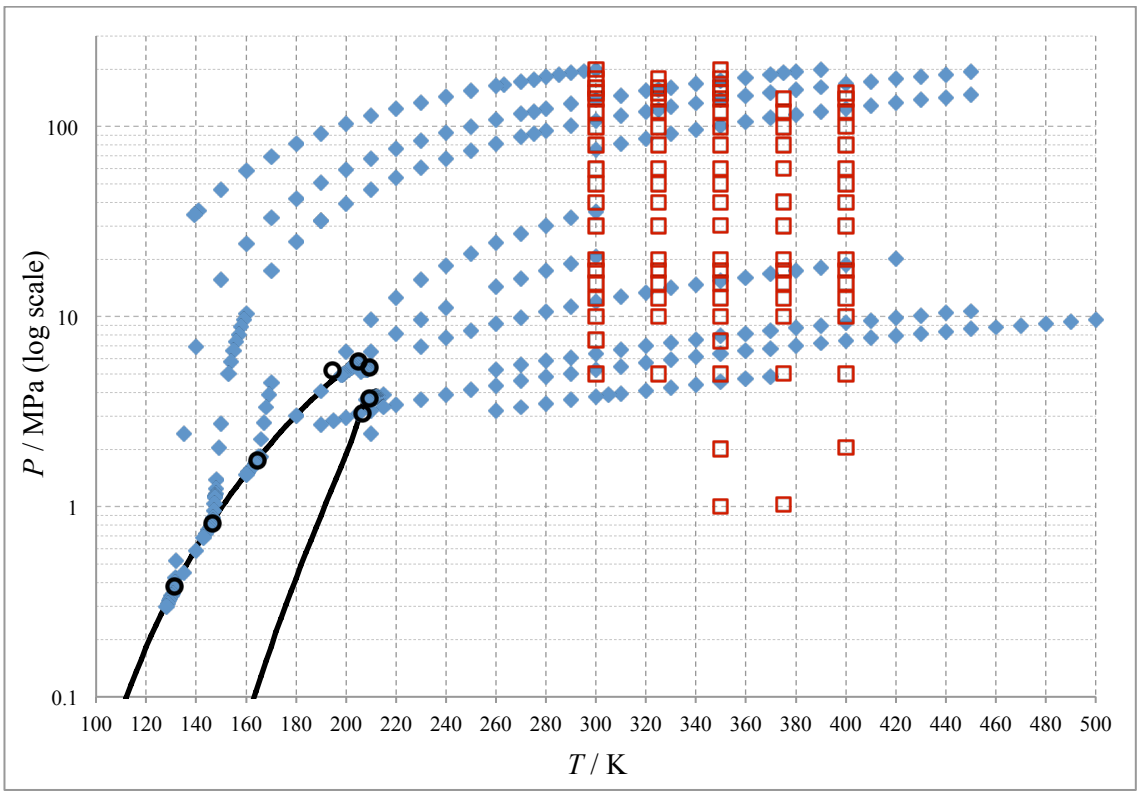

Figure 5.1. *PρT* data gathered for a residual gas sample. Red squares are conditions for density data collected isothermally with the MSD. Blue diamonds are isochoric data. Black open circles are experimental phase loop points. Dashed line is the phase loop prediction by GERG-2008 EoS.

A mathematical combination of isothermal and isochoric *PρT* data enables construction of a full thermodynamic characterization of a sample, by using the experimental techniques to compute all energy functions (*U*, *H*, *S*, *A*, and *G*). The first

step in this procedure is determination of experimental isochoric densities: experimental density values at each pair of coordinates *(P, T)* along the isochores reported in section 4.

Then, after selecting a reference density for each isochore to be the isochoric density, it is necessary to correct pressure data to provide a true isochore. A fit of these isochoric $P\rho T$ data provides a representative analytical function that allows calculation of the derivative with respect to temperature to obtain residual functions. These terms come separately from EoS predictions and differences are integrated over density to determine direct comparisons for energy functions.

5.1. Isochoric Densities

Coupling isochoric data with isothermal density measurements allows determination of experimental densities for the isochoric $P\rho T$ data. The density in the cell at any point along an experimental isochore is

$$\rho = \frac{n}{V} \tag{5.1}$$

in which n is the number of moles in the cell, and V is the total volume of the cell.

From the density data gathered with the MSD, we can compute an experimental density at a pair of conditions within the isochore. Having isothermal density data available at (300, 325, 350, 375, and 400) K, we have picked a convenient reference temperature (T_R) for each isotherm. Reference densities appear in table 5.1.

Table 5.1. Isochoric densities at reference conditions.

T_R / K	P_R / MPa	ρ_R / kg·m^{-3}	ρ_R / kmol·m^{-3}
300.000	199.8357	419.0196	24.8164
300.000	138.9426	385.5021	22.8313
300.000	107.9277	362.1485	21.4482
300.000	76.1276	329.0712	19.4892
299.999	35.7938	248.1891	14.6990
299.995	20.5670	172.9404	10.2424
350.000	15.4459	99.5641	5.8967
350.000	7.8710	49.1283	2.9096
350.001	6.3833	39.3823	2.3324
349.997	4.5335	27.5226	1.6300

As set by the calculation routine, these isochoric densities differ from RefProp values by the same amount as the experimental densities collected with the densimeter discussed in section 3. The ratio of the density at any point along an isochore to the reference density is

$$\frac{\rho}{\rho_R} = \frac{n}{n_R}\frac{V_R}{V} \tag{5.2}$$

For a true isochore, this ratio would be unity, but in the actual experiment, n changes from temperature to temperature because of the cell expansion and noxious volume effects. Knowing that the total amount of sample remains constant throughout the isochore,

$$n_{total} = n + n_x = const. \tag{5.3}$$

$$n = n_T - n_x \tag{5.4}$$

$$n = (n_R + n_{x,R}) - n_x = n_R + (n_{x,R} - n_x) \tag{5.5}$$

where subscript *R* refers to reference conditions, *x* refers to noxious volume, T denotes total and absence of subscript refers to the cell.

$$\frac{n}{n_R} = 1 + \frac{n_{x,R} - n_x}{n_R} = 1 + \frac{V_x\left(\rho_{x,R} - \rho_x\right)}{V_R \rho_R} \tag{5.6}$$

Using equation (5.2)

$$\frac{\rho}{\rho_R}\frac{V}{V_R} = 1 + \left[\frac{V_x}{V_R}\right]\frac{\left(\rho_{x,R} - \rho_x\right)}{\rho_R} \tag{5.7}$$

V/V_R is the ratio of the volume of the cell at a point along the isochore to the one at reference conditions. V_x/V is the ratio of the noxious volume to the volume of the cell. And solving eq (5.7) for ρ,

$$\rho = \left[\frac{V_R}{V}\right]\rho_R + \left[\frac{V_x}{V}\right]\left(\rho_{x,R} - \rho_x\right) \tag{5.8}$$

$$\frac{V_R}{V} = \exp\left[\beta\left(T_R - T\right) + \gamma\left(P_R - P\right)\right] \tag{5.9}$$

$$\frac{V_x}{V} = \frac{V_{x0}}{V_0}\exp\left[\beta_x\left(T_x - T_{x0}\right) + \gamma_x\left(P_x - P_{x0}\right) - \beta\left(T - T_0\right) - \gamma\left(P_x - P_{x0}\right)\right] \tag{5.10}$$

in which subscript 0 refers to calibration conditions. Expression (5.10) reduces to V_{x0}/V_0 when the cell and the noxious volume (pressure transducer and associated tubing) are the same material, as in the case of the low-pressure isochoric apparatus, assuming both the cell and the transducer have calibrations at the same conditions ($T_{x0} = T_0$, $P_{x0} = P_0$). V_{x0}/V_0 is also a good approximation for V_x/V knowing that it is a small number and it does not change much throughout the isochore. Table 5.2 contains isochoric densities of ten isochores for the residual gas sample.

Table 5.2. Experimental densities along isochores for the residual gas sample.

T / K	P / MPa	ρ_{Exp} / kg/m^3	ρ_{EoS} / kg/m^3	% dev
		ρ = 24.8164 kmol/m^3		
300.000	199.8357	419.0196	418.8352	0.044
295.000	195.5887	419.6515	419.2022	0.107
290.000	191.1118	420.3011	419.4833	0.195
285.000	186.5976	420.9551	419.7687	0.282
280.000	182.0546	421.6129	420.0628	0.368
275.000	177.3862	422.2814	420.3188	0.465
270.000	172.7979	422.9462	420.6388	0.546
263.061	166.3106	423.8807	421.0660	0.664
259.991	163.1169	424.3188	421.1063	0.757
249.998	153.5939	425.6881	421.7526	0.924
239.999	143.8741	427.0819	422.4197	1.092
229.997	133.9730	428.5004	423.1231	1.255
220.000	123.8466	429.9482	423.8434	1.420
210.000	113.4992	431.4280	424.5979	1.583
200.000	103.1503	432.9255	425.5329	1.708
190.000	92.1353	434.4978	426.2584	1.896
179.999	81.0710	436.1033	427.1705	2.048
169.999	69.7925	437.7659	428.1929	2.187
159.999	58.3007	439.5037	429.3595	2.308
150.001	46.6373	441.3470	430.7427	2.403
140.984	36.1367	443.1393	432.3565	2.433
		ρ = 22.8313 kmol/m^3		
390.000	200.5475	348.2174	380.6824	-1.250
380.000	194.0900	349.0893	381.1688	-1.106
375.000	190.8577	349.9717	381.4310	-1.040
370.000	187.5557	350.8579	381.6685	-0.965
360.000	180.8950	351.7539	382.1550	-0.817
350.000	174.1424	352.6486	382.6497	-0.670
340.000	167.2950	353.5592	383.1542	-0.524
330.000	160.3432	354.4782	383.6646	-0.376
325.000	156.7287	355.4059	383.8618	-0.285
320.000	153.2899	356.3433	384.1865	-0.229
310.000	146.1376	357.2886	384.7248	-0.084
300.000	138.9426	358.2427	385.3209	0.047
290.000	131.4393	359.2077	385.8019	0.215

Table 5.2. Continued

T / K	P / MPa	ρ_{Exp} / kg/m^3	ρ_{EoS} / kg/m^3	% dev
279.999	123.9472	359.6950	386.3867	0.356
275.000	120.0055	360.1843	386.5789	0.457
270.000	116.3288	361.1723	386.9892	0.497
260.000	108.6079	362.1485	387.6330	0.630
249.999	100.7470	363.1640	388.2991	0.763
239.999	92.7507	364.1952	389.0000	0.891
230.000	84.6076	364.7405	389.7365	1.016
219.991	76.3323	365.2421	390.5414	1.131
210.000	67.9246	366.3546	391.4092	1.237
199.994	59.3658	367.4190	392.3662	1.331
		ρ = 21.4482 kmol/m^3		
449.998	193.8001	348.2174	354.4615	-1.79
440.000	188.5609	349.0893	354.9107	-1.67
430.000	183.2007	349.9717	355.3277	-1.53
420.000	177.8295	350.8579	355.7812	-1.40
410.000	172.3511	351.7539	356.2125	-1.27
400.000	166.9505	352.6486	356.7434	-1.16
390.000	161.3494	353.5592	357.1946	-1.03
380.000	155.6739	354.4782	357.6487	-0.89
370.000	149.9239	355.4059	358.1078	-0.76
360.001	144.0859	356.3433	358.5638	-0.62
350.001	138.1950	357.2886	359.0447	-0.49
340.004	132.2390	358.2427	359.5450	-0.36
330.000	126.2030	359.2077	360.0570	-0.24
325.002	123.1401	359.6950	360.3065	-0.17
320.000	120.0714	360.1843	360.5715	-0.11
310.002	113.8592	361.1723	361.1039	0.02
300.000	107.9277	362.1485	361.9710	0.05
290.000	101.5192	363.1640	362.5341	0.17
280.000	95.0098	364.1952	363.1120	0.30
275.000	91.3860	364.7405	363.0945	0.45
270.000	88.4209	365.2421	363.7310	0.41
260.000	81.0900	366.3546	363.7320	0.72
250.000	74.6221	367.4190	364.7299	0.73
239.997	67.7519	368.5304	365.4722	0.83
229.999	60.8123	369.6690	366.3140	0.91

Table 5.2. Continued

T / K	P / MPa	ρ_{Exp} / kg/m^3	ρ_{EoS} / kg/m^3	% dev
220.000	53.7677	370.8448	367.2355	0.97
		ρ = 19.4892 kmol/m^3		
450.000	146.8766	316.9430	322.2395	-1.671
440.000	142.5187	317.7022	322.6377	-1.554
430.000	138.1020	318.4678	323.0294	-1.432
419.999	133.6299	319.2397	323.4182	-1.309
410.000	129.1274	320.0166	323.8259	-1.190
400.000	124.5640	320.8006	324.2287	-1.069
389.999	119.9614	321.5906	324.6476	-0.951
380.000	115.3127	322.3872	325.0772	-0.834
370.001	110.6114	323.1913	325.5146	-0.719
360.000	105.8506	324.0035	325.9558	-0.603
350.001	101.0393	324.8237	326.4103	-0.488
340.001	96.1758	325.6525	326.8810	-0.377
330.000	91.2519	326.4914	327.3624	-0.267
320.000	86.2662	327.3407	327.8546	-0.157
310.003	81.2292	328.2004	328.3730	-0.053
300.000	76.1276	329.0736	328.9124	0.049
		ρ = 14.6990 kmol/m^3		
299.999	35.7938	248.1891	248.1146	0.030
290.000	32.9943	248.8436	248.8315	0.005
279.998	30.1623	249.5223	249.5821	-0.024
270.000	27.3064	250.2280	250.4092	-0.072
260.000	24.4319	250.9658	251.3577	-0.156
250.000	21.5229	251.7434	252.3749	-0.251
240.000	18.5838	252.5645	253.4978	-0.370
230.000	15.6107	253.4288	254.7171	-0.508
220.000	12.5986	254.3268	255.9781	-0.649
		ρ = 10.2424 kmol/m^3		
299.995	20.5670	172.9404	172.9169	0.014
289.997	19.0228	173.0651	173.0645	0.000
279.999	17.4713	173.1912	173.2027	-0.007
270.000	15.9142	173.3185	173.3370	-0.011
260.000	14.3612	173.4465	173.5704	-0.071
250.000	12.7953	173.5755	173.7025	-0.073
239.999	11.2292	173.7048	173.8550	-0.086

Table 5.2. Continued

T / K	P / MPa	ρ_{Exp} / kg/m^3	ρ_{EoS} / kg/m^3	% dev
229.999	9.6663	173.8340	174.0745	-0.138
219.999	8.1088	173.9629	174.4033	-0.253
		ρ = 5.8967 kmol/m^3		
420.000	20.1203	99.1074	98.8347	0.275
400.004	18.7896	99.2366	98.9867	0.252
390.000	18.1280	99.3015	99.1033	0.200
379.999	17.4609	99.3668	99.2079	0.160
370.000	16.7911	99.4323	99.3163	0.117
360.000	16.1160	99.4982	99.4129	0.086
350.000	15.4459	99.5641	99.5641	0.000
340.002	14.7662	99.6304	99.6796	-0.049
330.000	14.0743	99.6972	99.7336	-0.036
320.000	13.3757	99.7643	99.7569	0.007
310.000	12.6772	99.8315	99.8034	0.028
300.001	11.9619	99.8992	99.7224	0.177
290.000	11.2683	99.9663	99.8753	0.091
280.001	10.5595	100.0339	99.9200	0.114
270.000	9.8629	100.1012	100.1745	-0.073
260.000	9.1356	100.1693	100.1057	0.063
250.000	8.4135	100.2372	100.1784	0.059
240.000	7.6915	100.3050	100.3858	-0.081
230.000	6.9525	100.3732	100.4302	-0.057
220.000	6.193	100.442	100.119	0.321
		ρ = 2.9096 kmol/m^3		
450.000	10.6829	48.8186	48.8189	-0.001
440.000	10.4061	48.8494	48.8530	-0.007
430.000	10.1284	48.8803	48.8861	-0.012
420.000	9.8503	48.9112	48.9210	-0.020
409.999	9.5266	48.9432	48.7240	0.448
400.000	9.2908	48.9731	48.9868	-0.028
390.000	9.0100	49.0040	49.0211	-0.035
380.000	8.7273	49.0350	49.0497	-0.030
369.998	8.4442	49.0661	49.0810	-0.030
360.000	8.1259	49.0980	48.8957	0.412
350.000	7.8710	49.1283	49.1155	0.026
340.000	7.5845	49.1594	49.1425	0.034

Table 5.2. Continued

T / K	P / MPa	ρ_{Exp} / kg/m^3	ρ_{EoS} / kg/m^3	% dev
330.000	7.2965	49.1905	49.1665	0.049
320.001	7.0076	49.2217	49.1909	0.062
309.998	6.7175	49.2528	49.2149	0.077
300.000	6.4207	49.2841	49.1933	0.184
290.001	6.1302	49.3153	49.2349	0.163
280.000	5.8407	49.3464	49.3039	0.086
270.000	5.5494	49.3775	49.3785	-0.002
260.000	5.2435	49.4090	49.3184	0.183
250.000	4.9443	49.4403	49.3542	0.174
240.000	4.6441	49.4716	49.4130	0.118
230.000	4.3360	49.5031	49.4086	0.191
220.000	4.0290	49.5345	49.4796	0.111
		ρ = 2.3324 kmol/m^3		
500.000	9.6248	39.0153	38.9859	0.075
490.000	9.4141	39.0397	39.0183	0.055
480.000	9.2024	39.0640	39.0492	0.038
470.000	8.9899	39.0884	39.0786	0.025
460.000	8.7767	39.1128	39.1080	0.012
450.000	8.5625	39.1372	39.1346	0.007
440.000	8.3478	39.1617	39.1618	0.000
430.000	8.1326	39.1861	39.1896	-0.009
420.000	7.9157	39.2106	39.2115	-0.002
410.000	7.6989	39.2351	39.2364	-0.003
399.999	7.4814	39.2596	39.2610	-0.004
390.000	7.2632	39.2841	39.2849	-0.002
379.999	7.0443	39.3087	39.3079	0.002
369.999	6.8248	39.3332	39.3312	0.005
359.999	6.6045	39.3578	39.3539	0.010
350.001	6.3833	39.3823	39.3745	0.020
339.999	6.1611	39.4069	39.3938	0.033
330.002	5.9385	39.4316	39.4143	0.044
320.000	5.7147	39.4562	39.4325	0.060
310.000	5.4899	39.4808	39.4491	0.080
300.000	5.2624	39.5055	39.4504	0.140
290.000	5.0378	39.5302	39.4825	0.121
280.000	4.8123	39.5548	39.5192	0.090

Table 5.2. Continued

T / K	P / MPa	ρ_{Exp} / kg/m^3	ρ_{EoS} / kg/m^3	% dev
270.000	4.5851	39.5795	39.5520	0.069
260.000	4.3528	39.6043	39.5480	0.142
250.000	4.1218	39.6290	39.5718	0.144
240.000	3.8911	39.6537	39.6236	0.076
230.000	3.6634	39.6784	39.7498	-0.180
220.000	3.4545	39.7026	40.2238	-1.313
		ρ = 1.6300 kmol/m^3		
369.998	4.8223	27.4890	27.4482	0.148
360.000	4.6818	27.5057	27.5048	0.003
349.997	4.5335	27.5226	27.5182	0.016
340.000	4.3838	27.5395	27.5243	0.055
330.005	4.2136	27.5569	27.3916	0.600
319.999	4.0836	27.5733	27.5387	0.126
310.001	3.9389	27.5901	27.5895	0.002
305.154	3.8681	27.5983	27.6127	-0.052
299.996	3.7885	27.6071	27.6038	0.012
290.001	3.6393	27.6240	27.6327	-0.032
279.998	3.4892	27.6409	27.6601	-0.069
270.000	3.3358	27.6579	27.6652	-0.026
260.000	3.1824	27.6749	27.6766	-0.006
240.000	2.8739	27.7089	27.7076	0.005
220.000	2.5606	27.7430	27.7340	0.032

5.2. Isochoric Temperature Derivative

The mathematical expressions to compute the energy functions that complete this full thermodynamic characterization are isothermal integrals in density

$$\frac{U^r}{RT} = \frac{1}{T}\int_0^{\rho}\left(\frac{\partial Z}{\partial(1/T)}\right)_{\rho}\frac{d\rho}{\rho} \tag{5.11}$$

$$\frac{A^r}{RT} = \int_0^\rho \left(Z-1\right)\frac{d\rho}{\rho} \tag{5.12}$$

$$\frac{S^r}{R} = \int_0^\rho \left[1 - \frac{1}{\rho R}\left(\frac{\partial P}{\partial T}\right)_\rho\right]\frac{d\rho}{\rho} = \frac{U^r}{RT} - \frac{A^r}{RT} \tag{5.13}$$

Superscript *r* stands for residual properties, which are the difference between the real value of the function and its ideal gas value at the same conditions.

$$X^r = X(T,P) - X^{ig}(T,P) \tag{5.14}$$

Besides experimental values of density (or *Z*), we must know the temperature derivative $(dP/dT)_\rho$, or $[dZ/d(1/T)]_\rho$. These two quantities have an exact mathematical equivalence:

$$\rho R\left(\frac{\partial Z}{\partial(1/T)}\right)_\rho = \left[P - T\left(\frac{\partial P}{\partial T}\right)_\rho\right] \tag{5.15}$$

Isochoric measurements are experimental determinations of this value at different conditions. First, we correct the experimental pressures to build true isochores using:

$$P^* = P + \left(\frac{\partial P}{\partial \rho}\right)_T \left(\rho^* - \rho\right) \tag{5.16}$$

in which the isothermal derivative of *P* with respect to ρ can come from an equation of state. These corrections are always smaller than 0.5%. The true isochore density ρ^* is the reference density calculated in the previous section (Table 5.1). It comes from density measurements in the MSD, usually at T = 300 K and the pressure of the corresponding isochore at that reference temperature. These corrected isochoric data fit into a fairly

regular polynomial form. For low density data a quadratic function in *1/T* fits *Z* values within a 0.1 % deviation band.

$$Z = \frac{P}{\rho RT} = a_0 + a_1 \frac{T_R}{T} + a_2 \left(\frac{T_R}{T} \right)^2 \tag{5.17}$$

At higher densities (high-pressure isochoric experiment), a cubic fit of *P* with *T* is sufficient.

$$P = a_0 + a_1 \frac{T}{T_R} + a_2 \left(\frac{T}{T_R} \right)^2 + a_3 \left(\frac{T}{T_R} \right)^3 \tag{5.18}$$

T_R is used here as a scaling factor. Table 5.3 contains the results of this fit procedure for 10 isochores of the residual gas sample.

Table 5.3. Isochoric fits for temperature derivative calculations.

ρ/kmol·m^{-3}	T / K	P / MPa	a_0	a_1	a_2	a_3	Σ
24.8164	200 - 300	78 - 200	-154.5868	286.3593	145.9441	-77.7786	0.093822
22.8313	200 - 400	45 - 218	-156.8632	319.4312	-22.1425	-1.5736	0.027238
21.4482	200 - 450	30 - 216	-134.4213	258.2736	-15.7666	-0.4802	0.163432
19.4893	300 - 450	76 - 161	-106.2381	190.9206	-8.4416	-0.1148	0.004763
14.6990	220 - 300	12 - 36	-51.7213	83.1363	6.8339	-2.4538	0.002296
10.2424	220 - 300	8 - 21	1.8546	-1.0644	0.0151	0.0000	0.000196
5.8967	220 - 420	6 - 20	1.3376	-0.3659	-0.0725	0.0000	0.000653
2.9096	220 - 450	4 - 11	1.1564	-0.1818	-0.0451	0.0000	0.000851
2.3324	220 - 500	3 - 10	1.1328	-0.1661	-0.0269	0.0000	0.001181
1.6300	220 - 370	2.5 - 5	1.0649	-0.0697	-0.0399	0.0000	0.000454

These fits provide analytical functions to compute the temperature derivative, key quantity for energy calculations.

$$\left(\frac{\partial(Z)}{\partial(1/T)}\right)_{\rho} = a_1 T_R + 2\frac{a_2 T_R^2}{T} \tag{5.19}$$

$$\left(\frac{\partial P}{\partial T}\right)_{\rho} = \frac{a_1}{T_R} + 2a_2\frac{T}{T_R^2} + 3a_3\frac{T^2}{T_R^3} \tag{5.20}$$

Table 5.4 contains temperature derivatives at all *(T, ρ)* data points for 10 isochores compared to theoretical values calculated with RefProp equation of state.

Table 5.4. Isochoric temperature derivatives for a residual gas sample.

***T* / K**	***P* / MPa**	Z_{Exp}	Z_{EoS}	$(dP/dT)_{Exp}$	$(dP/dT)_{EoS}$	**% dev *(dP/dT)***
ρ = 24.8164 kmol/m^3						
300.000	199.8357	3.2283	3.2348	1.1497	1.0039	12.685
295.000	194.2342	3.1910	3.2069	1.1592	1.0097	12.893
290.000	188.3850	3.1483	3.1775	1.1683	1.0158	13.053
285.000	182.5102	3.1036	3.1467	1.1769	1.0220	13.165
280.000	176.6198	3.0571	3.1141	1.1851	1.0283	13.233
275.000	170.6034	3.0066	3.0799	1.1929	1.0348	13.254
270.000	164.6980	2.9563	3.0437	1.2002	1.0414	13.230
263.061	156.3973	2.8814	2.9903	1.2097	1.0509	13.123
259.991	152.3636	2.8402	2.9653	1.2136	1.0552	13.048
249.998	140.2963	2.7198	2.8781	1.2252	1.0698	12.687
239.999	128.0895	2.5866	2.7804	1.2351	1.0851	12.145
229.997	115.7672	2.4394	2.6710	1.2433	1.1013	11.420
220.000	103.2842	2.2753	2.5479	1.2498	1.1185	10.506
210.000	90.6507	2.0921	2.4090	1.2545	1.1366	9.395
200.000	78.1283	1.8932	2.2517	1.2575	1.1559	8.079
ρ = 22.8313 kmol/m^3						
390.000	217.5117	2.6907	2.8330	0.8463	0.7534	10.970
380.000	209.0156	2.6633	2.8027	0.8525	0.7595	10.909
375.000	204.7797	2.6335	2.7866	0.8557	0.7627	10.868
370.000	200.4778	2.6024	2.7699	0.8588	0.7659	10.819
360.000	191.8453	2.5688	2.7343	0.8650	0.7724	10.702
350.000	183.1589	2.5351	2.6956	0.8711	0.7792	10.553
340.000	174.4176	2.4971	2.6536	0.8773	0.7863	10.374

Table 5.4. Continued

T / K	P / MPa	Z_{Exp}	Z_{EoS}	$(dP/dT)_{Exp}$	$(dP/dT)_{EoS}$	% dev (dP/dT)
330.000	165.6135	2.4565	2.6080	0.8834	0.7936	10.164
320.000	156.7525	2.4131	2.5582	0.8894	0.8012	9.920
310.000	147.8405	2.3665	2.5039	0.8954	0.8091	9.641
300.000	138.9426	2.3170	2.4446	0.9014	0.8173	9.327
290.000	129.7694	2.2641	2.3796	0.9074	0.8259	8.975
279.999	120.6768	2.2075	2.3084	0.9133	0.8349	8.584
270.000	111.5175	2.1773	2.2301	0.9192	0.8442	8.154
260.000	102.3214	2.1464	2.1438	0.9250	0.8540	7.681
249.999	93.0514	2.0807	2.0486	0.9308	0.8641	7.164
239.999	83.7175	2.0174	1.9431	0.9366	0.8748	6.604
230.000	74.3114	1.9409	1.8260	0.9423	0.8858	5.999
219.991	64.8534	1.8580	1.6954	0.9481	0.8974	5.347
210.000	55.3474	1.8066	1.5496	0.9537	0.9094	4.652
199.994	45.7731	1.7685	1.3858	0.9594	0.9218	3.914
			ρ = 21.4482 kmol/m^3			
449.998	215.9211	2.6907	2.5817	0.6924	0.6254	9.679
440.000	208.9798	2.6633	2.5604	0.6964	0.6294	9.618
430.000	201.9385	2.6335	2.5376	0.7004	0.6336	9.540
420.000	194.9182	2.6024	2.5131	0.7043	0.6378	9.442
410.000	187.8159	2.5688	2.4869	0.7083	0.6422	9.327
400.000	180.8331	2.5351	2.4587	0.7122	0.6468	9.191
390.000	173.6706	2.4971	2.4284	0.7162	0.6514	9.036
380.000	166.4662	2.4565	2.3958	0.7201	0.6563	8.860
370.000	159.2219	2.4131	2.3607	0.7240	0.6613	8.662
360.001	151.9247	2.3665	2.3229	0.7279	0.6664	8.442
350.001	144.6147	2.3170	2.2821	0.7317	0.6718	8.199
340.004	137.2807	2.2641	2.2380	0.7356	0.6773	7.933
330.000	129.9085	2.2075	2.1902	0.7395	0.6830	7.643
325.002	126.1932	2.1773	2.1649	0.7414	0.6859	7.488
320.000	122.4843	2.1464	2.1385	0.7433	0.6889	7.328
310.002	115.0267	2.0807	2.0823	0.7472	0.6950	6.986
300.000	107.9277	2.0174	2.0212	0.7510	0.7013	6.619
290.000	100.3734	1.9409	1.9547	0.7548	0.7078	6.224
280.000	92.7724	1.8580	1.8821	0.7586	0.7146	5.802
275.000	88.5982	1.8066	1.8432	0.7605	0.7181	5.581
270.000	85.1510	1.7685	1.8026	0.7624	0.7216	5.353

Table 5.4. Continued

T / K	P / MPa	Z_{Exp}	Z_{EoS}	$(dP/dT)_{Exp}$	$(dP/dT)_{EoS}$	% dev (dP/dT)
260.000	76.7982	1.6564	1.7156	0.7662	0.7288	4.878
250.000	69.4482	1.5577	1.6199	0.7700	0.7363	4.377
239.997	61.7397	1.4426	1.5144	0.7738	0.7439	3.853
229.999	54.0355	1.3174	1.3980	0.7775	0.7518	3.309
220.000	46.2993	1.1801	1.2689	0.7812	0.7598	2.751
ρ = 19.4892 kmol/m^3						
450.000	160.7549	2.2046	2.1353	0.5494	0.5057	7.960
440.000	155.2654	2.1777	2.1127	0.5514	0.5085	7.781
430.000	149.7408	2.1490	2.0886	0.5534	0.5114	7.586
419.999	144.1859	2.1186	2.0630	0.5554	0.5144	7.380
410.000	138.6284	2.0866	2.0357	0.5573	0.5174	7.160
400.000	133.0367	2.0525	2.0065	0.5593	0.5206	6.925
389.999	127.4353	2.0165	1.9753	0.5613	0.5238	6.678
380.000	121.8180	1.9783	1.9420	0.5633	0.5271	6.415
370.001	116.1793	1.9377	1.9063	0.5652	0.5306	6.138
360.000	110.5131	1.8944	1.8680	0.5672	0.5341	5.847
350.001	104.8307	1.8484	1.8269	0.5692	0.5376	5.542
340.001	99.1317	1.7993	1.7827	0.5711	0.5413	5.221
330.000	93.4089	1.7468	1.7351	0.5731	0.5451	4.884
320.000	87.6628	1.6906	1.6838	0.5751	0.5490	4.535
310.003	81.9067	1.6305	1.6285	0.5770	0.5530	4.170
300.000	76.1276	1.5660	1.5686	0.5790	0.5570	3.794
ρ = 14.6990 kmol/m^3						
299.999	35.7938	0.9763	0.9769	0.2981	0.2992	-0.344
290.000	32.8161	0.9259	0.9260	0.2982	0.2999	-0.569
279.998	29.8297	0.8717	0.8714	0.2983	0.3006	-0.765
270.000	26.8446	0.8135	0.8125	0.2982	0.3010	-0.912
260.000	23.8679	0.7511	0.7490	0.2982	0.3011	-0.987
250.000	20.8856	0.6836	0.6804	0.2980	0.3009	-0.954
240.000	17.9051	0.6104	0.6063	0.2979	0.3001	-0.760
230.000	14.9272	0.5310	0.5261	0.2976	0.2986	-0.320
220.000	11.9530	0.4446	0.4395	0.2973	0.2958	0.527
ρ = 10.2424 kmol/m^3						
299.995	20.5670	0.8050	0.8052	0.1566	0.1562	0.274
289.997	19.0070	0.7696	0.7696	0.1566	0.1564	0.089
279.999	17.4433	0.7315	0.7315	0.1565	0.1566	-0.075

Table 5.4. Continued

T / K	P / MPa	Z_{Exp}	Z_{EoS}	$(dP/dT)_{Exp}$	$(dP/dT)_{EoS}$	% dev (dP/dT)
270.000	15.8774	0.6905	0.6905	0.1564	0.1567	-0.201
260.000	14.3191	0.6467	0.6462	0.1562	0.1567	-0.263
250.000	12.7515	0.5989	0.5985	0.1561	0.1565	-0.271
239.999	11.1873	0.5474	0.5470	0.1559	0.1562	-0.177
229.999	9.6298	0.4916	0.4912	0.1557	0.1556	0.095
219.999	8.0808	0.4313	0.4307	0.1556	0.1545	0.668
ρ = 5.8967 kmol/m^3						
420.000	20.2194	0.9819	0.9848	0.0680	0.0686	-0.830
400.004	18.8547	0.9614	0.9640	0.0683	0.0688	-0.815
390.000	18.1779	0.9507	0.9527	0.0684	0.0690	-0.771
379.999	17.4965	0.9391	0.9407	0.0686	0.0691	-0.721
370.000	16.8137	0.9269	0.9280	0.0688	0.0692	-0.667
360.000	16.1267	0.9137	0.9145	0.0690	0.0694	-0.617
350.000	15.4459	0.9001	0.9001	0.0692	0.0695	-0.525
340.002	14.7567	0.8853	0.8848	0.0694	0.0697	-0.462
330.000	14.0564	0.8688	0.8685	0.0696	0.0699	-0.408
320.000	13.3506	0.8510	0.8510	0.0698	0.0701	-0.367
310.000	12.6462	0.8321	0.8323	0.0701	0.0703	-0.303
300.001	11.9263	0.8108	0.8121	0.0704	0.0706	-0.290
290.000	11.2293	0.7898	0.7904	0.0707	0.0708	-0.150
280.001	10.5183	0.7662	0.7669	0.0711	0.0711	-0.065
270.000	9.8209	0.7419	0.7415	0.0716	0.0715	0.113
260.000	9.0939	0.7134	0.7137	0.0720	0.0719	0.145
250.000	8.3735	0.6832	0.6835	0.0725	0.0724	0.233
240.000	7.6546	0.6505	0.6502	0.0732	0.0730	0.301
230.000	6.9199	0.6137	0.6135	0.0738	0.0737	0.235
220.000	6.1663	0.5717	0.5726	0.0746	0.0747	-0.125
ρ = 2.9096 kmol/m^3						
450.000	10.7509	0.9876	0.9876	0.0286	0.0286	0.151
440.000	10.4655	0.9832	0.9831	0.0287	0.0286	0.161
430.000	10.1795	0.9786	0.9785	0.0287	0.0287	0.141
420.000	9.8936	0.9737	0.9735	0.0287	0.0287	0.168
400.000	9.3196	0.9631	0.9628	0.0288	0.0288	0.173
390.000	9.0322	0.9573	0.9570	0.0289	0.0288	0.194
380.000	8.7434	0.9511	0.9508	0.0289	0.0289	0.183
369.998	8.4545	0.9445	0.9443	0.0290	0.0289	0.225

Table 5.4. Continued

T / K	P / MPa	Z_{Exp}	Z_{EoS}	$(dP/dT)_{Exp}$	$(dP/dT)_{EoS}$	% dev (dP/dT)
360.000	8.1307	0.9336	0.9373	0.0289	0.0290	-0.117
350.000	7.8710	0.9296	0.9298	0.0291	0.0290	0.176
340.000	7.5800	0.9216	0.9218	0.0291	0.0291	0.194
330.000	7.2880	0.9129	0.9133	0.0292	0.0292	0.194
320.001	6.9954	0.9036	0.9042	0.0293	0.0292	0.185
309.998	6.7021	0.8937	0.8943	0.0294	0.0293	0.204
300.000	6.4026	0.8822	0.8837	0.0294	0.0294	0.123
290.001	6.1097	0.8709	0.8721	0.0296	0.0295	0.128
280.000	5.8183	0.8590	0.8596	0.0297	0.0297	0.137
270.000	5.5256	0.8460	0.8459	0.0298	0.0298	0.158
260.000	5.2188	0.8297	0.8310	0.0300	0.0300	-0.063
250.000	4.9191	0.8134	0.8145	0.0301	0.0302	-0.181
240.000	4.6189	0.7955	0.7963	0.0303	0.0304	-0.379
230.000	4.3113	0.7748	0.7760	0.0305	0.0307	-0.734
220.000	4.0053	0.7526	0.7532	0.0307	0.0311	-1.198
$\rho = 2.3324$ kmol/m^3						
500.000	9.7166	1.0021	1.0028	0.0222	0.0221	0.414
490.000	9.4976	0.9995	1.0000	0.0222	0.0221	0.422
480.000	9.2780	0.9967	0.9971	0.0222	0.0221	0.420
470.000	9.0578	0.9938	0.9940	0.0222	0.0222	0.418
460.000	8.8373	0.9907	0.9908	0.0223	0.0222	0.410
450.000	8.6160	0.9873	0.9874	0.0223	0.0222	0.399
440.000	8.3945	0.9838	0.9838	0.0223	0.0222	0.384
430.000	8.1730	0.9801	0.9800	0.0223	0.0222	0.371
420.000	7.9499	0.9761	0.9760	0.0223	0.0223	0.345
410.000	7.7273	0.9719	0.9718	0.0224	0.0223	0.321
399.999	7.5043	0.9674	0.9674	0.0224	0.0223	0.294
390.000	7.2809	0.9627	0.9627	0.0224	0.0223	0.263
379.999	7.0571	0.9576	0.9577	0.0224	0.0224	0.228
369.999	6.8330	0.9523	0.9523	0.0224	0.0224	0.187
359.999	6.6085	0.9466	0.9467	0.0225	0.0224	0.145
350.001	6.3833	0.9404	0.9406	0.0225	0.0225	0.089
339.999	6.1575	0.9339	0.9342	0.0225	0.0225	0.025
330.002	5.9315	0.9268	0.9272	0.0226	0.0226	-0.045
320.000	5.7048	0.9193	0.9198	0.0226	0.0226	-0.127
310.000	5.4773	0.9111	0.9118	0.0226	0.0227	-0.229

Table 5.4. Continued

T / K	P / MPa	Z_{Exp}	Z_{EoS}	$(dP/dT)_{Exp}$	$(dP/dT)_{EoS}$	% dev (dP/dT)
300.000	5.2475	0.9020	0.9031	0.0227	0.0228	-0.369
290.000	5.0208	0.8928	0.8937	0.0227	0.0228	-0.479
280.000	4.7937	0.8828	0.8835	0.0228	0.0229	-0.611
270.000	4.5652	0.8719	0.8724	0.0228	0.0230	-0.787
260.000	4.3319	0.8591	0.8602	0.0229	0.0231	-1.072
250.000	4.1002	0.8457	0.8467	0.0230	0.0233	-1.377
240.000	3.8693	0.8313	0.8319	0.0230	0.0234	-1.732
230.000	3.6416	0.8164	0.8153	0.0232	0.0236	-2.106
220.000	3.4333	0.8047	0.7966	0.0234	0.0239	-2.205
ρ = 1.6300 kmol/m^3						
369.998	4.8280	0.9628	0.9642	0.0149	0.0150	-0.736
360.000	4.6845	0.9601	0.9602	0.0150	0.0150	-0.579
349.997	4.5335	0.9557	0.9559	0.0150	0.0151	-0.538
340.000	4.3812	0.9508	0.9513	0.0150	0.0151	-0.502
319.999	4.0765	0.9400	0.9411	0.0151	0.0151	-0.421
310.001	3.9298	0.9354	0.9354	0.0151	0.0152	-0.316
305.154	3.8582	0.9329	0.9325	0.0152	0.0152	-0.198
299.996	3.7777	0.9291	0.9292	0.0152	0.0152	-0.218
290.001	3.6270	0.9228	0.9225	0.0152	0.0152	-0.115
279.998	3.4755	0.9159	0.9153	0.0153	0.0153	0.024
270.000	3.3210	0.9076	0.9073	0.0153	0.0153	0.015
260.000	3.1667	0.8987	0.8986	0.0154	0.0154	0.076
240.000	2.8571	0.8784	0.8784	0.0156	0.0156	0.211
220.000	2.5435	0.8531	0.8533	0.0158	0.0158	0.204

5.3. Estimation of Energy Functions

All thermodynamic state functions (*S, U, H, A, G*) have an arbitrary reference state for which they have a known value. To avoid dealing with reference state calculations, and also knowing the particular characteristics of the data set built for this

sample, we obtain experimental values for these functions by computing differences between experimental and theoretical values.

$$U^r(T,P) = U^r(T,P)_{EoS} + \delta U^r \tag{5.21}$$

$$A^r(T,P) = A^r(T,P)_{EoS} + \delta A^r \tag{5.22}$$

$$S^r(T,P) = S^r(T,P)_{EoS} + \delta S^r \tag{5.23}$$

These δX values correspond to the difference between two integrals in density as defined in expressions (5.11 – 5.13), so that the difference in the integrands can be calculated first to observe its behavior with density and then integrate those differences.

$$\frac{\delta U^r}{RT} = \frac{1}{T}\int_0^\rho \left\{ \left[\left(\frac{\partial Z}{\partial(1/T)} \right)_\rho \right]_{\exp} - \left[\left(\frac{\partial Z}{\partial(1/T)} \right)_\rho \right]_{EoS} \right\} \frac{d\rho}{\rho} = \frac{1}{T}\int_0^\rho \Delta \left(\frac{\partial Z}{\partial(1/T)} \right)_\rho \frac{d\rho}{\rho} \tag{5.24}$$

$$\frac{\delta A^r}{RT} = \int_0^\rho \left\{ Z_{\exp} - Z_{EoS} \right\} \frac{d\rho}{\rho} = \int_0^\rho \Delta Z \frac{d\rho}{\rho} \tag{5.25}$$

$$\frac{\delta S^r}{R} = \int_0^\rho -\frac{1}{\rho R} \left\{ \left[\left(\frac{\partial P}{\partial T} \right)_\rho \right]_{\exp} - \left[\left(\frac{\partial P}{\partial T} \right)_\rho \right]_{EoS} \right\} \frac{d\rho}{\rho} = \int_0^\rho -\frac{1}{\rho R} \Delta \left(\frac{\partial P}{\partial T} \right)_\rho \frac{d\rho}{\rho} \tag{5.26}$$

In equations (5.24 – 5.26), δ means experimental minus equation of state. For the residual gas sample, table 5.5 contains values of these dimensionless integrands (Δ functions inside the integrals) calculated with RefProp equation of state.

Table 5.5. Dimensionless integrands for the calculation of thermodynamic functions.

ρ (kmol/m^3)	ΔU int	ΔA int	ΔS int
	T = 220 K		
24.8164	-0.9089	-0.2726	-0.6363
22.8313	-0.4094	-0.1424	-0.2670
21.4482	-0.2092	-0.0887	-0.1205
14.6990	-0.0077	0.0051	-0.0128
10.2424	-0.0116	0.0006	-0.0122
5.8967	0.0010	-0.0009	0.0019
2.9096	0.0146	-0.0006	0.0152
2.3324	0.0266	0.0081	0.0266
1.6300	-0.0026	-0.0002	-0.0024
	T = 240 K		
24.8164	-0.9208	-0.1938	-0.7270
22.8313	-0.4314	-0.1055	-0.3259
21.4482	-0.2391	-0.0719	-0.1672
14.6990	0.0227	0.0042	0.0185
10.2424	0.0036	0.0004	0.0032
5.8967	-0.0041	0.0004	-0.0045
2.9096	0.0040	-0.0007	0.0048
2.3324	0.0206	-0.0005	0.0206
1.6300	-0.0025	0.0000	-0.0024
	T = 260 K		
24.8164	-0.8925	-0.1251	-0.7674
22.8313	-0.4450	-0.0707	-0.3743
21.4482	-0.2688	-0.0592	-0.2096
14.6990	0.0263	0.0022	0.0241
10.2424	0.0053	0.0005	0.0048
5.8967	-0.0025	-0.0003	-0.0021
2.9096	-0.0005	-0.0013	0.0008
2.3324	0.0127	-0.0010	0.0127
1.6300	-0.0008	0.0001	-0.0009
	T = 280 K		
24.8164	-0.8171	-0.0570	-0.7600
22.8313	-0.4510	-0.0380	-0.4130
21.4482	-0.2709	-0.0241	-0.2468
14.6990	0.0190	0.0004	0.0187

Table 5.5. Continued

ρ (kmol/m^3)	ΔU int	ΔA int	ΔS int
10.2424	0.0014	0.0001	0.0014
5.8967	0.0002	-0.0007	0.0009
2.9096	-0.0023	-0.0006	-0.0017
2.3324	0.0072	-0.0007	0.0072
1.6300	0.0003	0.0006	-0.0003
T = 300 K			
24.8164	-0.7133	-0.0064	-0.7068
22.8313	-0.4477	-0.0048	-0.4429
21.4482	-0.2826	-0.0038	-0.2787
19.4893	-0.1381	-0.0026	-0.1356
14.6990	0.0078	-0.0006	0.0084
10.2424	-0.0052	-0.0001	-0.0050
5.8967	0.0029	-0.0013	0.0042
2.9096	-0.0030	-0.0015	-0.0015
2.3324	0.0043	-0.0011	0.0043
1.6300	0.0023	-0.0001	0.0024
T = 320 K			
22.8313	-0.4425	0.0223	-0.4648
21.4482	-0.2976	0.0079	-0.3054
19.4893	-0.1542	0.0068	-0.1609
5.8967	0.0052	-0.0001	0.0052
2.9096	-0.0028	-0.0005	-0.0022
2.3324	0.0015	-0.0005	0.0015
1.6300	0.0036	-0.0011	0.0047
T = 340 K			
22.8313	-0.4307	0.0488	-0.4794
21.4482	-0.3011	0.0262	-0.3272
19.4893	-0.1674	0.0166	-0.1840
5.8967	0.0070	0.0004	0.0065
2.9096	-0.0026	-0.0003	-0.0023
2.3324	-0.0003	-0.0003	-0.0003
1.6300	0.0051	-0.0005	0.0056
T = 350 K			
22.8313	-0.4232	0.0611	-0.4843
21.4482	-0.3016	0.0349	-0.3364

Table 5.5. Continued

ρ (kmol/m^3)	ΔU int	ΔA int	ΔS int
19.4893	-0.1731	0.0215	-0.1947
5.8967	0.0074	0.0000	0.0074
2.9096	-0.0023	-0.0002	-0.0021
2.3324	-0.0010	-0.0002	-0.0010
1.6300	0.0058	-0.0001	0.0059
T = 360 K			
22.8313	-0.4147	0.0730	-0.4876
21.4482	-0.3010	0.0435	-0.3446
19.4893	-0.1782	0.0265	-0.2047
5.8967	0.0079	-0.0008	0.0087
2.9096	-0.0023	-0.0037	0.0014
2.3324	-0.0017	-0.0001	-0.0017
1.6300	0.0064	0.0000	0.0064
T = 380 K			
22.8313	-0.3951	0.0948	-0.4899
21.4482	-0.2971	0.0607	-0.3577
19.4893	-0.1866	0.0364	-0.2230
5.8967	0.0085	-0.0015	0.0101
2.9096	-0.0019	0.0003	-0.0022
2.3324	-0.0026	0.0000	-0.0026
T = 400 K			
21.4482	-0.2907	0.0764	-0.3671
19.4893	-0.1931	0.0460	-0.2390
5.8967	0.0088	-0.0025	0.0113
2.9096	-0.0018	0.0003	-0.0021
2.3324	-0.0034	0.0000	-0.0034

Values in table 5.5 are fit to polynomial functions with density, then divided by ρ, and then integrated to result in the desired values of δX. In order to have some practical meaning, we translate these quantities into equivalent δTs by using the corresponding derivatives dX/dT.

$$\delta U^r = \left(\frac{\partial U}{\partial T}\right)_\rho \delta T_U = C_V \delta T_U \tag{5.27}$$

$$\delta A^r = \left(\frac{\partial A}{\partial T}\right)_\rho \delta T_A = -S\delta T_A \tag{5.28}$$

$$\delta S^r = \left(\frac{\partial S}{\partial T}\right)_\rho \delta T_S = \frac{C_V}{T}\delta T_S \tag{5.29}$$

Table 5.6 contains these δ values of the thermodynamic properties obtained by coupling isothermal density measurements and isochoric techniques.

Table 5.6. δX results from integration and corresponding equivalent δT.

ρ / kmol/m^3	δU / kJ/kmol	δT_U / K	δA / kJ/kmol	δT_A / K	δS / kJ/kmol·K	δT_S / K
			T = 220 K			
24.8164	-277.8684	-8.4279	-88.8886	3.5563	-0.8209	-5.4774
22.8313	-182.0901	-5.7178	-58.5690	2.0545	-0.5235	-3.6164
21.4482	-140.2486	-4.4901	-45.0247	1.4599	-0.3946	-2.7796
19.4893	-109.9214	-3.5328	-34.6826	0.8477	-0.3032	-2.1438
14.6990	-133.0314	-4.0220	-39.3786	0.8361	-0.3858	-2.5663
10.2424	-198.4125	-6.1839	-57.9576	1.0602	-0.6010	-4.1212
5.8967	-212.7037	-7.2795	-62.2283	0.9898	-0.6556	-4.9361
2.9096	-149.4098	-5.2282	-43.8082	0.6721	-0.4633	-3.5664
2.3324	-127.4887	-4.5874	-37.3967	0.5440	-0.3956	-3.1319
			T = 240 K			
24.8164	-327.0501	-9.8322	-74.9571	2.6890	-1.0527	-7.5953
22.8313	-219.6929	-6.8326	-50.9225	1.6274	-0.7055	-5.2660
21.4482	-173.3091	-5.4971	-40.0814	1.1940	-0.5574	-4.2434
14.6990	-140.5463	-4.5928	-31.6120	0.7251	-0.4563	-3.5784
10.2424	-170.2350	-5.4374	-34.2402	0.6864	-0.5691	-4.3625
5.8967	-245.0529	-7.9815	-47.7125	0.8314	-0.8246	-6.4455
2.9096	-257.3693	-8.9263	-50.0049	0.7647	-0.8658	-7.2066
2.3324	-179.2385	-6.3163	-34.9014	0.5159	-0.6024	-5.0951
1.6300	-152.7382	-5.4928	-29.7565	0.4182	-0.5133	-4.4301

Table 5.6. Continued

ρ / kmol/m^3	δU / kJ/kmol	δT_U / K	δA / kJ/kmol	δT_A / K	δS / kJ/kmol·K	δT_S / K
			T = 260 K			
24.8164	-354.6521	-10.5272	-55.0343	1.8012	-1.1572	-8.9311
22.8313	-239.2135	-7.3380	-37.6494	1.1112	-0.7801	-6.2216
21.4482	-188.6481	-5.9011	-29.5633	0.8187	-0.6167	-5.0159
14.6990	-151.7045	-4.9534	-22.8306	0.4959	-0.5006	-4.2499
10.2424	-177.5448	-5.7596	-22.5875	0.4314	-0.6011	-5.0700
5.8967	-253.0013	-8.3659	-30.5937	0.5114	-0.8602	-7.3958
2.9096	-265.4566	-9.1970	-32.0307	0.4732	-0.9015	-8.1205
2.3324	-184.9592	-6.4849	-22.4123	0.3205	-0.6274	-5.7190
1.6300	-157.6327	-5.6123	-19.1190	0.2605	-0.5346	-4.9484
			T = 280 K			
24.8164	-358.1768	-10.4583	-28.2795	0.8551	-1.1813	-9.6582
22.8313	-240.8548	-7.2590	-19.5121	0.5373	-0.7936	-6.6973
21.4482	-188.3988	-5.7880	-15.4121	0.4003	-0.6210	-5.3416
14.6990	-148.2244	-4.7873	-11.9606	0.2475	-0.4899	-4.4300
10.2424	-165.3858	-5.3615	-11.6250	0.2127	-0.5525	-5.0147
5.8967	-235.2100	-7.7712	-15.4498	0.2489	-0.7880	-7.2896
2.9096	-248.3056	-8.5065	-16.0458	0.2297	-0.8319	-7.9795
2.3324	-173.6794	-6.0052	-11.1977	0.1554	-0.5817	-5.6316
1.6300	-148.1185	-5.1833	-9.5488	0.1265	-0.4961	-4.8605
			T = 300 K			
24.8164	-325.6550	-9.3226	-9.4538	0.2666	-1.0580	-9.0861
22.8313	-208.6918	-6.1586	-8.2759	0.2142	-0.6720	-5.9495
21.4482	-150.4936	-4.5247	-7.6470	0.1876	-0.4802	-4.3308
19.4893	-95.9382	-2.9489	-6.9741	0.1596	-0.3006	-2.7721
14.6990	-63.4450	-2.0129	-6.0129	0.1191	-0.1957	-1.8623
10.2424	-97.3700	-3.1211	-5.3052	0.0934	-0.3109	-2.9895
5.8967	-117.3973	-3.8339	-4.0156	0.0626	-0.3810	-3.7327
2.9096	-87.6312	-2.9465	-2.4022	0.0334	-0.2859	-2.8840
2.3324	-75.5183	-2.5581	-1.9979	0.0270	-0.2466	-2.5056
1.6300	-57.4637	-1.9655	-1.4599	0.0188	-0.1878	-1.9267
			T = 320 K			
22.8313	-239.5116	-6.9014	4.3489	-0.1065	-0.7764	-7.1587
21.4482	-178.9728	-5.2506	2.2093	-0.0515	-0.5791	-5.4364
19.4893	-119.8452	-3.5932	-0.0803	0.0018	-0.3868	-3.7108

Table 5.6. Continued

ρ / kmol/m^3	δU / kJ/kmol	δT_U / K	δA / kJ/kmol	δT_A / K	δS / kJ/kmol·K	δT_S / K
5.8967	-72.7676	-2.3314	-2.6949	0.0407	-0.2356	-2.4151
2.9096	-93.7157	-3.0762	-2.5052	0.0339	-0.3063	-3.2171
2.3324	-107.1877	-3.5399	-1.2171	0.0160	-0.3515	-3.7149
1.6300	-79.1640	-2.6354	-0.3611	0.0045	-0.2598	-2.7679
			T = 340 K			
22.8313	-244.4265	-6.8619	14.0739	-0.3275	-0.7989	-7.6251
21.4482	-180.5660	-5.1576	8.5614	-0.1901	-0.5915	-5.7439
19.4893	-117.1808	-3.4187	2.5565	-0.0534	-0.3861	-3.8298
5.8967	-62.3525	-1.9497	-4.8230	0.0709	-0.2106	-2.2386
2.9096	-80.2800	-2.5626	-5.1772	0.0684	-0.2708	-2.9385
2.3324	-95.5943	-3.0671	-2.6324	0.0338	-0.3197	-3.4878
1.6300	-72.0248	-2.3265	-0.7943	0.0098	-0.2399	-2.6352
			T = 350 K			
22.8313	-244.9270	-6.7828	35.6530	-0.8101	-0.8030	-7.7828
21.4482	-179.6879	-5.0612	26.9008	-0.5841	-0.5916	-5.8317
19.4893	-114.3932	-3.2899	18.4125	-0.3768	-0.3808	-3.8328
5.8967	-55.6323	-1.7161	11.8971	-0.1724	-0.1943	-2.0978
2.9096	-71.7617	-2.2566	15.1134	-0.1973	-0.2495	-2.7460
2.3324	-88.0870	-2.7831	16.8672	-0.2141	-0.3008	-3.3268
1.6300	-67.3103	-2.1399	12.3175	-0.1499	-0.2281	-2.5379
			T = 360 K			
22.8313	-245.0539	-6.6923	36.2534	-0.8050	-0.7820	-7.6883
21.4482	-178.6589	-4.9607	25.3136	-0.5379	-0.5672	-5.6696
19.4893	-111.6714	-3.1650	14.7680	-0.2962	-0.3518	-3.5898
5.8967	-49.1321	-1.4942	7.1952	-0.1029	-0.1571	-1.7199
2.9096	-63.3264	-1.9607	12.4437	-0.1605	-0.2111	-2.3526
2.3324	-80.4913	-2.5031	16.6716	-0.2092	-0.2703	-3.0266
1.6300	-62.4788	-1.9542	12.9587	-0.1560	-0.2098	-2.3624
			T = 380 K			
22.8313	-296.9897	-7.8821	75.0189	-1.5946	-0.9790	-9.8734
21.4482	-228.7463	-6.1681	59.6612	-1.2166	-0.7590	-7.7771
19.4893	-159.6507	-4.3910	44.7964	-0.8649	-0.5381	-5.6234
5.8967	-92.8332	-2.7397	33.1791	-0.4626	-0.3317	-3.7194
2.9096	-101.2832	-3.0369	37.6120	-0.4744	-0.3656	-4.1651

Table 5.6. Continued

ρ / kmol/m^3	δU / kJ/kmol	δT_U / K	δA / kJ/kmol	δT_A / K	δS / kJ/kmol·K	δT_S / K
2.3324	-107.9646	-3.2495	37.7445	-0.4635	-0.3835	-4.3859
			T = 400 K			
21.4482	-180.3095	-4.7193	29.7035	-0.5828	-0.5249	-5.4955
19.4893	-104.2673	-2.7815	10.5074	-0.1957	-0.2868	-3.0605
5.8967	-5.2235	-0.1494	3.5036	-0.0477	-0.0216	-0.2467
2.9096	-11.1392	-0.3232	5.8021	-0.0716	-0.0422	-0.4895
2.3324	-10.6358	-0.3096	5.4165	-0.0651	-0.0400	-0.4655

With these δ values, we only need the prediction from the equation of state to obtain experimental values of all thermodynamic properties.

Equivalent temperature differences (δT) are useful and more meaningful for practical purposes, to evaluate the performance of equations of state and make conscious judgments about them in real operations and design applications.

6. CONCLUSIONS AND FUTURE WORK

In summary, this dissertation contains a full thermodynamic characterization that includes *P, ρ, T, S, U, H, A,* and *G* constructed from isothermal and isochoric volumetric data collected for a typical residual gas sample (95 % methane, 4 % ethane, 1 % propane). Such experimental information is useful for testing, validating and improving existing predictive models, and contributes to the improvement of natural gas design and business operations.

Sophisticated, state-of-the-art techniques provide reference quality (high accuracy and precision) data. Deep understanding of these techniques and apparatus is necessary for the estimation and assessment of uncertainties and errors, as well as for the manipulation and statistical treatment of the data. Pure substance data reported validate and expand the applicability ranges of existing reference equations of state for nitrogen and carbon dioxide.

High accuracy $P\rho T$ data are always in demand. So are simple and powerful predictive models. This work comprises an overview of some of the principal capabilities of the thermodynamics research group at Texas A&M University: theoretical correlations, and experimental characterization and data manipulation.

Magnetic suspension densimeters currently provide the most accurate density data. During this work, we reached a deep understanding and exploitation of the technique from quantification of its inherent force transmission error, and rigorous, first-principles estimation of uncertainties including all experimental variables as well as

sample composition effects, to the coupling of its accurate yield into independent isochoric measurements to provide isochoric densities. Identification and explicit calculation of temperature derivatives from isochoric measurements allowed extension of experimental volumetric characterizations up to a full thermodynamic characterization that includes energy functions.

In the area of phase equilibrium, the behavior of isochores inside the two-phase (vapor-liquid) region is currently under study. This includes study of the behavior of isentropic lines and their sensitivity to phase changes. Also, alternative experimental techniques involving vibrating tubes and resonant cavities for phase boundary determinations in the region between the cricondentherm (CT) and criocondenbar (CB) points, and more direct experimental determinations of thermal and volumetric derivatives are envisioned.

Preliminary results from experimental tests of the MSD system using sinkers of lighter materials, suggest possible reductions in the apparatus contribution to the force transmission error, and a more accurate determination of fluid effects. Having achieved the uncertainty levels reported in this work, such a modification combined with a lower-pressure transducer could improve the accuracy of the low-density range of the apparatus.

REFERENCES

(1) Annual Energy Outlook 2012 Early Release Overview. US Energy Information Administration. *http://www.eia.gov/forecasts/aeo/er/early_introduction.cfm*.

(2) *Annual Energy Outlook 2011 with Projections to 2035*; US Energy Information Administration: Washington, DC, 2011.

(3) Scenarios and Projections. *http://www.iea.org/* Accessed March, 2012.

(4) Voser, P. The Natural Gas Revolution: A Secure, Abundant Force for Good. *http://www.shell.us/home/content/usa/aboutshell/media_center/speeches_and_webcasts/2012/speech_03072012.html*.

(5) ExxonMobil The Outlook for Energy: A View to 2040. *exxonmobil.com/energyoutlook*. Accessed February, 2012.

(6) DOW The Future of Energy. *http://www.dow.com/energy/* Accessed March, 2012.

(7) Redlich, O.; Kwong, J. N. S., On the thermodynamics of solutions. V. An equation of state. Fugacities of gaseous solutions. *Chemical Reviews* **1949,** 44, (1), 233-244.

(8) Peng, D.-Y.; Robinson, D. B., A new two-constant equation of state. *Industrial & Chemistry Engineering Fundamentals* **1976,** 15, (1), 59-64.

(9) Span, R.; Lemmon, E. W.; Jacobsen, R. T.; Wagner, W.; Yokozeki, A., A reference equation of state for the thermodynamic properties of nitrogen for temperatures from 63.151 to 1000 K and pressures to 2200 MPa. *Journal of Physical and Chemical Reference Data* **2000,** 29, (6), 1361-1433.

(10) Span, R.; Wagner, W., A new equation of state for carbon dioxide covering the fluid region from the triple-point temperature to 1100 K at pressures up to 800 MPa. *Journal of Physical and Chemical Reference Data* **1996,** 25, (6), 1509-1596.

(11) Starling, K. E.; Savidge, J. L. *Compressibility Factors of Natural Gas and Other Related Hydrocarbon Gases*; American Gas Association: Arlington, VA, November, 1992, 1992.

(12) Kunz, O.; Klimeck, R.; Wagner, W.; Jaeschke, M., *The GERG-2004 wide-range equation of state for natural gases and other mixtures*. Fortschritt-Berichte. VDI Verlag: Dusseldorf, 2007.

(13) Jaeschke, M.; Humphreys, A. E. *GERG Technical Monograph 5. Standard GERG Virial Equation for Field Use.*; TM 5; GERG: Dusseldorf, 1991.

(14) International Organization for Standarization. *International Standard 12213-3:2006(E). Natural Gas - Calculation of Compression Factor - Part 3: Calculation Using Physical Properties.* ISO: Geneva, 2006.

(15) Holste, J. C.; Hall, K. R.; Eubank, P. T.; Marsh, K. N., High pressure PVT measurements. *Fluid Phase Equilibria* **1986,** 29, (C), 161-176.

(16) Ewing, M. B.; Goodwin, A. R. H., An apparatus based on a spherical resonator for measuring the speed of sound in gases at high pressures. Results for argon at temperatures between 255 K and 300 K and at pressures up to 7 MPa. *The Journal of Chemical Thermodynamics* **1992,** 24, (5), 531-547.

(17) Goodwin, A. R. H.; Moldover, M. R., Thermophysical properties of gaseous refrigerants from speed of sound measurements. I. Apparatus, model, and results for 1,1,1,2-tetrafluoroethane R134a. *The Journal of Chemical Physics* **1990,** 93, (4), 2741-2753.

(18) Daridon, J. L.; Lagourette, B.; Grolier, J. P. E., Experimental measurements of the speed of sound in n-hexane from 293 to 373 K and up to 150 MPa. *International Journal of Thermophysics* **1998,** 19, (1), 145-160.

(19) Hozumi, T.; Sato, H.; Watanabe, K., Speed of sound in gaseous difluoromethane. *Journal of Chemical & Engineering Data* **1994,** 39, (3), 493-495.

(20) Charnley, A.; Isles, G. L.; Townley, J. R., The direct measurement of the isothermal Joule-Thomson coefficient for gases. *Proceedings of the Royal Society of London. Series A. Mathematical and Physical Sciences* **1953,** 218, (1132), 133-143.

(21) Stokes, R. H.; Marsh, K. N.; Tomlins, R. P., An isothermal displacement calorimeter for endothermic enthalpies of mixing. *The Journal of Chemical Thermodynamics* **1969,** 1, (2), 211-221.

(22) Ewing, M. B.; Marsh, K. N.; Stokes, R. H.; Tuxford, C. W., The isothermal displacement calorimeter: design refinements. *The Journal of Chemical Thermodynamics* **1970,** 2, (5), 751-756.

(23) Battino, R.; Marsh, K., An isothermal displacement calorimeter for the measurement of the enthalpy of solution of gases. *Australian Journal of Chemistry* **1980,** 33, (9), 1997-2003.

(24) Dix, M.; Fareleira, J.; Takaishi, Y.; Wakeham, W., A vibrating-wire densimeter for measurements in fluids at high pressures. *International Journal of Thermophysics* **1991,** 12, (2), 357-370.

(25) Pádua, A. A. H.; Fareleira, J. M. N. A.; Calado, J. C. G.; Wakeham, W. A., A vibrating-wire densimeter for liquids at high pressures: The density of 2,2,4-trimethylpentane from 298.15 to 348.15 K and up to 100 MPa. *International Journal of Thermophysics* **1994,** 15, (2), 229-243.

(26) Pádua, A. A. H.; Fareleira, J. M. N. A.; Calado, J. C. G.; Wakeham, W. A., Validation of an accurate vibrating-wire densimeter: Density and viscosity of liquids over wide ranges of temperature and pressure. *International Journal of Thermophysics* **1996,** 17, (4), 781-802.

(27) Picker, P.; Tremblay, E.; Jolicoeur, C., A high-precision digital readout flow densimeter for liquids. *Journal of Solution Chemistry* **1974,** 3, (5), 377-384.

(28) Albert, H. J.; Wood, R. H., High-precision flow densimeter for fluids at temperatures to 700 K and pressures to 40 MPa. *Review of Scientific Instruments* **1984,** 55, (4), 589-593.

(29) Hynek, V.; Hnedkovsky, L.; Cibulka, I., A new design of a vibrating-tube densimeter and partial molar volumes of phenol(aq) at temperatures from 298 K to 573 K. *The Journal of Chemical Thermodynamics* **1997,** 29, (11), 1237-1252.

(30) Blencoe, J. G.; Drummond, S. E.; Seitz, J. C.; Nesbitt, B. E., A vibrating-tube densimeter for fluids at high pressures and temperatures. *International Journal of Thermophysics* **1996,** 17, (1), 179-190.

(31) Hnědkovský, L.; Cibulka, I., An automated vibrating-tube densimeter for measurements of small density differences in dilute aqueous solutions. *International Journal of Thermophysics* **2004,** 25, (4), 1135-1142.

(32) Burnett, E. S., Compressibility determinations without volume measurements. *Journal of Applied Mechanics* **1936,** 3, A136.

(33) Silberberg, I. H.; Kobe, K. A.; McKetta, J. J., Gas compressibilities with the burnett apparatus. Methods and apparatus. *Journal of Chemical & Engineering Data* **1959,** 4, (4), 314-323.

(34) Hall, K. R.; Canfield, F. B., Isotherms for the He-N2 system at 190°C, 170°C and 160°C up to 700 atm. *Physica* **1970,** 47, (2), 219-226.

(35) Hall, K. R.; Canfield, F. B., A least-squares method for reduction of burnett data to compressibility factors and virial coefficients. *Physica* **1970,** 47, (1), 99-108.

(36) Bosart, L. W., An improved pycnometer for glycerin. *Journal of Industrial & Engineering Chemistry* **1911,** 3, (7), 508-508.

(37) Burgess, G. K. A micropyrometer. *Bulletin of the Bureau of Standards* **1913,** 9, 475-478.

(38) Guon, J.; Bodine, J. E., Remote operating gas pycnometer. *Review of Scientific Instruments* **1965,** 36, (12), 1885-1885.

(39) Beams, J. W., Magnetic suspension densimeter. *Review of Scientific Instruments* **1969,** 40, (1), 167-168.

(40) Senter, J. P., Magnetic densimeter utilizing optical sensing. *Review of Scientific Instruments* **1969,** 40, (2), 334-338.

(41) Kleinrahm, R.; Wagner, W., Measurement and correlation of the equilibrium liquid and vapour densities and the vapour pressure along the coexistence curve of methane. *The Journal of Chemical Thermodynamics* **1986,** 18, (8), 739-760.

(42) Toscani, S.; Figuiere, P.; Szwarc, H., A magnetic-suspension apparatus to measure densities of liquids as a function of temperature at pressures up to 100 MPa Application to n-heptane. *The Journal of Chemical Thermodynamics* **1989,** 21, (12), 1263-1277.

(43) Masui, R., Development of a magnetic suspension densimeter and measurement of the density of toluene. *International Journal of Thermophysics* **2002,** 23, (4), 921-935.

(44) Bignell, N., Magnetic flotation in densimetry. *Measurement Science and Technology* **2006,** 17, (10), 2574-2580.

(45) Joint Committee for Guides in Metrology / Working Group 1, *ISO/IEC Guide 98-3:2008. Uncertainty of Measurement - Part 3: Guide to the Expression of Uncertainty in Measurement (GUM:1995).* ISO: Geneva, 2008.

(46) Taylor, B. N.; Kuyatt, C. E. *Guidelines for Evaluating and Expressing the Uncertainty of NIST Measurement Results*; NIST: Gaithersburg, MD, 1994.

(47) NIST Uncertainty of Measurement Results. *http://physics.nist.gov/cuu/Uncertainty/international1.html* Accessed July, 2011.

(48) Krouwer, J. S., Critique of the guide to the expression of uncertainty in measurement method of estimating and reporting uncertainty in diagnostic assays. *Clinical Chemistry* **2003,** 49, (11), 1818-1821.

(49) Abbott, M. M., Low-pressure phase equilibria: Measurement of VLE. *Fluid Phase Equilibria* **1986,** 29, (C), 193-207.

(50) Marsh, K. N., New methods for vapor-liquid-equilibria measurements. *Fluid Phase Equilibria* **1989,** 52, (0), 169-184.

(51) Gibbs, R. E.; Van Ness, H. C., Vapor-liquid equilibria from total-pressure measurements. A new apparatus. *Industrial & Engineering Chemistry Fundamentals* **1972,** 11, (3), 410-413.

(52) Bobbo, S.; Stryjek, R.; Elvassore, N.; Bertucco, A., A recirculation apparatus for vapor-liquid equilibrium measurements of refrigerants. Binary mixtures of R600a, R134a and R236fa. *Fluid Phase Equilibria* **1998,** 150-151, (0), 343-352.

(53) Malanowski, S., Experimental methods for vapour-liquid equilibria. Part I. Circulation methods. *Fluid Phase Equilibria* **1982,** 8, (2), 197-219.

(54) Malanowski, S., Experimental methods for vapour-liquid equilibria. II. Dew- and bubble-point method. *Fluid Phase Equilibria* **1982,** 9, (3), 311-317.

(55) Kolbe, B.; Gmehling, J., Thermodynamic properties of ethanol + water. I. Vapour-liquid equilibria measurements from 90 to 150°C by the static method. *Fluid Phase Equilibria* **1985,** 23, (2-3), 213-226.

(56) Kneisl, P.; Zondlo, J. W.; Whiting, W. B., An apparatus for measurement of multiple-phase equilibria at elevated pressures. *Industrial and Engineering Chemistry Research* **1988,** 27, (8), 1541-1543.

(57) D'Souza, R.; Patrick, J. R.; Teja, A. S., High pressure phase equilibria in the carbon dioxide-n-hexadecane and carbon dioxide-water systems. *Canadian Journal of Chemical Engineering* **1988,** 66, (2), 319-323.

(58) McLinden, M. O.; Splett, J. D., A liquid density standard over wide ranges of temperature and pressure based on toluene. *Journal of Research of the National Institute of Standards and Technology* **2008,** 113, 29-67.

(59) McLinden, M.; Kleinrahm, R.; Wagner, W., Force transmission errors in magnetic suspension densimeters. *International Journal of Thermophysics* **2007,** 28, (2), 429-448.

(60) Cristancho, D. E.; Mantilla, I. D.; Ejaz, S.; Hall, K. R.; Iglesias-Silva, G. A.; Atilhan, M., Force transmission error analysis for a high-pressure single-sinker magnetic suspension densimeter. *International Journal of Thermophysics* **2010,** 31, (4-5), 698-709.

(61) Mantilla, I. D.; Cristancho, D. E.; Ejaz, S.; Hall, K. R.; Atilhan, M.; Iglesias-Silva, G. A., New P-rho-T data for nitrogen at temperatures from (265 to 400) K at pressures up to 150 MPa. *Journal of Chemical & Engineering Data* **2010,** 55, (10), 4227-4230.

(62) Klimeck, J.; Kleinrahm, R.; Wagner, W., An accurate single-sinker densimeter and measurements of the (p, [rho],T) relation of argon and nitrogen in the temperature range from (235 to 520) K at pressures up to 30 MPa. *The Journal of Chemical Thermodynamics* **1998,** 30, (12), 1571-1588.

(63) Michels, A.; Wouters, H.; De Boer, J., Isotherms of nitrogen between 0° and 150° and at pressures from 20 to 80 atm. *Physica* **1934,** 1, (7-12), 587-594.

(64) Wiebe, R.; Gaddy, V. L., The compressibilities of hydrogen and of four mixtures of hydrogen and nitrogen at 0, 25, 50, 100, 200 and 300° and to 1000 atmospheres. *Journal of the American Chemical Society* **1938,** 60, (10), 2300-2303.

(65) Nowak, P.; Kleinrahm, R.; Wagner, W., Measurement and correlation of the (p,[rho],T) relation of nitrogen. I. The homogeneous gas and liquid regions in the temperature range from 66 K to 340 K at pressures up to 12 MPa. *The Journal of Chemical Thermodynamics* **1997,** 29, (10), 1137-1156.

(66) Duschek, W.; Kleinrahm, R.; Wagner, W.; Jaeschke, M., Measurement and correlation of the (pressure, density, temperature) relation of nitrogen in the temperature range from 273.15 to 323.15 K at pressures up to 8 MPa. *The Journal of Chemical Thermodynamics* **1988,** 20, (9), 1069-1077.

(67) Pieperbeck, N.; Kleinrahm, R.; Wagner, W.; Jaeschke, M., Results of (pressure, density, temperature) measurements on methane and on nitrogen in the temperature range from 273.15 K to 323.15 K at pressures up to 12 MPa using a

new apparatus for accurate gas-density measurements. *The Journal of Chemical Thermodynamics* **1991,** 23, (2), 175-194.

(68) Ewing, M. B.; Trusler, J. P. M., Second acoustic virial coefficients of nitrogen between 80 and 373 K. *Physica A: Statistical and Theoretical Physics* **1992,** 184, (3-4), 415-436.

(69) Huff, J. A.; Reed, T. M., Second virial coefficients of mixtures of non-polar molecules from correlations on pure components. *Journal of Chemical & Engineering Data* **1963,** 8, (3), 306-311.

(70) Otto, J.; A., M.; Wouters, H., *Phys. Z.* **1934,** 35, 97.

(71) Canfield, F. B.; Leland, T. W.; Kobayashi, R., *Advances in Cryogenic Engineering* **1963,** 8.

(72) Pocock, G.; Wormald, C. J., Isothermal Joule-Thomson coefficient of nitrogen. *Journal of the Chemical Society-Faraday Transactions I* **1975,** 71, (4), 705-725.

(73) Holborn, L.; Otto, J., The isotherms of several gases between+400 degrees and-183 degrees. *Z. Phys.* **1925,** 33, 1-11.

(74) Kamerlingh, H.; Urk, A. T. van, Isotherms of diatomic substances and their binary mixtures. Communications Physical Laboratory, University of Leiden **1924,** 169d.

(75) Roe, D. R.; Saville, G., Unpublished results. *[Reference to 13]* **1972**, 239.

(76) Lemmon, E. W.; Huber, M. L.; McLinden, M. O., NIST Standard Reference Database 23: Reference Fluid Thermodynamic and Transport Properties-REFPROP, Version 8.0. National Institute of Standards and Technology, Standard Reference Data Program: Gaithersburg, 2007.

(77) Holste, J. C.; Hall, K. R.; Iglesias-Silva, G. A., Log-linear plots for data representation. *AIChE Journal* **1996,** 42, (1), 296-297.

(78) Gokmenoglu, Z.; Xiong, Y.; Kiran, E., Volumetric properties of carbon dioxide + sulfur hexafluoride at high pressures. *Journal of Chemical & Engineering Data* **1996,** 41, (2), 354-360.

(79) Mantilla, I. D.; Cristancho, D. E.; Ejaz, S.; Hall, K. R.; Atilhan, M.; Iglesias-Silva, G. A., P-rho-T data for carbon dioxide from (310 to 450) K up to 160 MPa. *Journal of Chemical & Engineering Data* **2010,** 55, (11), 4611-4613.

(80) Klimeck, J.; Kleinrahm, R.; Wagner; W, Measurements of the(p,[rho],T) relation of methane and carbon dioxide in the temperature range 240 K to 520 K at pressures up to 30 MPa using a new accurate single-sinker densimeter. *The Journal of Chemical Thermodynamics* **2001,** 33, (3), 251-267.

(81) Michels, A.; Michels, C.; Wouters, H., Isotherms of CO2 between 70 and 3000 Atmospheres (Amagat Densities between 200 and 600). *Proceedings of the Royal Society of London. Series A - Mathematical and Physical Sciences* **1935,** 153, (878), 214-224.

(82) Juza, J.; Kmonícek, V.; Sifner, O., Measurements of the specific volume of carbon dioxide in the range of 700 to 4000b and 50 to 475°C. *Physica* **1965,** 31, (12), 1735-1744.

(83) Holste, J. C.; Hall, K. R.; Eubank, P. T.; Esper, G.; Watson, M. Q.; Warowny, W.; Bailey, D. M.; Young, J. G.; Bellomy, M. T., Experimental (p, Vm, T) for pure CO2 between 220 and 450 K. *The Journal of Chemical Thermodynamics* **1987,** 19, (12), 1233-1250.

(84) Duschek, W.; Kleinrahm, R.; Wagner, W., Measurement and correlation of the (pressure, density, temperature) relation of carbon dioxide I. The homogeneous gas and liquid regions in the temperature range from 217 K to 340 K at pressures up to 9 MPa. *The Journal of Chemical Thermodynamics* **1990,** 22, (9), 827-840.

(85) Patel, M. R.; Joffrion, L. L.; Eubank, P. T., A simple procedure for estimating virial coefficients from burnett PVT data. *AIChE Journal* **1988,** 34, (7), 1229-1232.

(86) Butcher, E. G.; Dadson, R. S., The virial coefficients of the carbon dioxide-ethylene system. I. Pure gases. *Proceedings of the Royal Society of London. Series A. Mathematical and Physical Sciences* **1964,** 277, (1371), 448-467.

(87) Dadson, R. S.; Evans, E. J.; King, J. H., The second virial coefficient of carbon dioxide. *Proceedings of the Physical Society* **1967,** 92, (4), 1115-1121.

(88) Michels, A.; Michels, C., Isotherms of CO2 between 0 degrees and 150 degrees and pressures from 16 to 250 atm (Amagat densities 18-206). *Proceedings of the Royal Society of London. Series A - Mathematical and Physical Sciences* **1935,** 153, (878), 201-214.

(89) Waxman, M.; Davis, H. A.; Hastings, J. R., A new determination of the second virial coefficient of carbon dioxide at temperatures between 0 and 150°C and an evaluation of its reliability. In *Proceedings of the Sixth Symposium on Thermophysical Properties*, ASME: New York, 1973; pp 245-255.

(90) Albaiges, J., Quantities, units and symbols in physical chemistry, 3rd edition. *Int. J. Environ. Anal. Chem.* **2008,** 88, (8), 594-595.

(91) Griffiths, R. B., Critical phenomena and tricritical points in multicomponent systems. *Physica* **1974,** 73, (1), 174-183.

(92) Hall, K. R.; Eubank, P. T.; Myerson, A. S.; Nixon, W. E., A new technique for collecting binary vapor-liquid equilibrium data without measuring composition: The method of intersecting isochores. *AIChE Journal* **1975,** 21, (6), 1111-1114.

(93) Hall, K. R.; Eubank, P. T., Rectilinearity rule for isochoric slopes issuing from the coexistence curve. *Industrial & Engineering Chemistry Fundamentals* **1976,** 15, (1), 80-81.

(94) Cristancho, D. E. Experimental Characterization and Molecular Study of Natural Gas Mixtures. Ph.D. thesis. Texas A&M University, College Station, 2010.

VITA

Name:	Ivan Dario Mantilla
Address:	Bryan Research & Engineering P.O. Box 4747 Bryan, TX 77805
Email Address:	I.Mantilla@bre.com
Education:	B.S., Chemical Engineering Universidad Industrial de Santander, Colombia, 2005 Ph.D., Chemical Engineering Texas A&M University, 2012